DEVELOPMENT OF NINE-CHANNEL 10-MICROMETER (Hg,Cd)Te PUSHBROOM IR/CCD SYSTEM

W.J. WHITE

S. IWASA

Prepared for

NASA/GODDARD SPACE FLIGHT CENTER

DECEMBER 1977

FINAL REPORT

HONEYWELL
Electro-Optics Center
2 Forbes Road
Lexington, Massachusetts 02173

DEVELOPMENT OF A NINE CHANNEL 10.5 μm - 12.5 μm (Hg,Cd)Te DETECTOR ARRAY SENSOR WITH Si-CCD READOUT FOR PUSHBROOM CAMERA SYSTEMS

W.J. WHITE

S. IWASA

Prepared for

NASA/GODDARD SPACE FLIGHT CENTER

DECEMBER 1977

FINAL REPORT

HONEYWELL
Electro-Optics Center
2 Forbes Road
Lexington, Massachusetts 02173

PREFACE

This report is intended to serve the dual role of a documentation of the engineering development of the 9-channel array and an operating manual for the user of the array. The development was supported by NASA Contract NAS 5-~~22339~~. 22339

The authors are indebted to the contract monitor, K. L. Hallam, and also L. Thompson and L. Goldberg of NASA/ GSFC for their many helpful discussions.

Also appreciated were the observations and guidance of R. M. Broudy, D. E. Marshall, N. R. Butler, and T. J. Tredwell. The detector array was supplied by W. G. Rae, the CCD by J. S. T. Huang, and the hardware was assembled by A. R. Carson.

TABLE OF CONTENTS

SECTION 1
INTRODUCTION

It has long been recognized that a technology for making self scanned multi-element infrared detector focal planes was needed. The invention of charge coupled devices in 1969 sparked an enthusiasm for such focal planes using both monolithic (CCD as the detector) and hybrid (detector connected to the CCD) approaches. The ultimate realization of such a focal plane would embody multi-elements closely packed, moderate operating temperature, high IR sensitivity and low power consumption. Currently these goals are for the most part readily achievable for the thermal (10.5 to 12.5 μm) infrared in hybrid focal planes employing (Hg,Cd)Te photodiodes and silicon charge coupled devices. In a Push-broom camera configuration, a focal plane is configured in a long linear array multiplexed by a CCD, and the array is oriented perpendicular to the vehicle motion. For earth resources applications, detector arrays sensitive to wavelengths from visible to 12.5 μm would be needed.

The work reported here demonstrates and verifies in the laboratory the feasibility of such an approach, through the development of a simple, 9-element focal plane detector array for the 10.5 - 12.5 μm spectral range, using available technology. Since (Hg,Cd)Te photodiodes sensitive in the 10.5 to 12.5 region having sufficiently high performance for direct coupling to CCDs were unavailable at the time, the array of (Hg,Cd)Te photoconductive detectors was parallel coupled to the CCD through cryogenically cooled preamps. An array of high performance detectors was mounted in a variable temperature (80 to 120 K) test dewar along with 9 matched preamps and a 30-channel CCD multiplexer. A self-contained breadboard system of 9-channel Pushbroom 10 μm peak PC (Hg,Cd)Te IR/CCD MUX system was designed and fabricated, as depicted in Figure 1. Tests showed a 9-channel average D^*_λ peak value of 7.5×10^9 cm $Hz^{\frac{1}{2}}/W$ (17 Hz, 60^o FOV, 1 Hz, 105 K) at the output of the CCD multiplexer. This value exceeds the work statement objective by a factor of 5. The detector array alone exhibits an average D^*_λ peak value of 9.6×10^9 cm $Hz^{\frac{1}{2}}/W$ and hence the total S/N degradation suffered in the multiplexing electronics has been limited to only 22%.

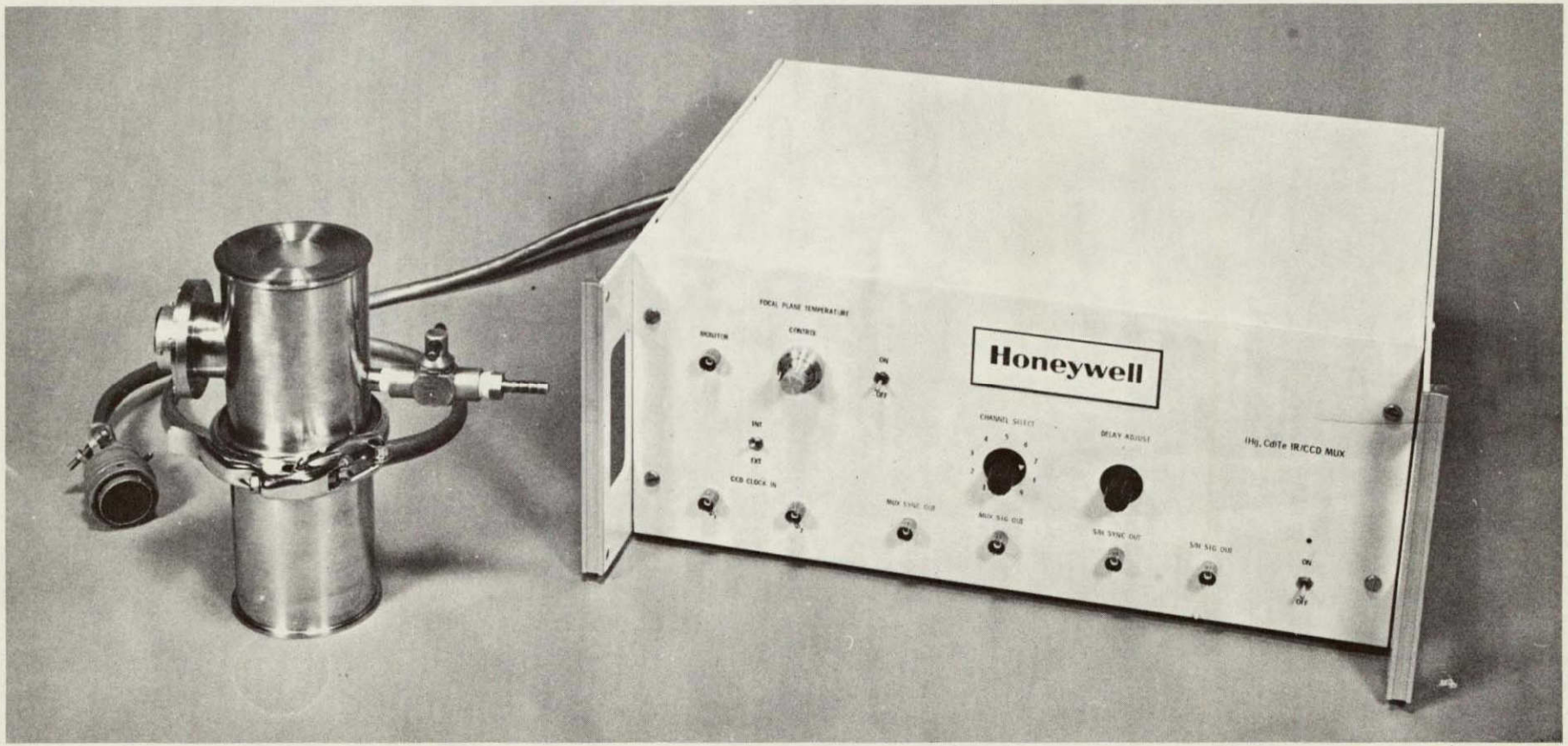

Figure 1 THE 9-CHANNEL 10 μm PC (Hg,Cd)Te IR/CCD MUX BREADBOARD

Ideally, photovoltaic (Hg,Cd)Te diodes would best be suited towards the realization of a large focal plane, since they permit direct coupling (no preamplifiers) and consume very little power. Analysis shows that a 12.5 μm PV (Hg,Cd)Te IR/CCD Pushbroom focal plane operating at 105 K could become a reality in the near future, providing certain requisite (Hg,Cd)Te special materials properties can be realized in practice, through further development efforts. To test the direct coupling concept, a 5 μm PV (Hg,Cd)Te was directly connected to a Si CCD MUX. No degradation in signal-to-noise-ratio was experienced and D^*_λ peak value of 1.6×10^{11} cm $Hz^{\frac{1}{2}}/W$ (BLIP) was obtained after the CCD multiplexer, when the photodiode at 77 K was irradiated by the 300 K background with 180 degree field of view. These results represent the achievement of a major milestone towards the realization of a hybrid focal plane.

Finally, on the basis of the present 9-channel Pushbroom PC IR/CCD breadboard, Honeywell has proposed a 90-element Aircraft Pushbroom Focal Plane Hardware to NASA Goddard SFC and a program NAS5-24323 has been subsequently awarded.

SECTION 2

BURIED CHANNEL CCD MULTIPLEXER

2.1 HONEYWELL CCD DESCRIPTION

A buried n-channel CCD was designed and fabricated by Honeywell to satisfy the requirements of the Goddard Space Flight Center Pushbroom Camera Development Program. The Honeywell CCD 2058 is a multifunction test circuit that contains a multiplexer (MUX) with 30 parallel inputs, a time delay and integration (TDI) with 9 inputs; two circuits for two dimensional IR/CCD arrays, a digital filter, and a series of special amplifiers. Figure 2 is a photograph of the 2058 CCD 30 channel MUX circuit.

It has a 2 phase shift register 60 bits long. Two adjacent inputs are separated by an empty bit to minimize interchannel crosstalk (2 bits/channel). Two separate readouts are provided. A floating gate amplifier is placed after the ninth input, and can non-destructively readout the multiplexed output of the first nine input channels. In addition, a floating diffusion amplifier placed at the end of the shift register can readout all the 30 input channels. A fat zero input structure precedes the shift register for the optimization of transfer efficiency.

2.2 SIGNAL INJECTION METHODS

In an IR/CCD MUX system, the IR detector outputs (voltage, current, or charge) are introduced into the CCD shift register as analog signals. Two types of signal injection methods have been studied in depth in conjunction with the 2058 CCD, i.e., potential equilibration (fill and spill) and dynamic current injection (current integration)[1].

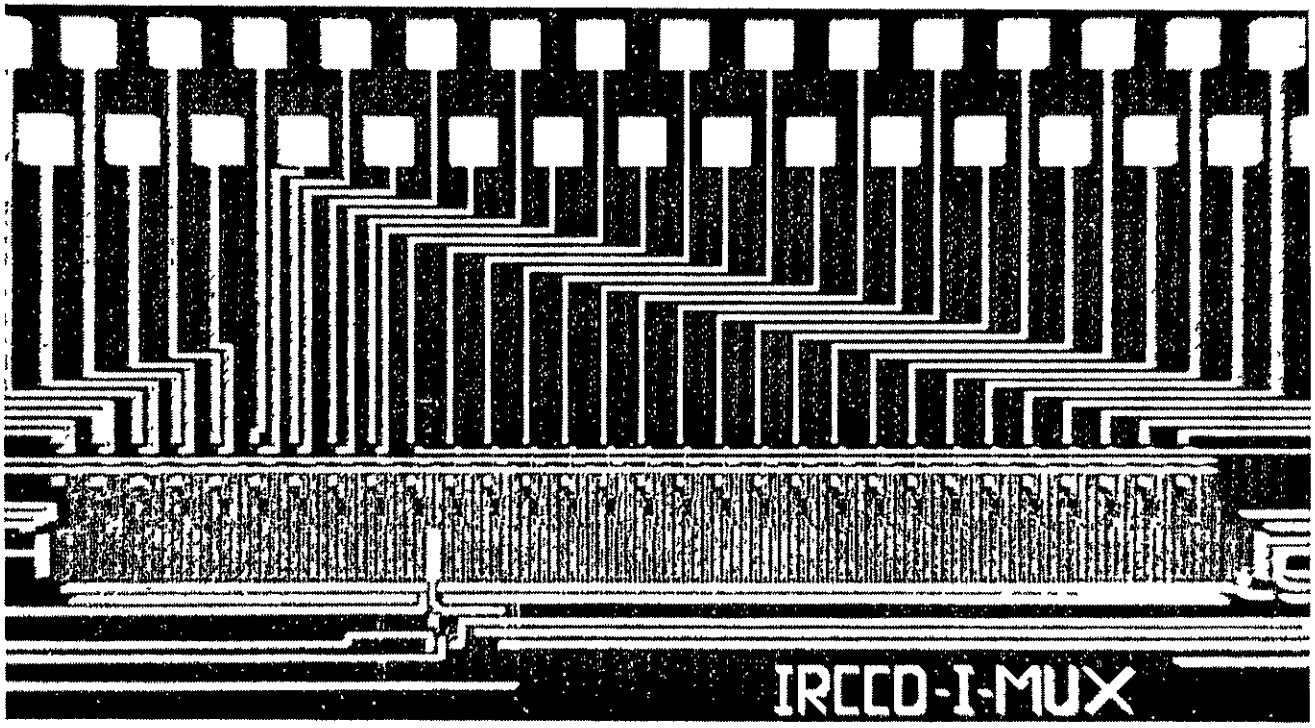

Figure 2 2058 CCD 30-CHANNEL MUX CHIP

Potential Equilibration

Figure 3 gives the signal injection sequence of the fill and spill mode. The input voltage signal V_{in} is applied to the signal gate and after the fill and spill sequence, the shift register receives a charge packet of size:

$$\Delta Q = C_w(V_w - V_{in}) \qquad (1)$$

where C_w and V_w respectively are the capacitance and potential of the storage well. Due to the proximity of the two gates, the threshold voltage difference is negligable, and results in a linear relationship given in Figure 4. The injected charge Q is transferred down the shift register and is ultimately converted into a dc level via the floating diffusion capacitance C_{FD}, and a single stage MOSFET source follower with a gain g, so that the input/output relationship is described by

$$V_{out} = \frac{C_{wu}}{C_{FD}} (V_w - V_{in})g \qquad (2)$$

In the 2058 CCD output design, g = 0.7 and $C_w/C_{FD} = 2/7$, consistent with the device geometry. The characteristics are unchanged at 77 K. The channel non-uniformity is seen to be small.

Current Integration

Figure 5 depicts the signal injection sequence for the current integration mode. For the range of the integration times shown, the channel under the control gate is strongly inverted and the I/O characteristic is given by

$$V_{out} = \frac{\mu_n C_{ox} Z\tau}{2L} \left[V_{in} - (V_G - V_T)\right]^2 \frac{1}{C_{FD}} g \qquad (3)$$

where $\mu_n = 650$ $cm^2/V\text{-}s$ at 300 K is the surface channel electron mobility, $C_{ox} = 3.0 \times 10^{-8}$ fd/cm^2 the gate oxide capacitance per unit area, Z/L = 4 the gate aspect ratio, τ the integration time, and V_{in}, V_G and V_T respectively refer to the source, gate and the threshold voltage. Figure 6 describes this relationship. In the current integration mode, one has the option of signal entry either

at the source diffusion or at the control gate, leading to an identical I/O relationship as given in equation 3. The input impedance is different for the two entries, however. In the source input case, the transconductance is given by

$$g_m = \sqrt{\frac{\mu C_{ox}^2}{2L} I_s} \qquad (4)$$

where I_s is the source diffusion current. The gate is nearly open except for a small capacitance. The nonuniformity among the 9 inputs originate mainly from variations in the threshold voltage of ΔV_T = 20 mV as evidenced by translation and not slope change in Figure 6. The effect of the integration time τ is a change in the slope. Figure 7 illustrates the I/O characteristics of the current integration mode at 300 K and at 77 K, where the major changes occur in V_T (translation) and in μ_n (slope change).

2.3 NOISE AND DYNAMIC RANGE

Figure 8 shows the difference in input referred noise and receiving well noise for current integration and fill and spill signal injection. The fill and spill technique has a lower receiving well noise and, therefore, better dynamic range but it has a higher input referred noise than current integration. The input referred noise at low frequencies is dominated by the input MOS generated 1/f noise. Figure 9 is the measured noise of the two signal injection techniques at 300 K and at 77 K.

2.4 INJECTION METHODS TRADEOFF

Table 1 gives the tradeoff between the two methods. Since the interface between the PC (Hg,Cd)Te and CCD is a single stage bipolar amplifier at a cryogenic temperature, not much signal gain can be expected. Hence, the current integration method is chosen for its lower input noise. Table 2 summarizes the operational characteristics of the Honeywell 2058 CCD, 30 Channel MUX used in the Pushbroom IR/CCD experiments and hardware.

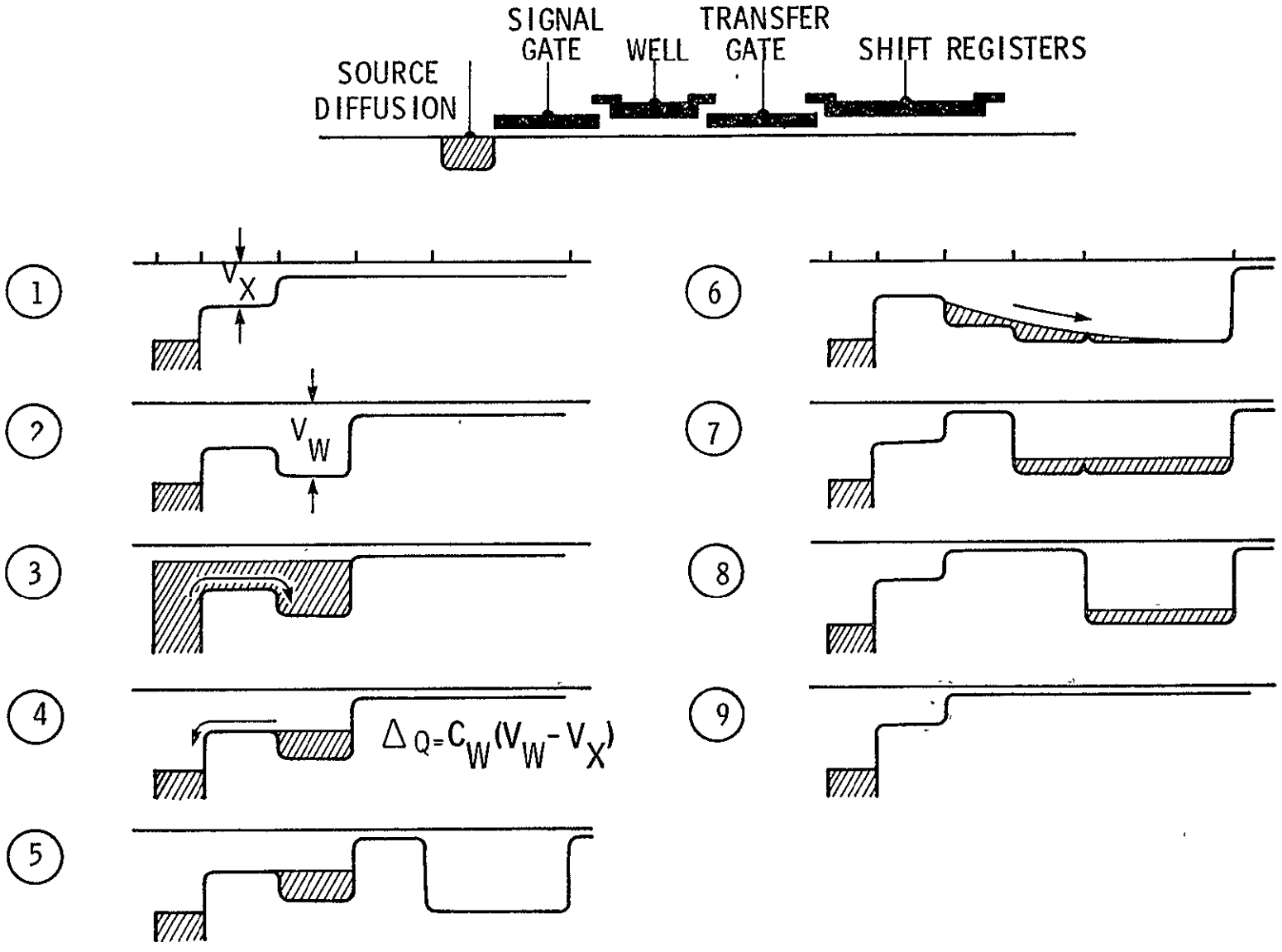

Figure 3 FILL AND SPILL INPUT SEQUENCE

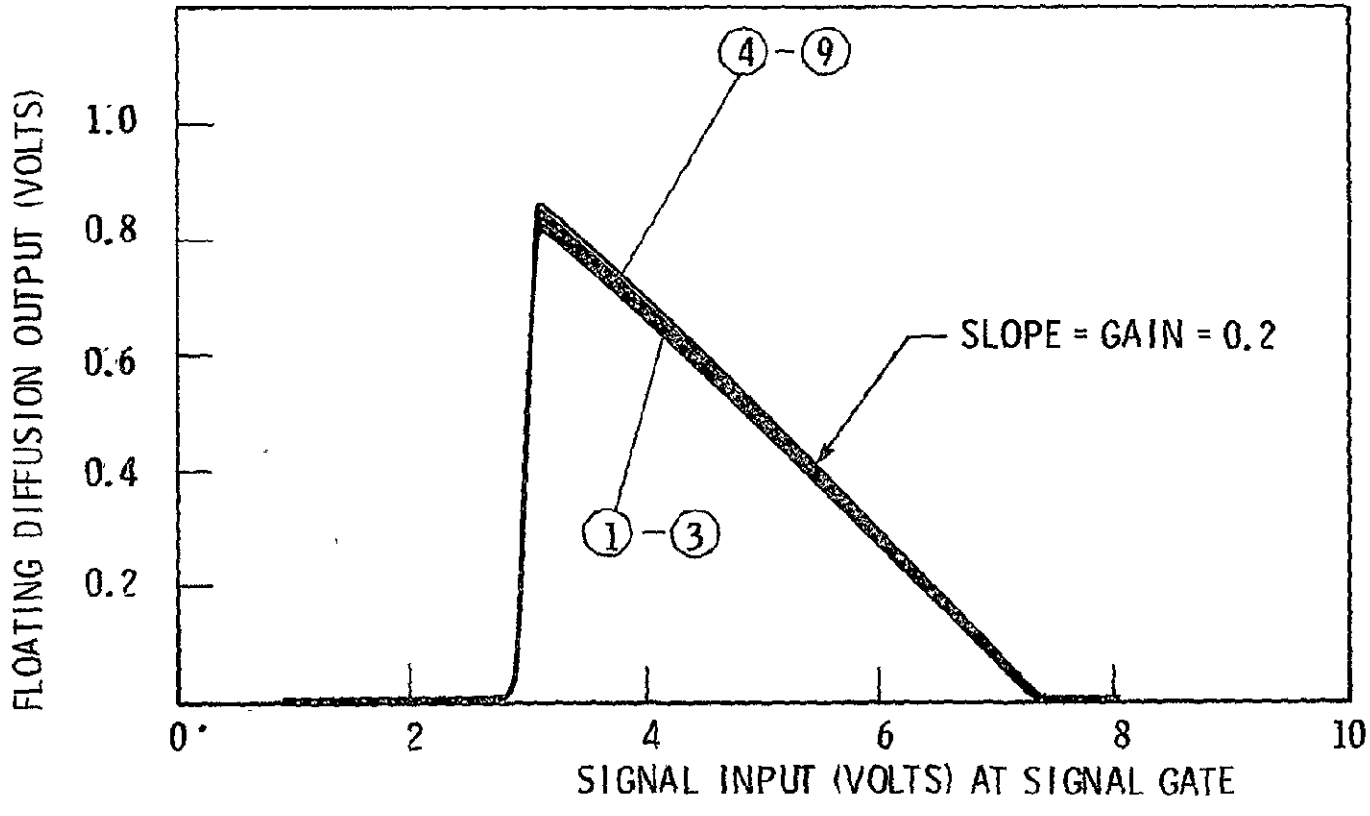

Figure 4 INPUT VS OUTPUT RELATIONSHIP FOR FILL & SPILL

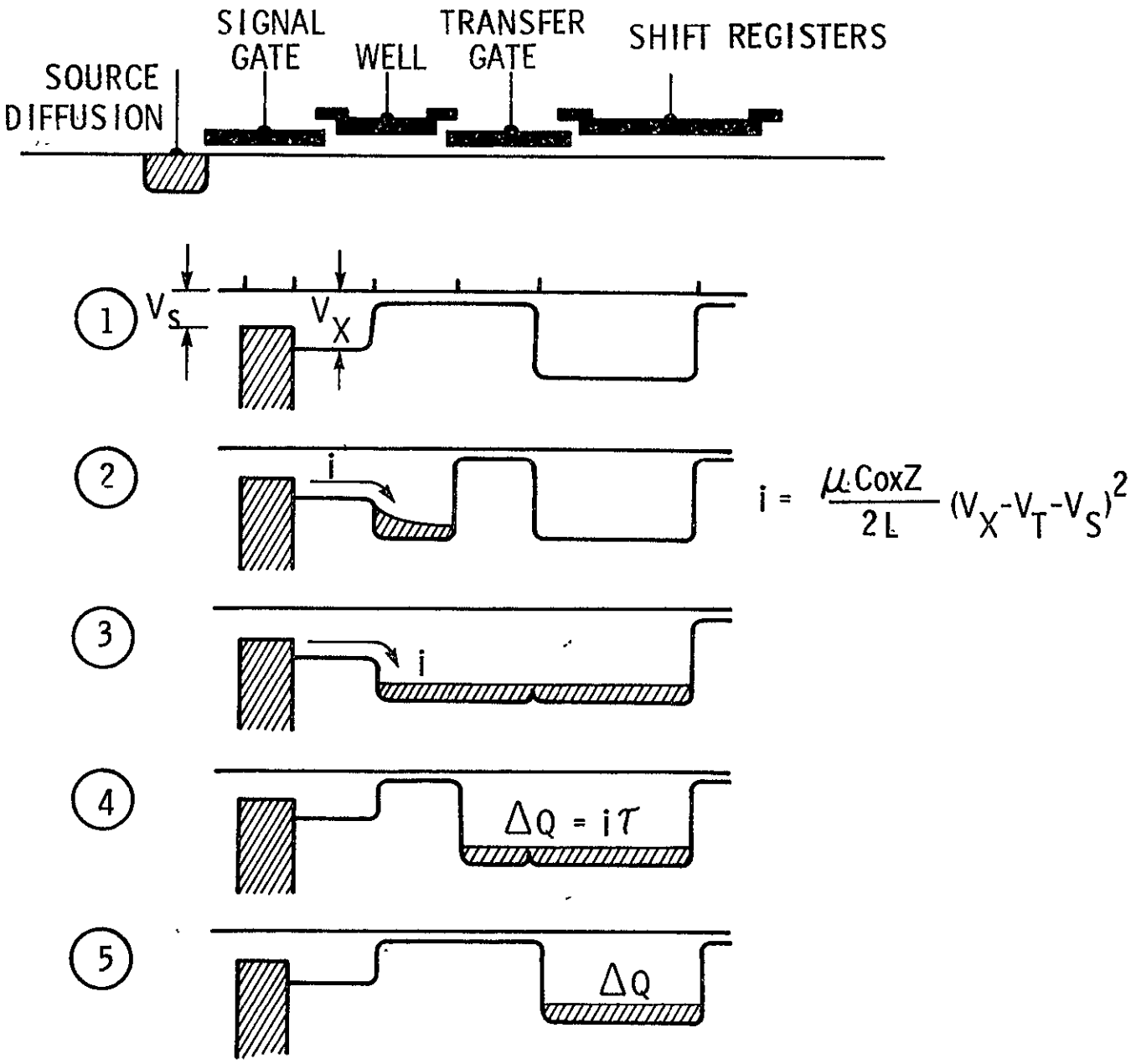

Figure 5 CURRENT INTEGRATION INPUT SEQUENCE

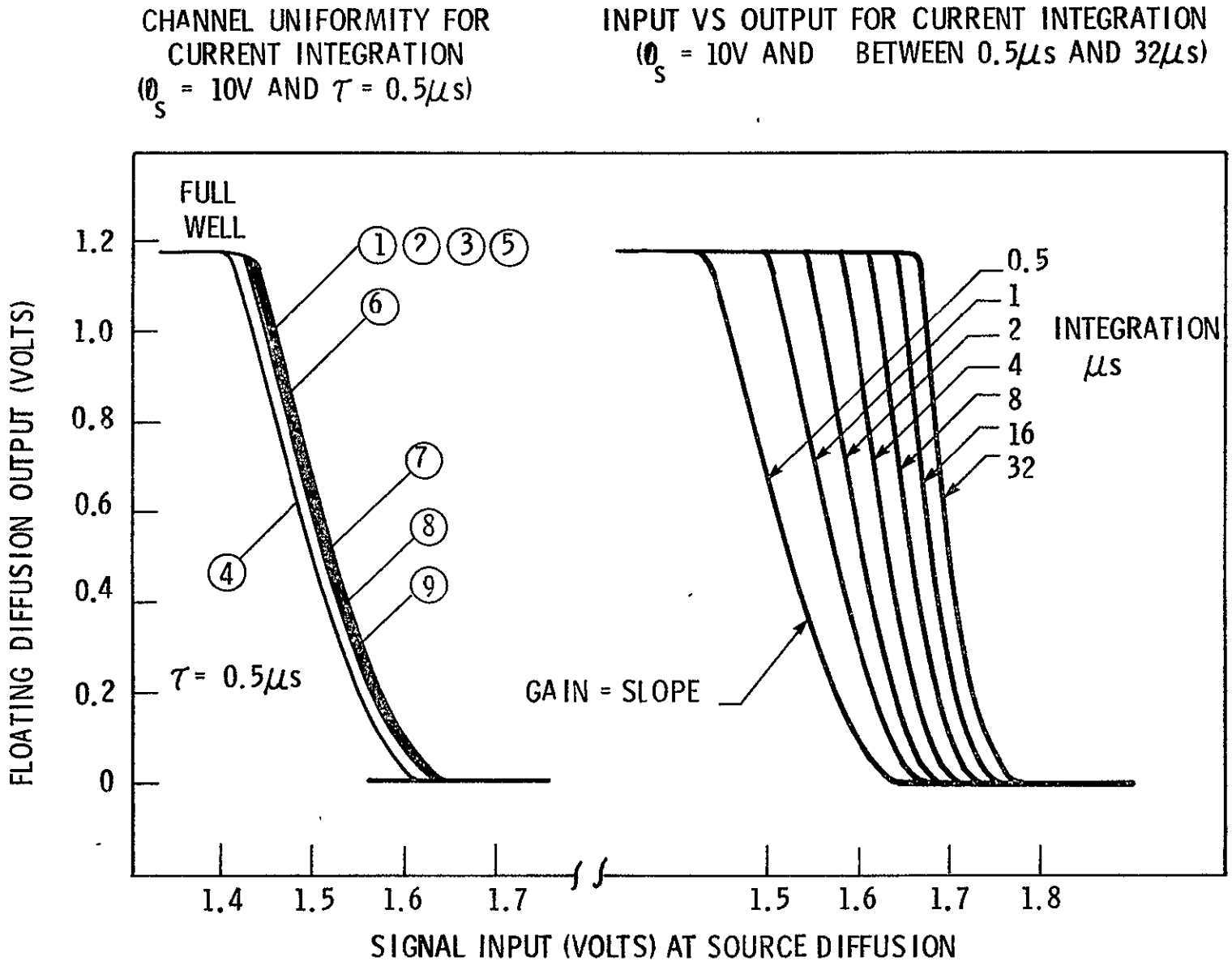

Figure 6 INPUT VS OUTPUT RELATIONSHIP FOR CURRENT INTEGRATION

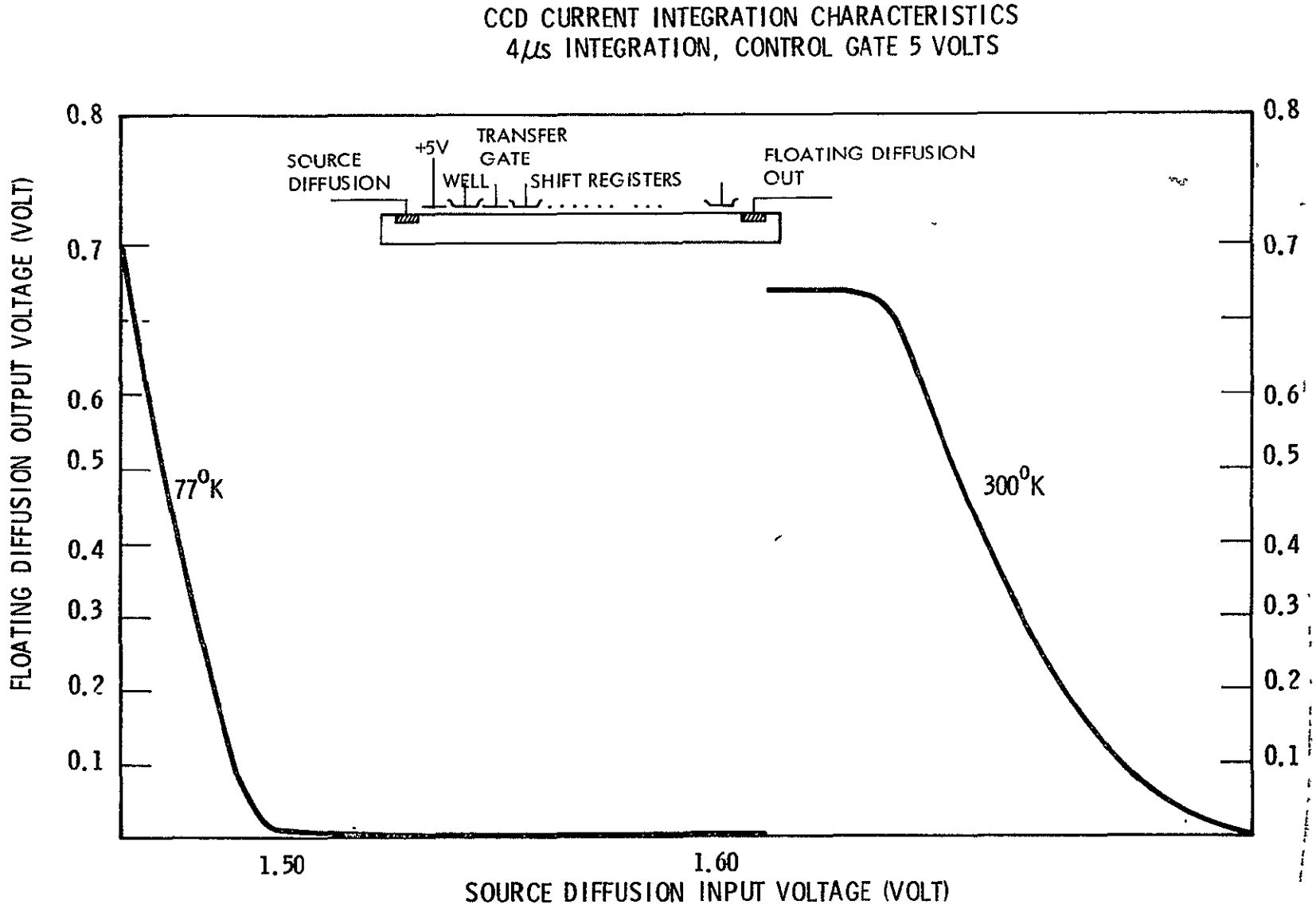

Figure 7 TEMPERATURE DEPENDENCE OF CURRENT INTEGRATION

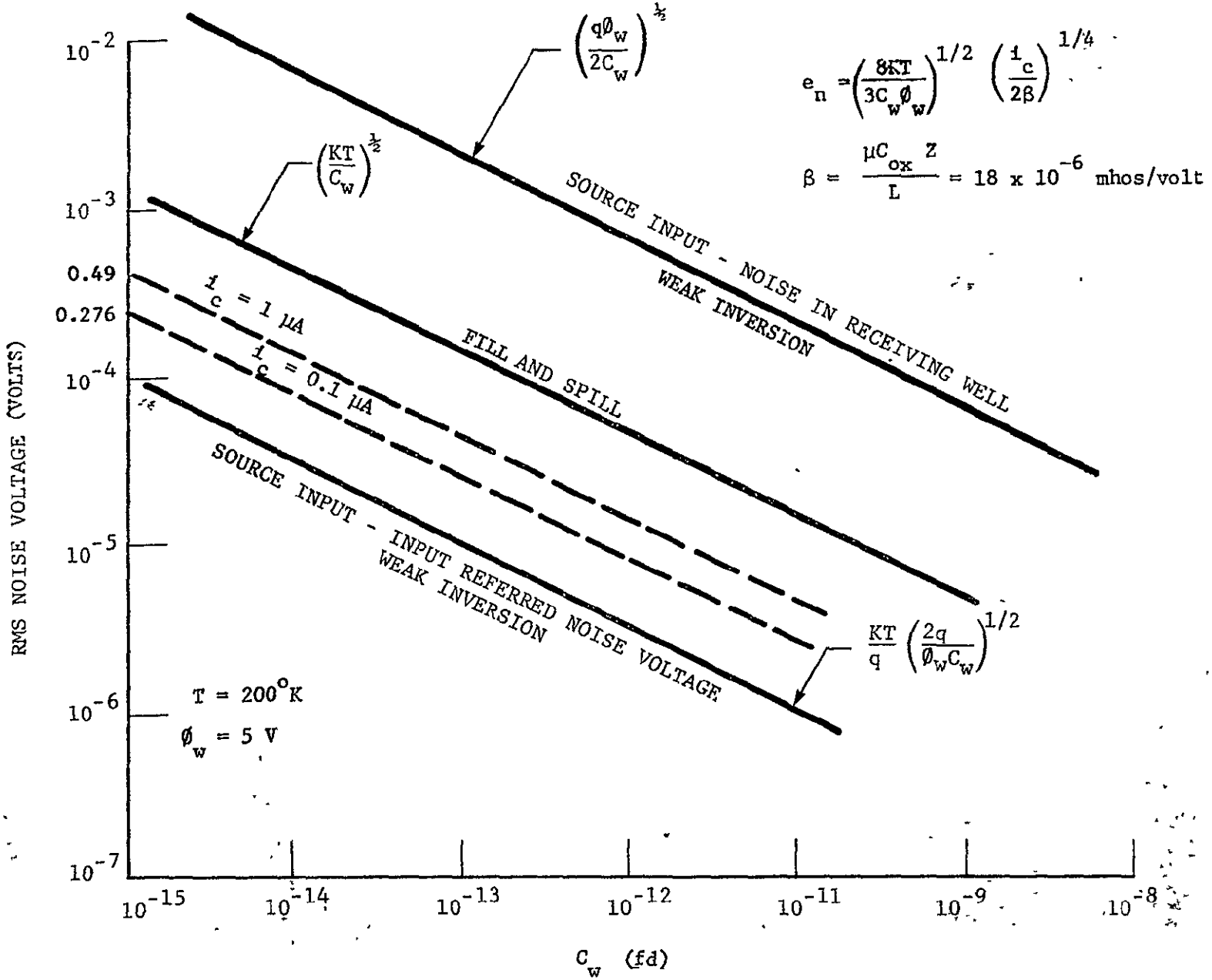

Figure 8 THEORETICAL INPUT REFERRED NOISE (FLATBAND)

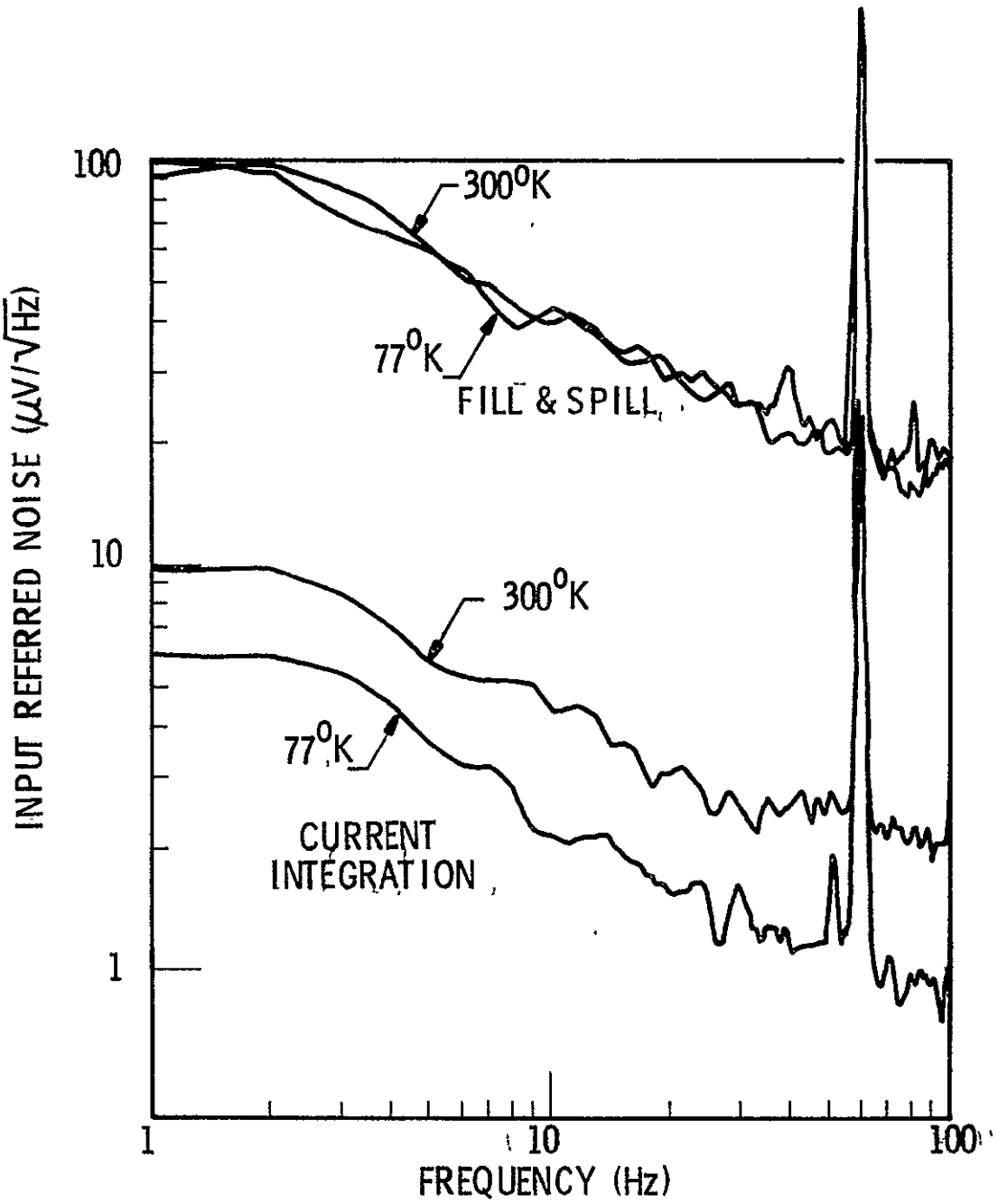

Figure 9 EXPERIMENTAL INPUT REFERRED NOISE (1/f)

SECTION 3

PC IR/CCD BREADBOARD DEMONSTRATION

3.1 PC (Hg,Cd)Te DETECTOR ARRAY

3.1.1 PC HCT Detector Theory

Mercury Cadmium Telluride (Hg,Cd)Te detectors are conductivity modulated quantum detectors made from an alloy of HgTe and CdTe.[2] Their band gap, and thus their quantum threshold is determined by the ratio of HgTe to CdTe, and by the temperature at which they are operated. This quantum threshold is relatable to the detectors infrared spectral sensitivity by the relationship

$$\lambda_o = \frac{1.24}{E_g} \qquad (5)$$

where E_g is the bandgap in electron volts and λ_o is in micrometers.

For any given application, such as the Pushbroom array, (Hg,Cd)Te crystal material having the proper ratio of HgTe to CdTe is found using the relationship[1]

$$E_g = 1.59x - 0.25 + 5.23 \times 10^{-4}(1-2.08x)T + 0.327\ x^3$$

where x = is the CdTe mole fraction and T is the temperature in K.

For this work, x = 0.197, at T = 105 K, λ_o = 12.5 μm.

In theory, photoconductive detectors are limited in performance only by quantum efficiency and background, provided that a low enough temperature is selected for operation. This is expressed

$$D^*_\lambda = \frac{\lambda}{2hc}\sqrt{\frac{\eta}{Q_B}} \qquad (6)$$

1 JAP 41 2576 (1970) J. Schmitt eta l

where λ is the wavelength, η the quantum efficiency and Q_B the background in photons/cm^2 s.

In practice, however, other noise mechanisms become important. They are 1/f noise, amplifier noise, and at sufficiently high frequencies the detector Johnson noise.

The photoconductive detector is a low resistance (10~1000 Ω) device, which is normally biased from a battery V_b with a series resistance R_L which is much larger than the detector resistance (R_d). This produces a current V_b/R_L, which in turn produces an electric field in the detector given by

$$E = \frac{R_d V_b}{R_L d} \text{ volts} \qquad (7)$$

where d is the interelectrode spacing of the detector. The signal produced by infrared photons illuminating the detector is then

$$i_s = \eta q \; A \; Q \; G \; A_d \qquad (8)$$

where

A_d is the detector sensitive area in cm^2
Q is the signal in photons/cm^2 s
G is the photoconductive gain = $\mu E \tau / d$
E is the electric field in the detector
d is the detector thickness
τ is the response lifetime
μ is the detector mobility

Table 1

INJECTION METHODS TRADEOFF

FILL & SPILL	CURRENT INTEGRATION
$Q = C_W (V_X - V_W)$	$O \mp \frac{\mu Cox\ Z\tau}{2L} (V_X - V_T - V_S)^2$
FIXED GAIN	ADJUSTABLE GAIN
LINEAR	NON-LINEAR
UNIFORM	VARIATIONS
GATE INPUT	GATE OR SOURCE INPUT (THE LATTER PROVIDES CURRENT SINK)
NOISE ALIASING DUE TO SAMPLING	NOISE REDUCTION DUE TO INTEGRATION

This signal current is developed as a voltage across R_d in parallel with R_L. In the background limited case the shot noise current is

$$i_n = G\sqrt{4qI} \qquad (9)$$

with $I = \eta q\ A_d Q_B$, where Q_B is the background in photons/cm^2s. The expressions for signal and noise currents (or voltages) can be used to find the D* as follows

$$D^* = \frac{R_i\sqrt{A_d}}{i_n}\ \text{cm Hz}^{\frac{1}{2}}/\text{W} \qquad (10)$$

where $R_i = \frac{i_s\ \lambda/hc}{Q\ A_d}$ A/watt.

Table 2

OPERATIONAL CHARACTERISTICS OF HONEYWELL 2058 CCD

1) Type: Buried n-channel CCD

2) Function: 30 parallel input MUX

3) Input configuration: Current integration for 5 μs

4) Uniformity: 10% (9 inputs, current integration)

5) Transfer efficiency: 0.99995 at 1 MHz

6) Dark current: 5% of full well at 1 kHz T = 300 K

7) Input referred noise: 1.8 $\mu V/\sqrt{Hz}$ at 17 Hz at 105 K

8) Voltage gain at half well: 23 at 17 Hz at 105 K

9) Dynamic Range: 25,000$/\sqrt{Hz}$ at 17 Hz

The responsivity for a (Hg,Cd)Te element can be expressed as:

$$R_v = \eta \lambda \tau V_o / hc \, \ell \, wt \, n_o \quad \text{volts/watt} \qquad (11)$$

which clearly shows the basic requirements for high photoconductivity at a given wavelength: one must have high quantum efficiency η, long excess carrier lifetime τ, the highest possible bias voltage V_o, the smallest possible piece of crystal (ℓ is length, w width and t thickness), and a low thermal equilibrium carrier concentration n_o. In the Pushbroom array, the 9 channel average R_i is 30,000 volts/watt at 105 K. This value together with the average D* value of 9.6×10^{10} cm $Hz^{\frac{1}{2}}/W$ represents a state-of-the-art PC array performance.

3.1.2 9-Channel 10 μm PC (Hg,Cd)Te Array Performance

Figure 10 is a photograph of the array of PC (Hg,Cd)Te detectors used in the breadboard demonstration. Figure 11 gives its relative spectral response. They have an average resistance at 105 K of 60Ω and are operated with best signal to noise at approximately 0.3 volt. The D^*_λ peak values of the array measured at 105 K are plotted in Figure 12 as a function of frequency. The average spectral noise of an element at 105 K at 17 Hz is of the order of 40 $nV/\sqrt{Hz}$.

3.2 CRYOGENIC PREAMPLIFIER

3.2.1 Bipolar Preamp Design

The input noise at 17 Hz at 105 K for current integration in the 2058 CCD is 1.8 $\mu V/\sqrt{Hz}$, while the nine channel 10 μm PC (Hg,Cd)Te array exhibits an average noise of 50 $nV/\sqrt{Hz}$ as will be discussed shortly. Clearly one must insert in the cryogenic enclosure a preamplifier which amplifies the detector noise by, say, 100 times to render the CCD noise insignificant. With 40 dB gain amplifier, the expected degradation in the detector D* is given by

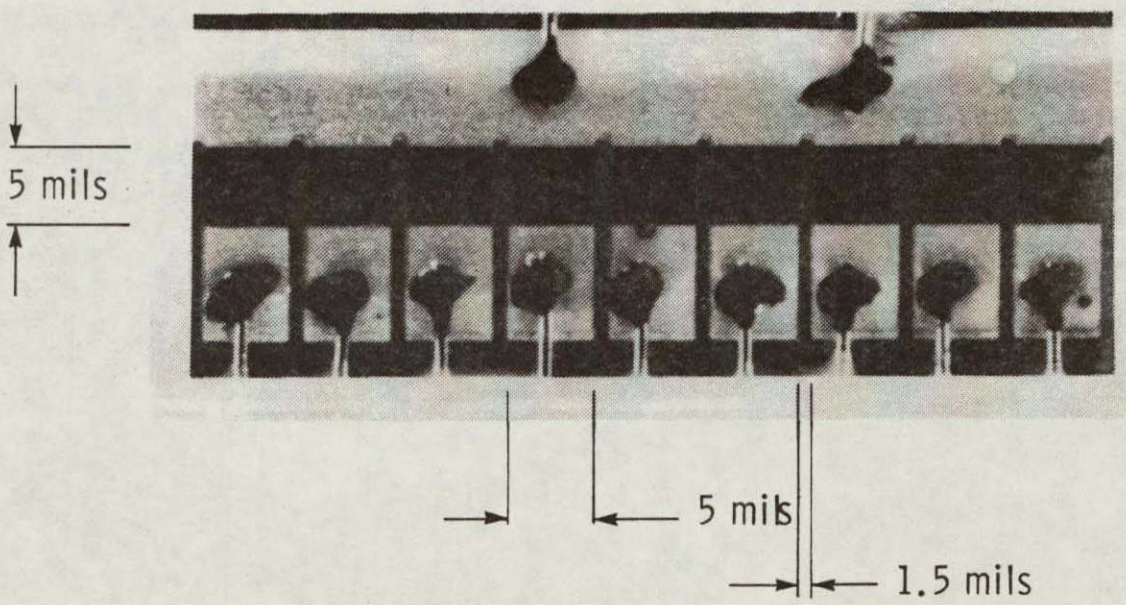

Figure 10 9-CHANNEL 10 μm PEAK PC (Hg,Cd)Te ARRAY

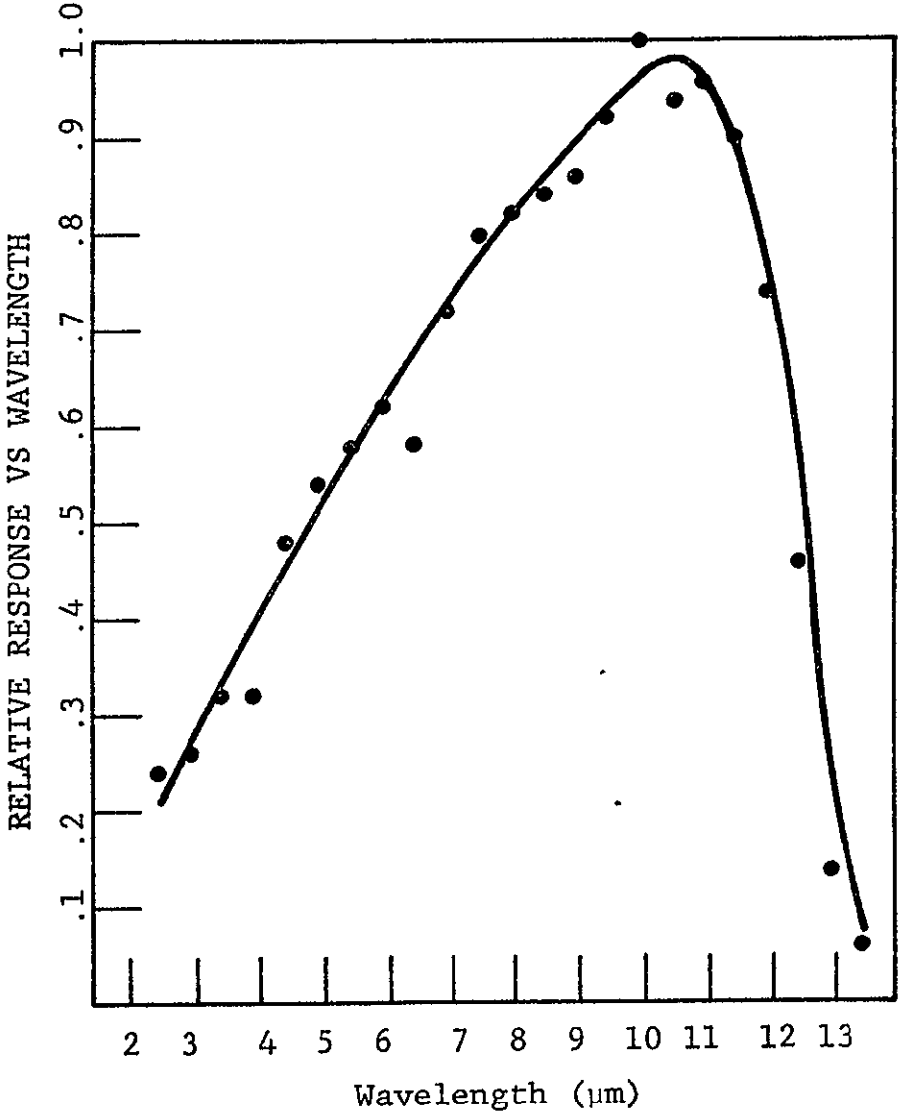

Figure 11 SPECTRAL RESPONSE OF PUSHBROOM ARRAY

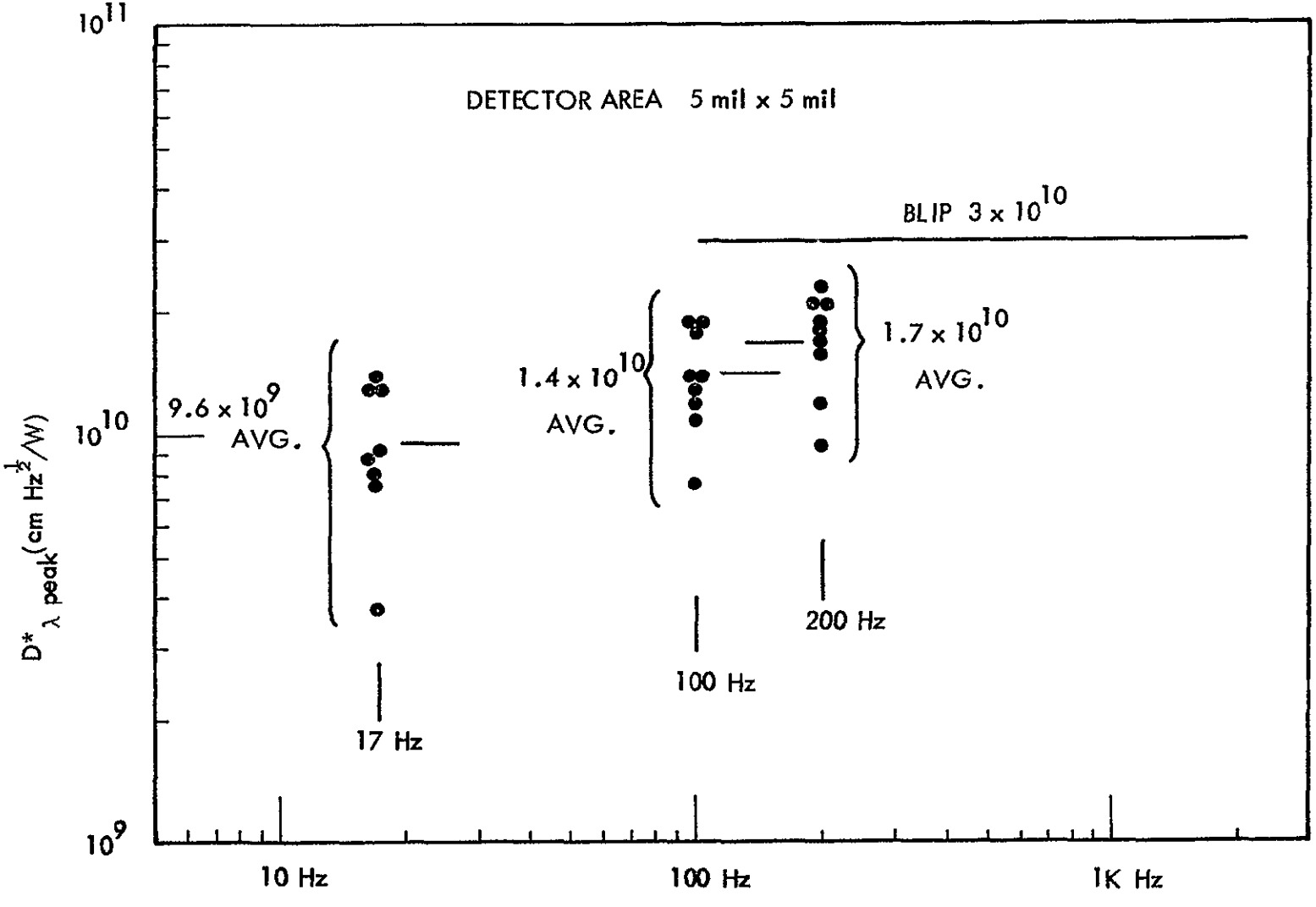

Figure 12 D^*_λ PEAK VS SIGNAL FREQUENCY

$$D^*_{IR/CCD} = \frac{D^*_{DETECTOR}}{\sqrt{\frac{(1.8 \times 10^{-6})^2 + (5 \times 10^{-6})^2}{(5 \times 10^{-6})^2}}} = 0.94\ D^*_{DETECTOR},$$

i.e., 6 %.

For this purpose, we have selected a common base bipolar transistor amplifier, as depicted in Figure 13. The main advantage of a bipolar rather than a J-FET or a MOS is that the bipolar noise is the lowest for the same device area. The common base offers the lowest input impedance to match the 50Ω PC (Hg,Cd)Te elements. The following gives an analysis of the circuit.

Table 3

9-CHANNEL 10 μm PEAK PC (Hg,Cd)Te ARRAY

1) Material: Photoconductive (Hg,Cd)Te

2) Array configuration: Linear 9 contiguous elements

3) Element size: 125 x 125 μm ± 20% average

4) Spacing between elements: 25 μm

5) Operating temperature: 80 to 120 K

6) Background temperature: 300 K
Spectral Response: 10.6 μm peak, 13 μm cutoff

7) D^*_λ peak (17 Hz, 60° FOV, 1 Hz): 9.6×10^{10} cm $Hz^{\frac{1}{2}}/W$

8) Responsivity: 30,000 volts/watt 9-channel average

9) Resistance: 55 ohm 9-channel average

10) Power consumption: 1.5 mW/element

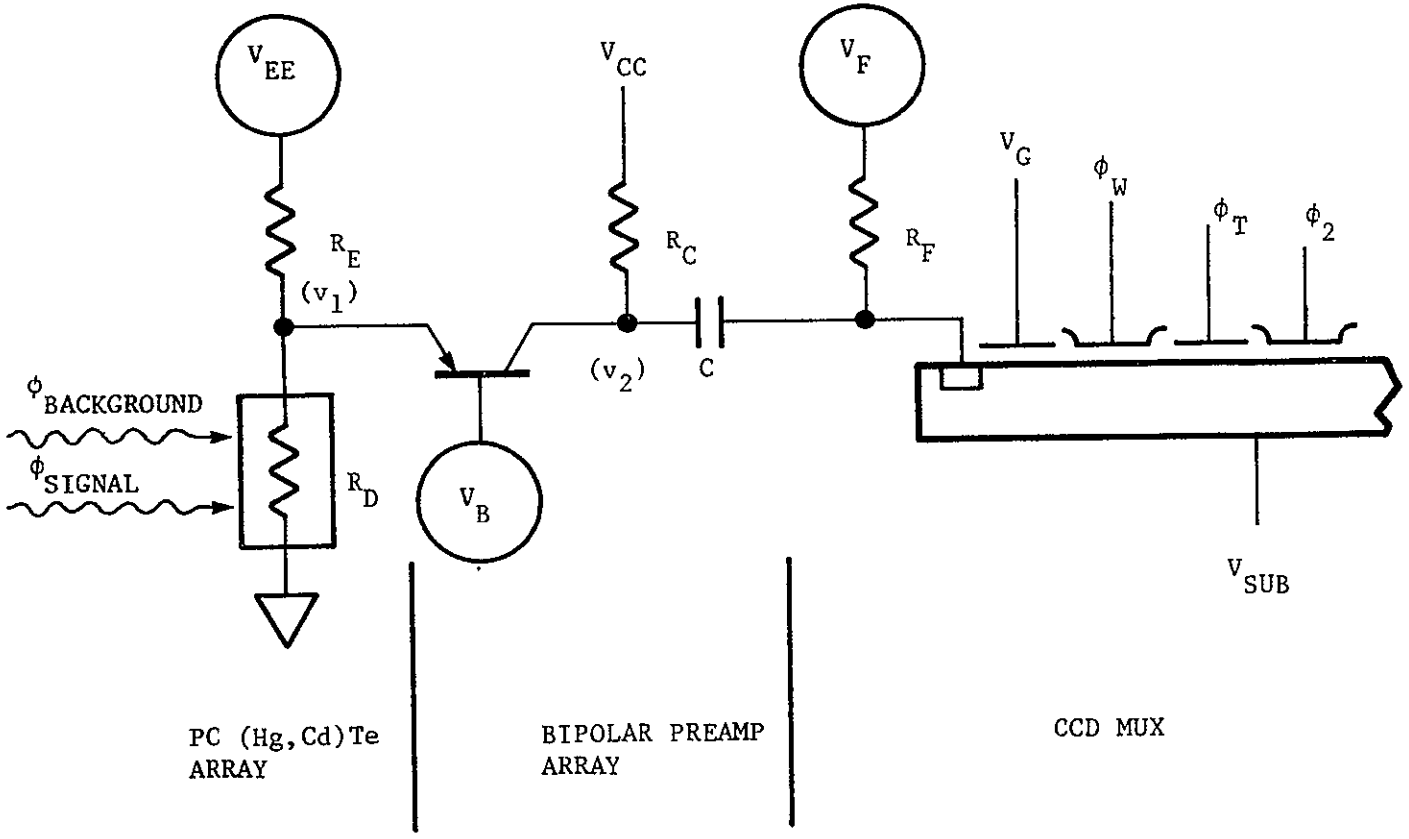

Figure 13 COMMON BASE BIPOLAR PREAMPLIFIER DESIGN

3.2.2 Noise Analysis

The voltage and current noise of a bipolar preamp in Figure 13 is expressed by

$$e_n^2 = 4\ kT\ r_{bb'} + 2\ kT\ r_e + i_n^2\ r_{b'b}$$

$$i_n^2 = 2q\ I_B\ (1 + \frac{fo}{f})$$

where $r_{b'b}$ is the base resistance, $r_e = kT/qI_c$ the emitter resistance, I_c the collector current, $I_B = I_c/h_{FE}$ the base current, h_{FE} the current gain, and fo is the break frequency of the transistor 1/f noise. The observed value for fo in bipolar transistors 2N 4405 and 2N 3964 operated at 80~120 K is of the order of 0.5~4 kHz. When the transistor is configured as in Figure 13 with an effective detector impedance R_d (a parallel combination of detector and bias resistances), the voltage noise is expressed by

$$e_n^2 = 4\ kT\ (r_{bb'} + R_d) + \frac{2(kT)^2}{qI_c} + 2q\ \frac{I_c}{h_{FE}}\ (1 + \frac{fc}{f})(r_{bb'} + R_d)^2$$

It is readily seen that there is an optimum collector current I_c that minimizes the expression. That I_c is given by

$$I_c^2 = \frac{(kT)^2\ h_{FE}}{q^2(r_{bb'} + R_d)^2\ (1 + \frac{fc}{f})}$$

A minimum collector current of I_c = 100 μA has been calculated using h_{FE} = 30, $r_{b'b}$ = 40Ω , T = 110 K, f_c = 0.5 kHz, and f = 17 Hz. The input noise at the minimum noise current I_c is given by

$$e_n^2 = 4\ kT \left[r_{b'b} + R_d + \frac{kT}{2qI_c} \right] =$$

$$4\ kT \left[r_{b'b} + R_d + \frac{(r_{b'b}+R_d)\sqrt{1 + \frac{fo}{fc}}}{2\sqrt{h_{FE}}} \right]$$

For the present case, the three terms equally contribute, and the calculated noise is 1 $nv\sqrt{Hz}$, whereas the measured noise at 77 K at 17 Hz was less than $10^{'}$ $nV\sqrt{Hz}$. The discrepancy is due to the change in fo and h_{FE} at 77 K rather than at 110 K.

3.3.3 Small Signal Gain

Figure 14 illustrates the small signal equivalent circuit of the bipolar cryogenic preamplifier. The following expressions are readily derived.

$$V_{out} = -G_m V_{b'e} R_c$$

$$V_{b'e} = - \frac{e_s r_{b'e} R_E}{(R_D + R_E)(R_E + r_{b'e} + r_{b'b}) - R_E^2}$$

$$- \frac{G_m r_{b'e} R_D R_E r_{b'e}}{R_D R_E + (r_{b'e} + r_{b'b})(R_D + R_E)}$$

$$V_{b'e} = \frac{\frac{e_s r_{b'b} R_E}{(R_D + R_E)(R_E + r_{b'e} + r_{b'b}) - R_E^2}}{\frac{G_m R_D R_E r_{b'e}}{R_D R_E + (r_{b'e} + r_{b'b})(R_D + R_E)}} -$$

The gain of the preamplifier (V_{out}/e_s) is readily seen to reduce to

$$\frac{V_{out}}{e_s} = \frac{R_c}{\frac{R_D R_E}{R_D + R_E} + \frac{kT}{qI_c}} \quad \frac{}{\frac{r_{b'b}}{1 + h_{FE}}}$$

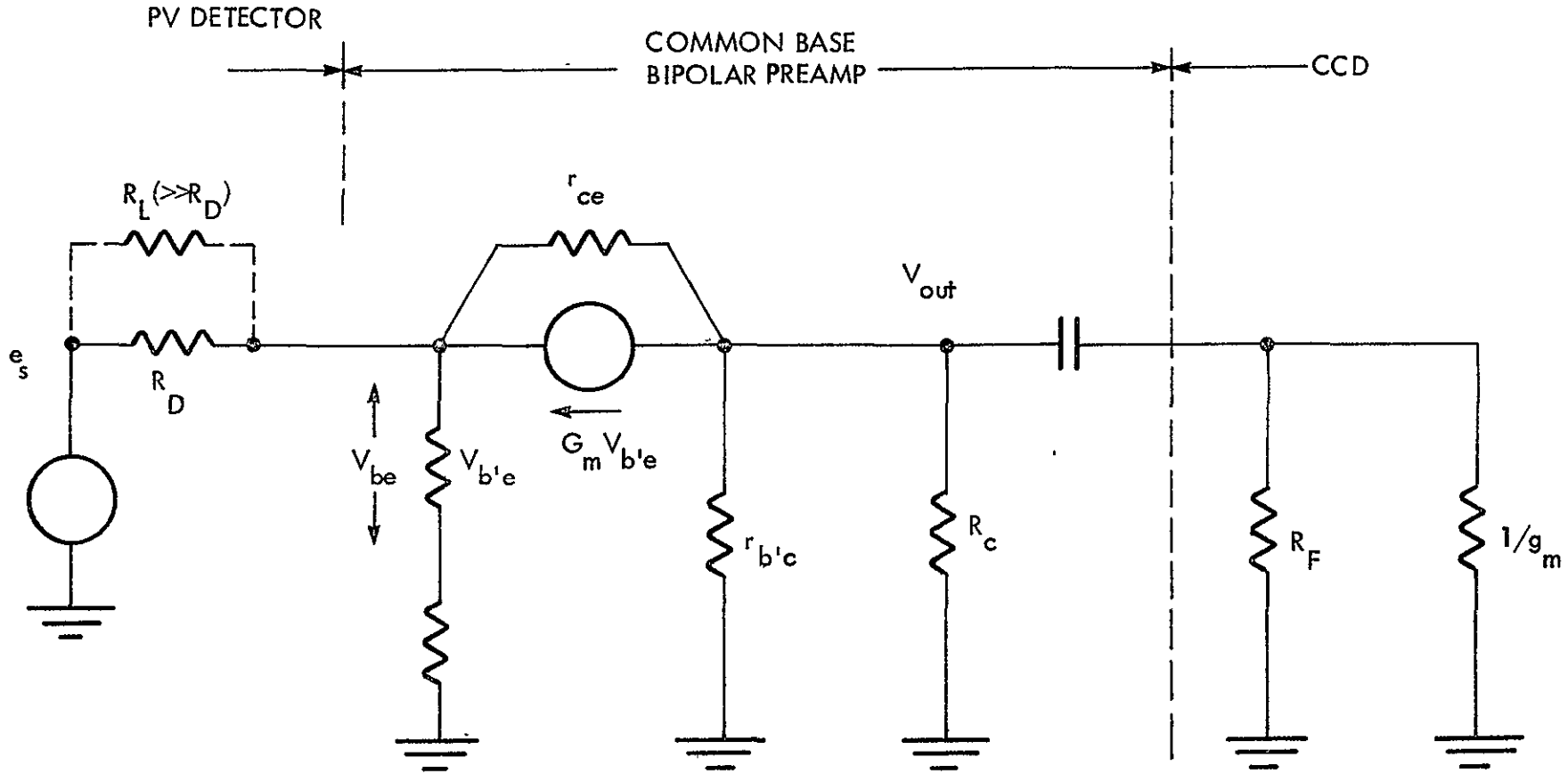

Figure 14 SMALL SIGNAL EQUIVALENT OF COMMON BASE AMPLIFIER

The values of $R_c = 10^4$, $R_D = (1/5)$, $R_E = 50\Omega$, $I_c = 10^{-4}$ amp, T = 110 K, $r_{b'b} = 40\Omega$ and $h_{FE} \sim 10$, yield a gain of 100, which is closely matched by the measured gain. Table 4 summarizes the bipolar cryogenic preamplifier characteristics.

3.2.4 Preamplifier/CCD Interface Analysis

The ac loading effect of the CCD input stage on the bipolar preamp has been neglected in the previous discussion. The justification may be found in the following analysis. The CCD MUX circuit samples each of the nine bipolar output voltages during a $\tau = 5$ μs time window fc/18 times a second. Figure 15a shows the CCD clock waveforms, whereas Figure 15b gives the detail.

The sampled bipolar output ac voltage V_2 is converted into a charge packet of a size Q with the conversion factor given by:

$$Q = g_m V_2 \tau$$

$$g_m = \frac{Z}{L} \mu C_{ox} \left(\frac{kT}{q}\right) \left[\left(1 + \frac{2I}{\frac{Z}{L}\mu C_{ox}} \left(\frac{q}{kT}\right)^2\right)^{\frac{1}{2}} - 1\right]$$

$$\text{and } I = \frac{V_w C_{ox}}{2\tau} = \frac{V_w C_{ox} Ag}{2\tau}$$

where $\tau = 5$ μs is the integration period, g_m the CCD transconductance during integration, Z/L = 4 the 2058 CCD input gate aspect ratio, $\mu = 700$ $cm^2 V^{-1}$ the electron mobility, $C_{ox} = 3 \times 10^{-8}$ farads cm^{-2} the gate oxide capacitance, $V_w = 10$ volts the charge well depth and $Ag = 10^{-5}$ cm^2 is the storage gate area. Calculations yield $I = 3.2 \times 10^{-7}$ amp; $g_m = 6.6 \times 10^{-6}$ and $Q = 3.3 \times 10^{-11}$ x coloumb. The effective transconductance is further reduced by the integration duty factor, i.e.,

Table 4

BIPOLAR CRYOGENIC PREAMP CHARACTERISTICS

1) Transistor: 2N3964 PNP

2) Configuration: Common Base

3) Gain: 40 dB

4) Input voltage noise: 10 $nV/\sqrt{Hz}$ at 17 Hz at 105 K

5) Current gain: $\beta > 10$ at 77 K

6) Collector current: 200 nA

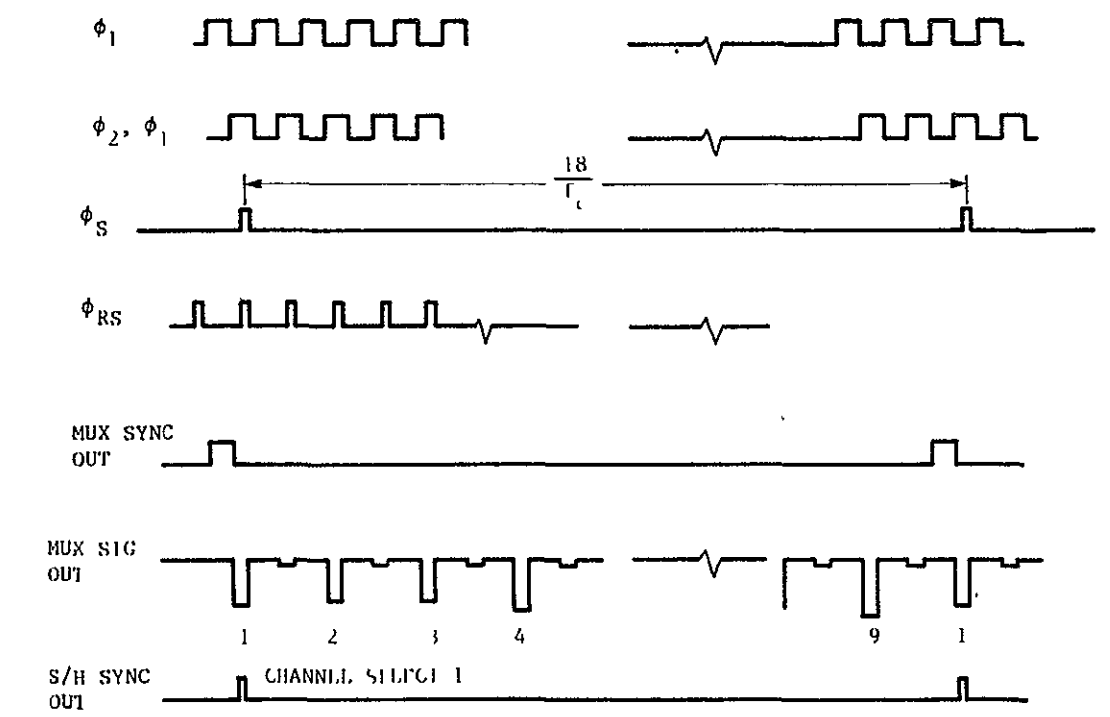

(a)

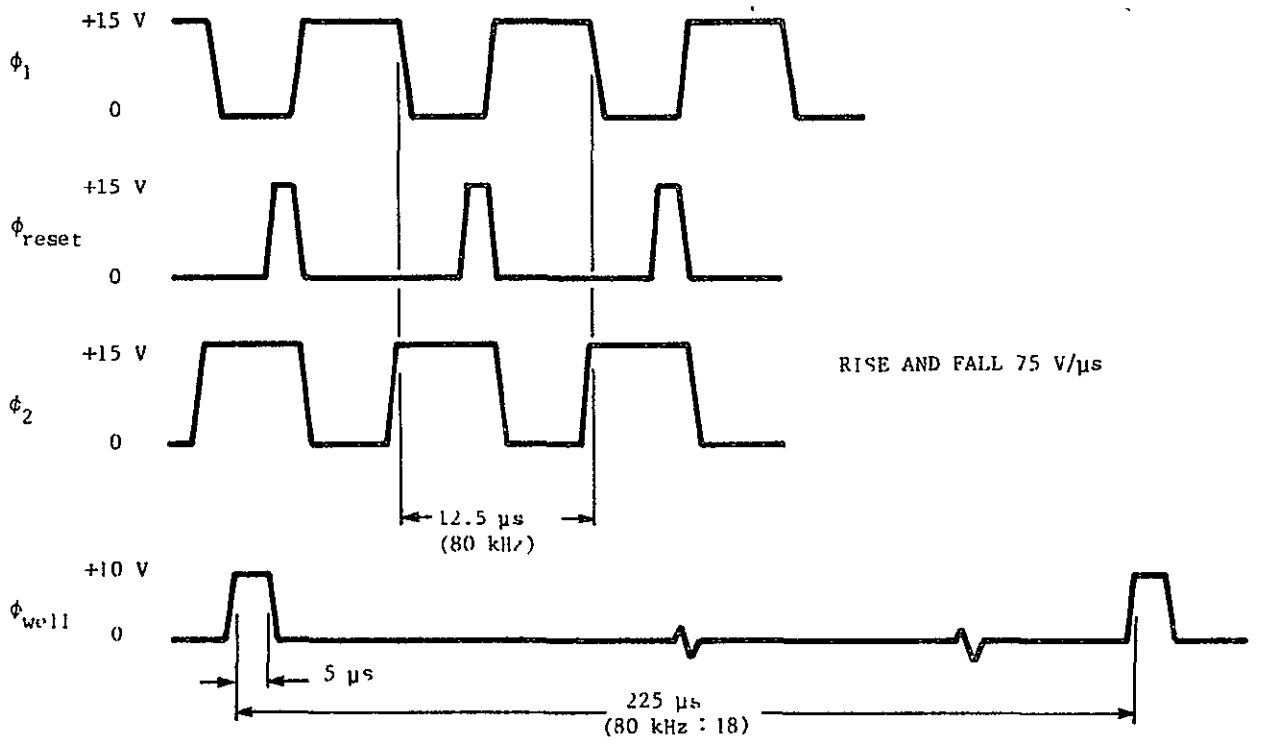

(b)

Figure 15 PUSHBROOM IR/CCD MUX CLOCKING WAVEFORMS

$$g_{m_{eff}} = \frac{\tau}{\tau_c} g_m = \frac{f_c \tau}{18} g_m = 1.5 \times 10^{-7} \nu = \frac{1}{6.6\ M\Omega}$$

Thus, the bipolar collector load impedance R_c = 10 K Ω is not loaded down by the CCD impedance of 6.8 M Ω. Because of the high CCD impedance, interestingly enough, the ac coupling capacitor need be only of the order of 0.05 μF to pass 17 Hz ac signal without a significant attenuation.

3.3 VARIABLE TEMPERATURE DETECTOR DEWAR AND PEDESTAL DESIGN

In its natural space environment aboard an orbiting satellite having a radiatively cooled finger, the pushbroom array is simply mounted and wired to post amplifiers. The laboratory environment must simulate these conditions as nearly as possible. This means a vacuum vessel and a 105 K pedestal. A variable temperature pedestal (80~120 K) was built in conjunction with a three inch diameter stainless steel dewar. This is depicted in Figure 16, where the spacer serves as the thermal resistor. The heater dissipates 18 watts, with the result that with liquid nitrogen in the cold well at 77 K, the cold pedestal assembly stabilizes at 105 K. This is done with an increased boiloff rate of liquid nitrogen, however it is easily replenished in the laboratory. A photograph of the three inch diameter dewar is shown in Figure 17.

3.4 SUPPORT ELECTRONICS

3.4.1 Clock Waveform Generator Circuit

Figure 18 is the pushbroom MUX clock waveform generator circuit. All the logic and timing sequence is generated by CMOS chips which are low power consumption and noise-immune devices. There is a provision for both internal clock generation as well as external clock tracking. The internal clock is fixed at 80 kHz. The external tracking circuit will trigger on an externally supplied clock in the frequency range of 1~80 kHz.

3.4.2 Demultiplexer Circuit

The 2058 CCD MUX is a 2 bit CCD and there are therefore 18 analog bits per a "frame". A decade counter together with a JKFF divides the clocking pulse train by a factor of 18. The resulting fc/18 pulse is used to strobe and load in the 9 parallel inputs into the shift register. Another set of a BCD counter and a JKFF generates a sliding sampling window which activates a sample and hold

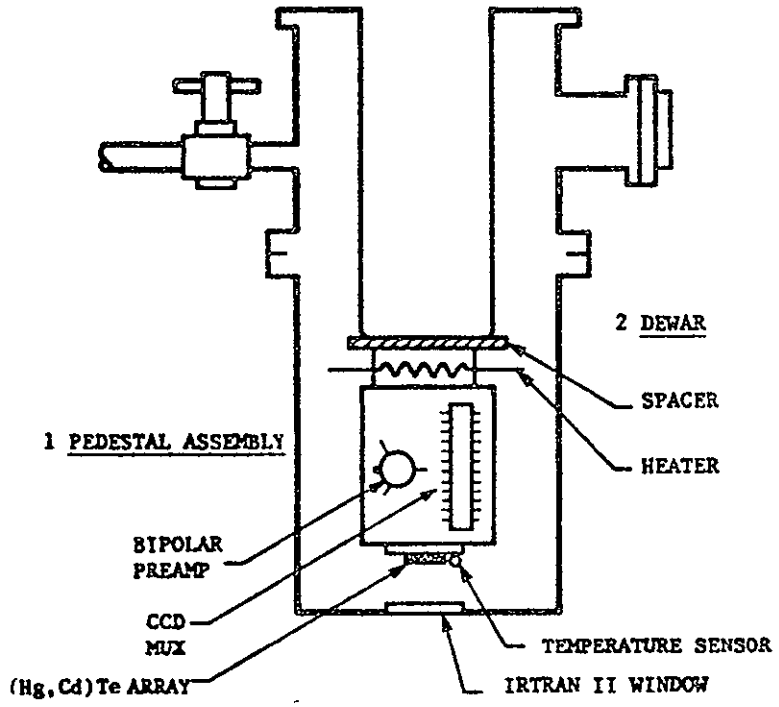

Figure 16 VARIABLE TEMPERATURE PEDESTAL DESIGN

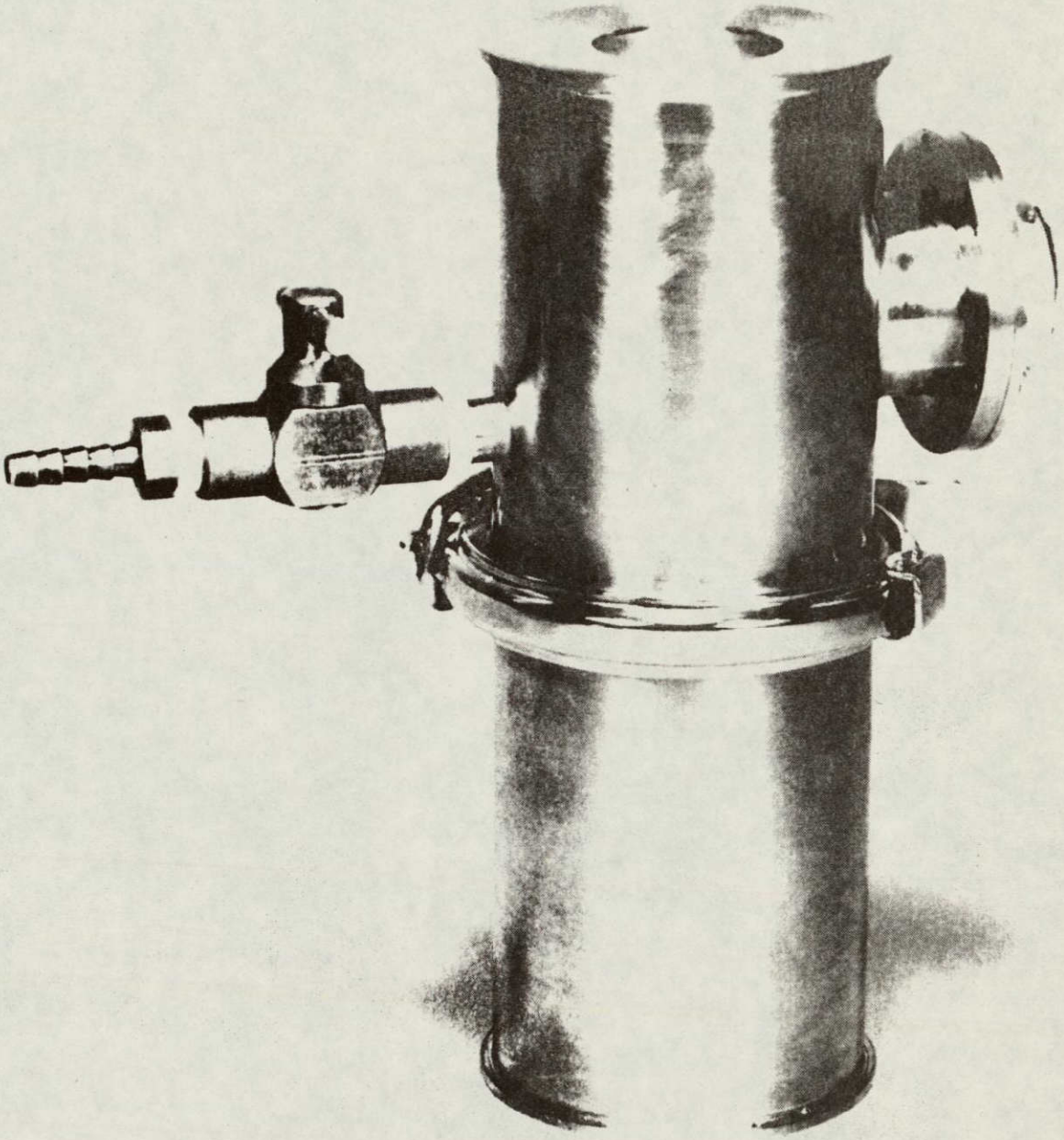

Figure 17 VARIABLE TEMPERATURE DEWAR

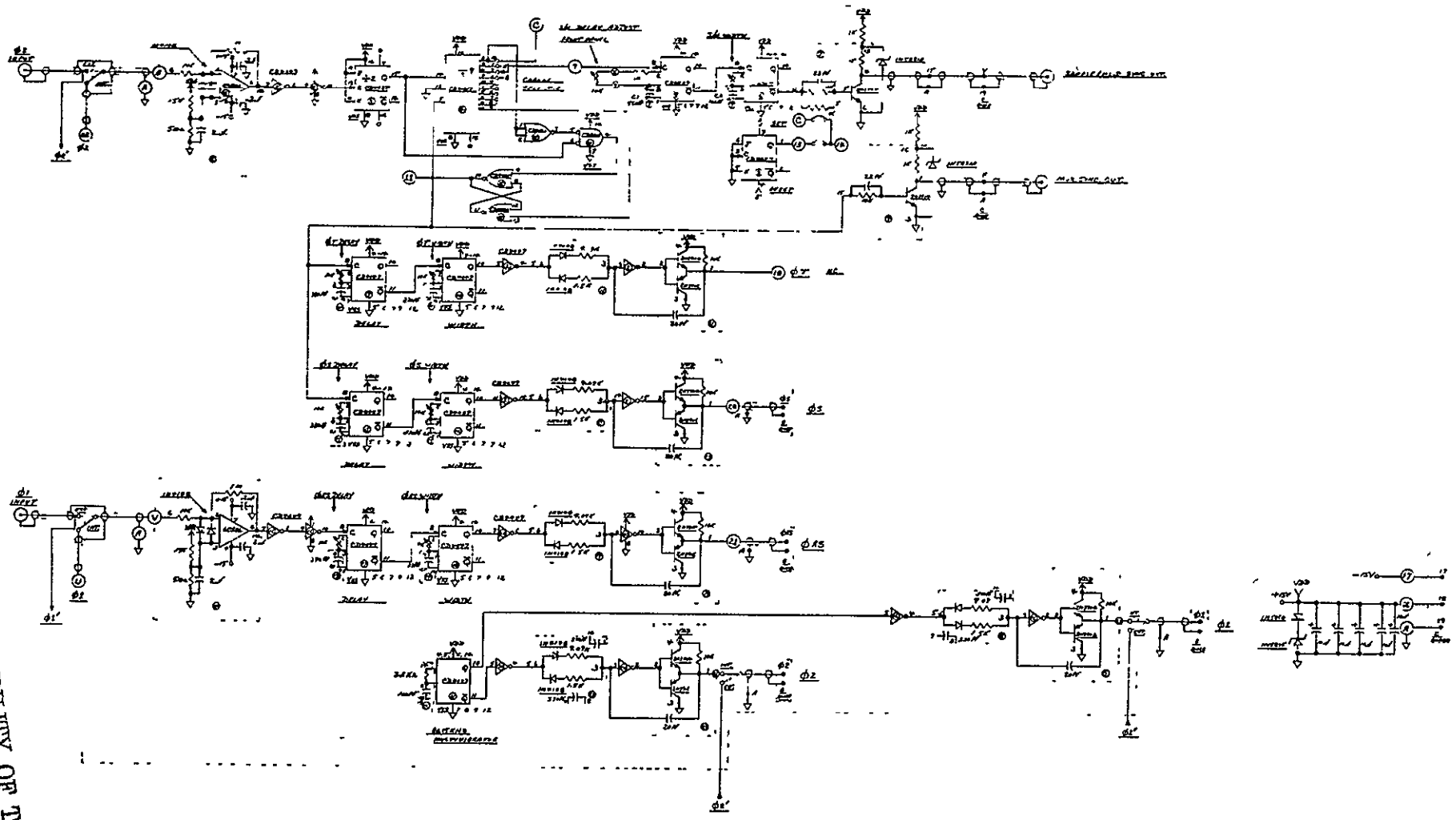

Figure 18 PUSHBROOM MUX CLOCK WAVEFORM GENERATOR CIRCUIT

amplifier. The output of the sample and hold amplifier is the sampled (fc/18 times a second) excursion of the designated PC (Hg,Cd)Te element.

3.4.3 Low Noise Bias

Figure 19 contains the low noise bias supply network. In particular, one dc bias voltage which biases the common base of the bipolar preamp is of critical importance in that the noise level must not exceed a fraction of the detector noise seen at the emitter. This is achieved by a voltage divider and a π filter with an extremely large time constant. In spite of the 1/f encountered in a commercial power module, a noise of 2 $nV/\sqrt{Hz}$ at 17 Hz is achieved.

3.4.4 Direct Reading Temperature Monitor

The silicon diode temperature monitor located on the focal plane is linear and stable to within 1% in the temperature range 77 K and 300 K. By taking advantage of this, a circuit has been devised, whereby the focal plane temperature is directly converted into (T in K)/100 volts. This is a very convenient feature. The filamental heater inside the dewar pedestal assembly powers and controls the focal plane temperature in the range 80 - 120 K.

3.4.5 Pushbroom Breadboard Front Panel Description

Figure 20 describes the arrangement of the front panel of the Pushbroom IR/CCD MUX Breadboard. It consists of a power switch, clocking waveform I/O, MUX synchronization, MUX signal out, S/H synchronization and tuning, S/H signal out, channel select, and focal plane temperature controller and monitor. The operation manual deals with the details of the instrumentation.

3.5 9 CHANNEL PUSHBROOM PC (Hg,Cd)Te IR/CCD MUX RESULTS

Figure 21 illustrates the multiplexed output waveform as well as the sample/hold waveform of a selected channel, showing the chopped blackbody signal.

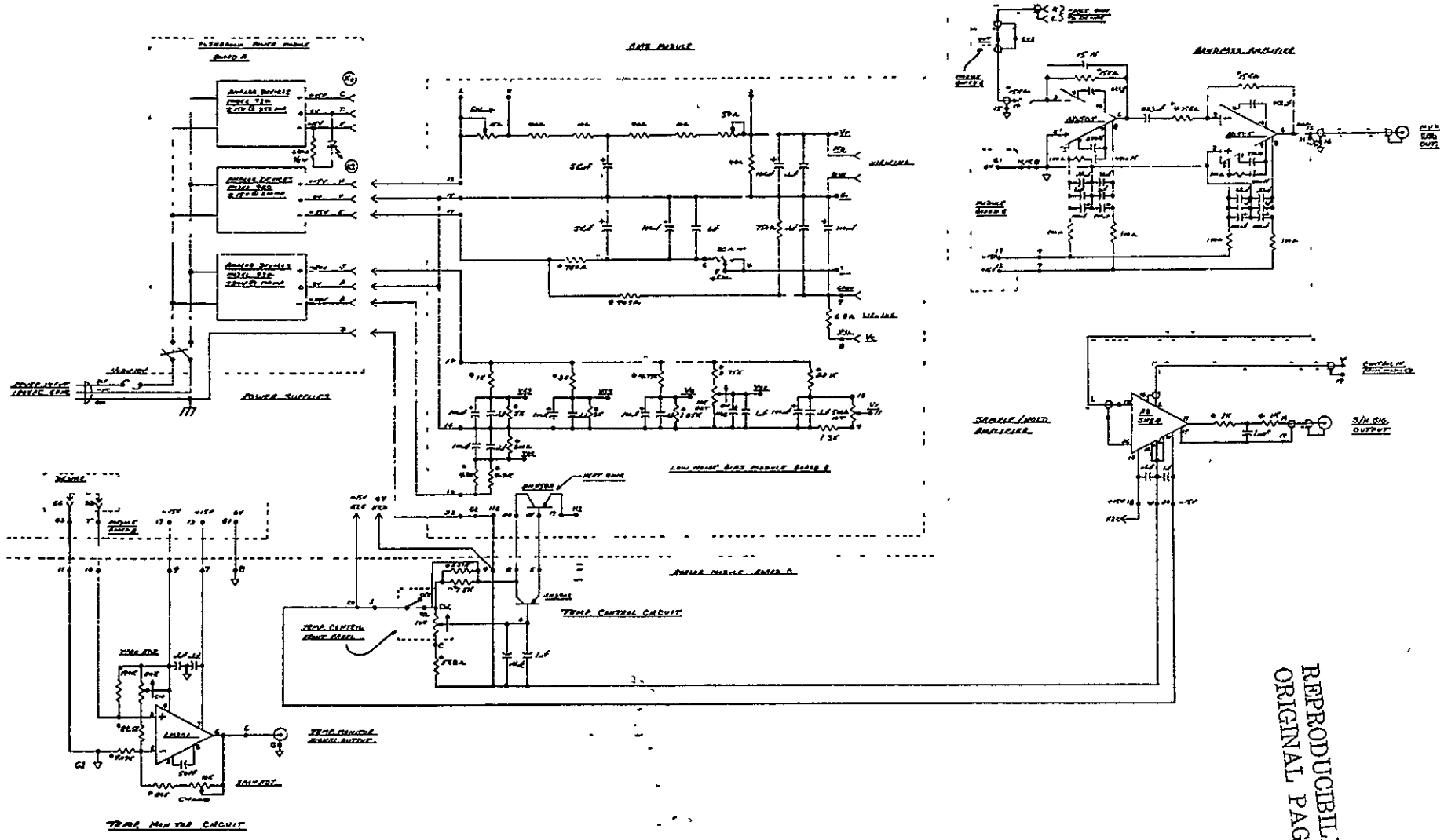

Figure 19 BIAS NETWORK, S/H AMPLIFIER, TEMPERATURE CONTROL AND MONITOR CIRCUIT

Figure 20 FRONT PANEL ARRANGEMENT OF PUSHBROOM IR/CCD MUX OUTPUT WAVEFORMS

FOCAL PLANE TEMPERATURE 82°K, f_c = 100KHz, CHOPPER FREQUENCY 41 Hz

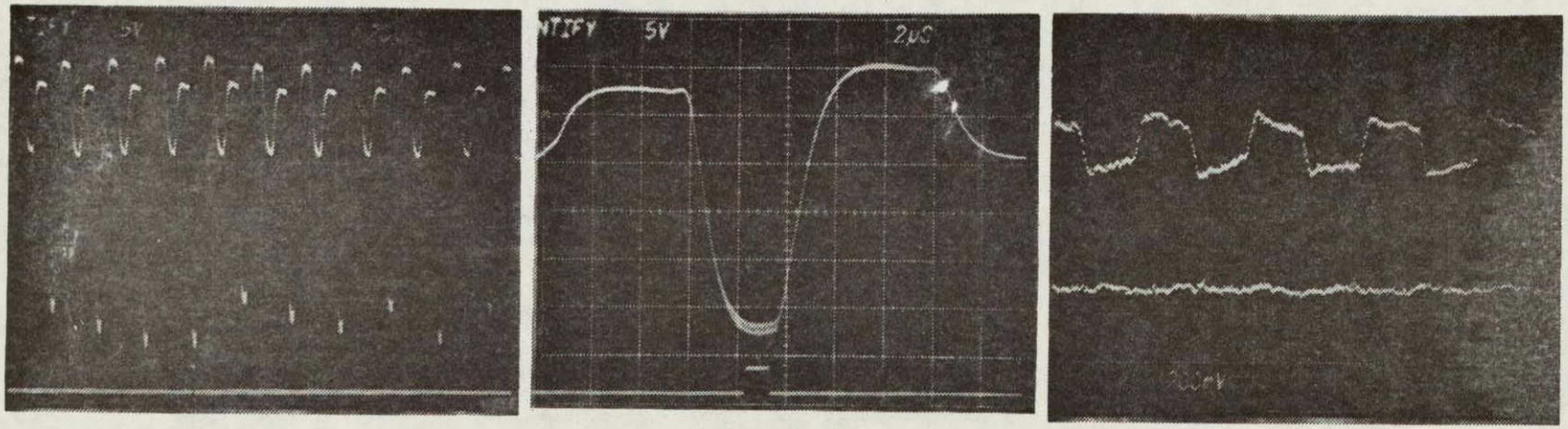

MULTIPLEXED OUTPUT FOR 9 CHANNELS

SAME OUTPUT EXPANDED FOR ONE CHANNEL

SAMPLE AND HOLD OUTPUT OF THE SAME CHANNEL

Figure 21 PUSHBROOM IR/CCD MUX OUTPUT WAVEFORMS

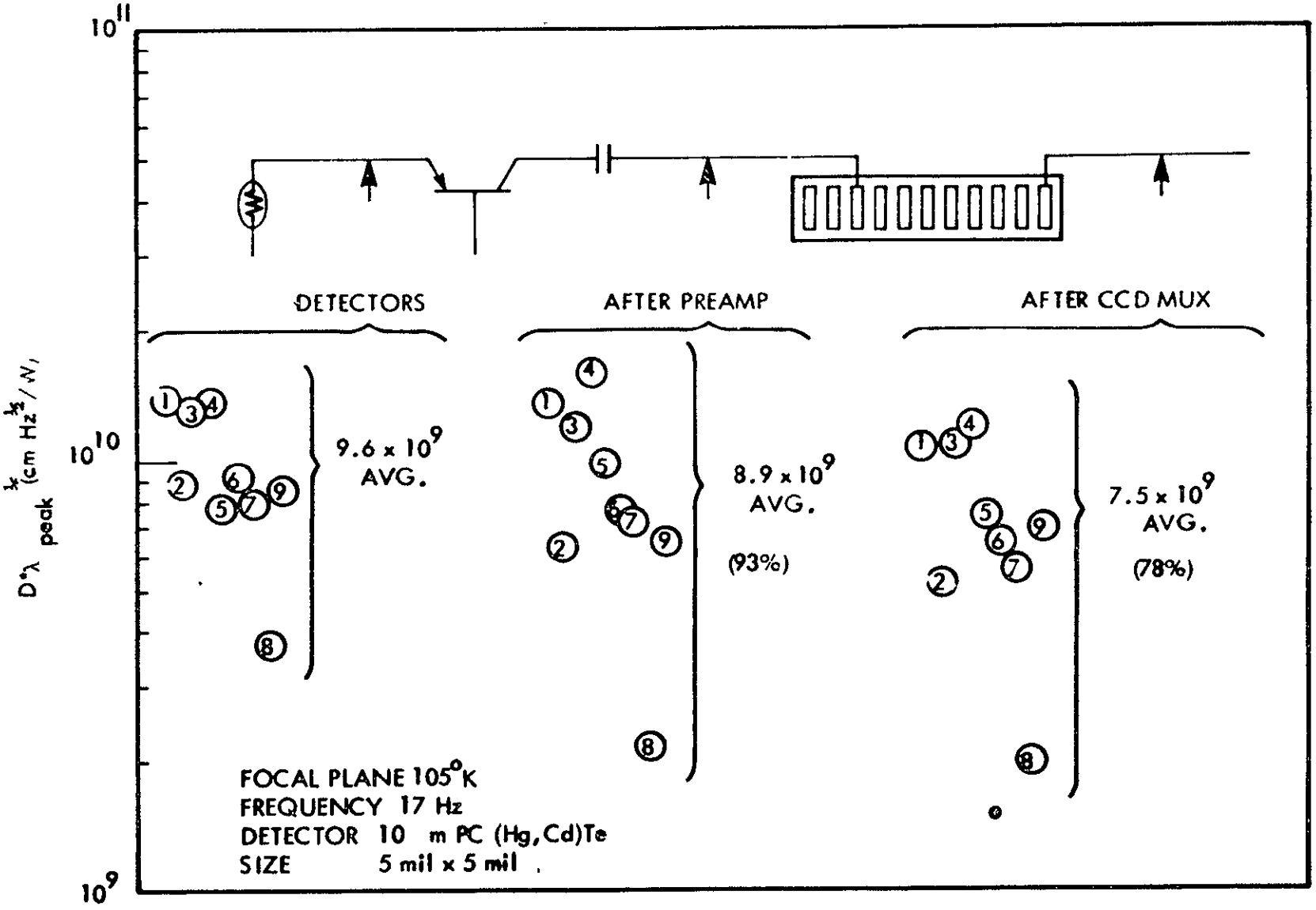

Figure 22 D^*_λ HISTOGRAM OF PUSHBROOM IR/CCD BREADBOARD

The signal-to-noise ratios of the PC (Hg,Cd)Te IR/CCD at various stages, namely, that of the PC detectors, after the preamplifiers and after the multiplexer, are expressed as D^*_λ peak and plotted in Figure 22. On the average, a 7% degradation in the S/N is experienced after the preamplifiers and 22% after the CCD multiplexer. The detector noise is 40 $nV/\sqrt{Hz}$ and the input noise of the amplifier 10 $nV/\sqrt{Hz}$, therefore, the expected average loss in the S/N is given by

$$\left[\left((10\ nV/\sqrt{Hz})^2 + (40\ nV/\sqrt{Hz})^2\right)/\ (40\ nV/\sqrt{Hz})^2\right]^{\frac{1}{2}} = 0.97$$

which is to say a loss of 3% is accounted for. The S/N loss in going through the multiplexer is computed to be

$$\left[\left((40\ nV/\sqrt{Hz})^2 + (10\ nV/\sqrt{Hz})^2 + (1.8\ \mu V/\sqrt{Hz}/100)^2\right)/\ (40\ nV/\sqrt{Hz})^2\right]^{\frac{1}{2}} = 0.89$$

There is an 11% discrepancy between the observed 0.78 and the calculated 0.89. The discrepancy is a direct result of the noise aliasing suffered when the CCD multiplexer samples the detector signal. In a sampled system, the noise spectrum beyond the integral multiple of the sampling frequency is reflected back into the base signal bandwidth. One method of minimizing aliasing is to reduce the noise bandwidth of the detector/amplifier to less than the sampling frequency. This can be achieved by adding a capacitor next to the collector resistance and forming a low pass filter. This was tried on one channel after which a near theoretical degradation has been observed. Table 5 lists the performance of the Pushbroom Breadboard.

The essence of the 9-channel Pushbroom 10 μm PC (Hg,Cd)Te IR/CCD MUX demonstration under NAS5-22339 was published at the conference on Charge Coupled Device Technology and Applications, Washington D.C., November 1976. The article by S. Iwasa and W.J. White, entitled "A CCD Scanned (Hg,Cd)Te Array For Earth Viewing Applications" is included in Appendix A.

Table 5

PUSHBROOM IR/CCD MUX PERFORMANCE

1) D* peak: 7.5×10^{9} cm $Hz^{\frac{1}{2}}/W$ 9-channel average: focal plane temperature 105 K, 10.6 μm peak, 300 K background, 60° FOV, 17 Hz, 1 Hz bandwidth

2) Responsivity uniformity: $\pm$ 40%

3) Temperature dependence: $D^*/T = -1.4 \times 10^{8}/K$ (90~120) K range

SECTION 4

5 μm PV (Hg,Cd)Te IR/CCD

A photovoltaic detector (also called a photodiode) is a quantum detector in which the photo-generated carriers within the diffusion length of the p-n junction are separated by the built-in electric field in the depletion region. By this mechanism, an incoming photon is converted into an externally measurable current flow. A description of the principles of (Hg,Cd)Te PV detectors has been reported.[2,4] A direct coupling experiment between a 5 micrometer peak wavelength (Hg,Cd)Te PV diode and a CCD was carried out at Honeywell. No detectable degradation in the signal-to-noise ratio was experienced in the CCD MUX, and D^*_λ peak value of 1.6×10^{11} cm $Hz^{\frac{1}{2}}/W$ (BLIP) was obtained after the CCD MUX, when the photodiode at 77 K was irradiated by the 300 K background with 180 degree field of view, chopped at 123 Hz.

This is an encouraging result towards the realization of a large integrated focal plane, since both the PV diode and CCD consume very little power. The detail of the experiment and the analysis are included in Appendix B in which the partial support of the NASA/Goddard Space Flight Center Contract NAS5-22339 is acknowledged.

SECTION 5

CONCEPTUAL FOCAL PLANE DESIGN

A focal plane design has been submitted for an aircraft flight instrument under separate cover (Honeywell document 7-4-31 in response to NASA/GSFC RFP5-45005-253 dated May 17, 1977). This focal plane is similar in function to the 9 channel breadboard except that there are 90 channels and the dewar is flyable and will have a long operational time without need to replenish the liquid nitrogen. This dewar is depicted in Figure 23 and the focal plane is functionally described in Figure 24.

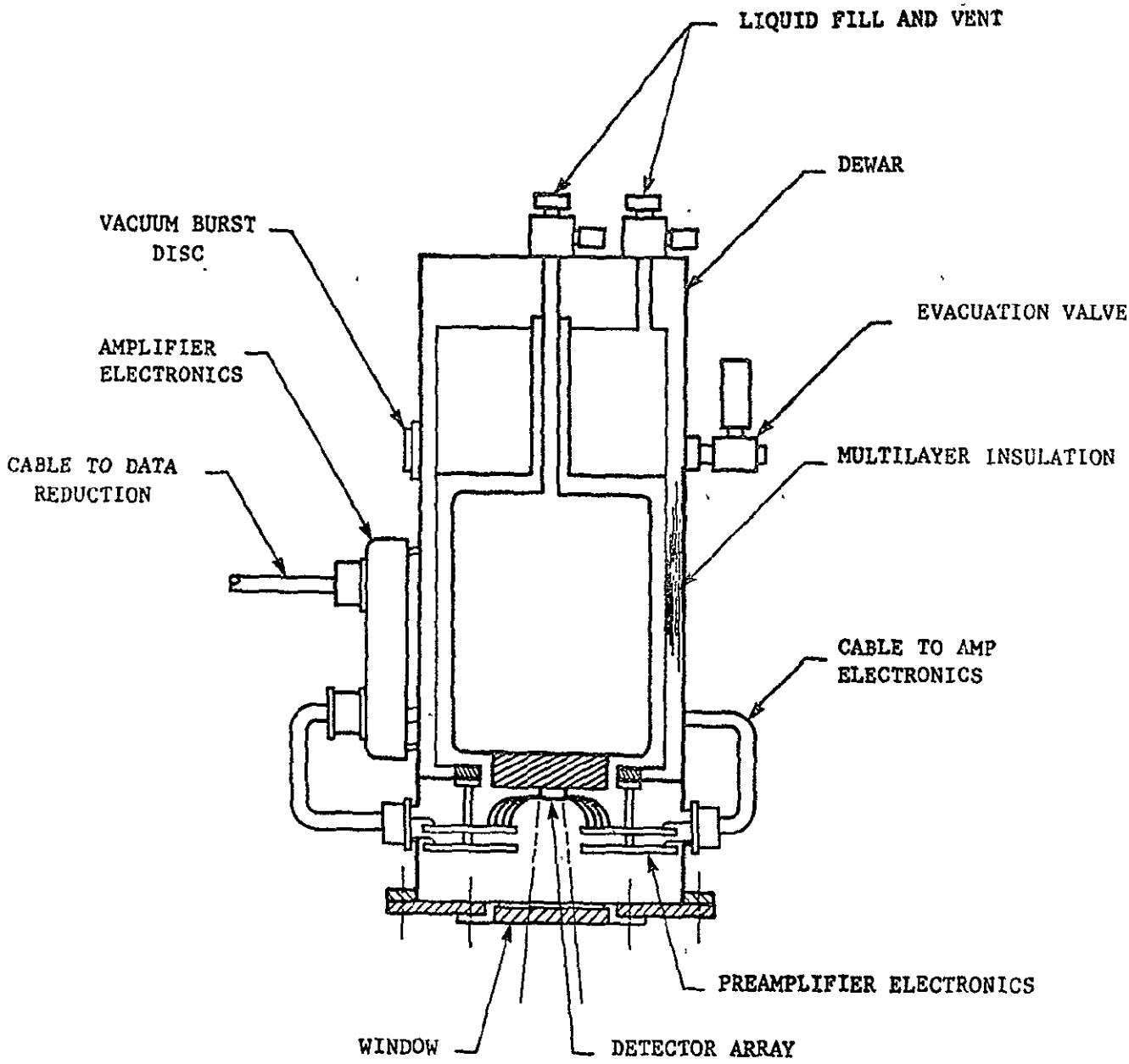

Figure 23 DEWAR CONFIGURATION

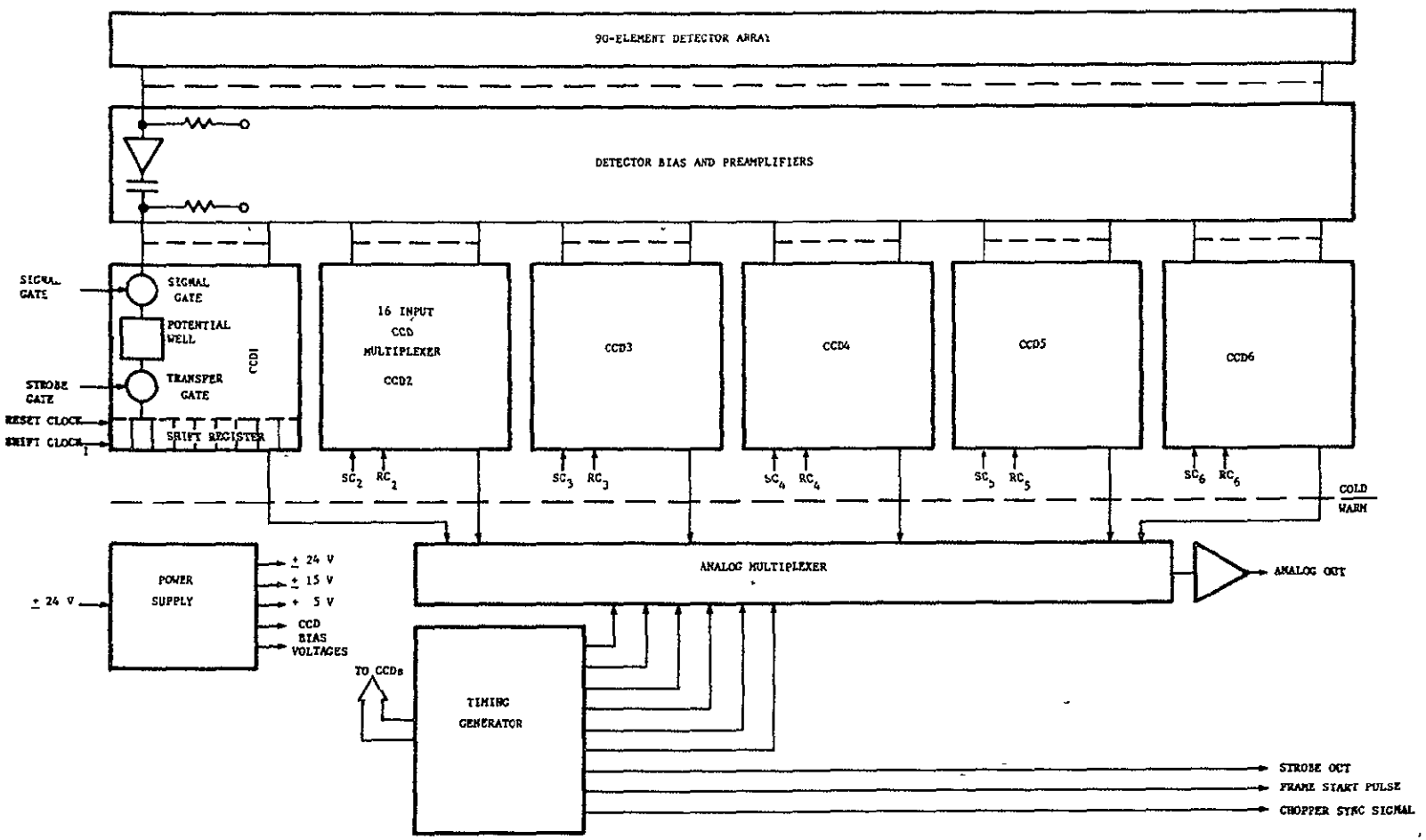

Figure 24 AIRCRAFT PUSHBROOM FOCAL PLANE ELEC. CONFIGURATION

LIST OF REFERENCES

1) Sequin and Tompsett, "Charge Transfer Devices", Academic Press (New York), 1975

2) D. Long, "Photovoltaic and Photoconductive Infrared Detectors", Topics in Applied Physics (ed. by R.J. Keyes), Chapter 3 (to be published) also M.B. Reine and R.M. Broudy, "A review of (Hg,Cd)Te Infrared Detector Technology

3) C.D. Motchenbacher and F.C. Fitchen, "Low-Noise Electronic Design" Wiley (New York), 1973

4) T.J. Tredwell, "(Hg,Cd)Te Photodiodes for Detection of Two-Micrometer Infrared Radiation", Optical Engineering 16, 237 (1977).

APPENDIX A

A CCD SCANNED (Hg,Cd)Te ARRAY FOR EARTH VIEWING APPLICATIONS

S. Iwasa and W.J. White

Honeywell Radiation Center
Lexington, Massachusetts

ABSTRACT

A 9-channel demonstration of 10-micrometer photoconductive mercury cadmium telluride detector array, bipolar preamplifiers, and a Si CCD multiplexer, integrated into a focal plane assembly and operating at 105°K and at 17 Hz is reported. An average $D^*_{\lambda peak} = 7.5 \times 10^9$ cmHz$^{\frac{1}{2}}$/W is obtained after the electronic scanning by the CCD. Reported also is the result of a direct coupling experiment between a 5-micrometer photovoltaic mercury cadmium telluride photodiode and a CCD. No appreciable degradation in the signal-to-noise ratio was experienced and $D^*_{\lambda peak} = 1.6 \times 10^{11}$ cmHz$^{\frac{1}{2}}$/W at 723Hz and at 77°K was obtained after the CCD.

I. INTRODUCTION

Present generation earth resources sensors flying in near earth orbit use a single infrared detector in each spectral region and scan by means of a moving mirror to obtain a full field of coverage in the direction orthogonal to the vehicle motion. In future systems it would be desirable to eliminate the need for the mirror, which is physically large and heavy, requires considerable drive power, and has the inherent reliability problems of mechanical devices.

Electronic scanning can be done simply by multiplexing, however, a large number of resolution elements (detectors) will be required. Any consideration of the benefits of electronic scanning must take into account not only relative system performance but also any tradeoffs between extra cooling power required for the extra elements, and operating power for the mirror. If low level radiative cooling is provided for example, then low power dissipation per element becomes a controlling factor.

Photoconductive (Hg,Cd)Te detectors are ideally suited for 10.5 to 12.5-micrometer earth resources applications. Detectors having $D^*(500, 3kHz, 1Hz) > 2 \times 10^{10}$ cmHz$^{\frac{1}{2}}$/W at 110°K are readily available. Recent advancements in 1/f noise reduction have been made also. Detectors operating at 82°K have shown $D^*(500, 17, 1)$ of 1.2×10^{10} cm Hz$^{\frac{1}{2}}$/W.

The resistance of these detectors has been improved to the 50-200 Ω range for square detectors, which results in power dissipations in the 100μW to 1mW range. Even with on focal plane parallel to serial conversion this amount of power may prove to be undesirable.

The (Hg,Cd)Te photodiodes, on the other hand would dissipate little or no power and would appear to be a better choice for the future earth resources, long life satellite applications. It will be shown in the text that (Hg,Cd)Te PV detectors can be direct coupled into buried channel CCD shift registers, thus providing the potential for an on focal plane parallel to serial conversion at power dissipation levels acceptable to radiative cooler requirements. Recent developments have been made in (Hg,Cd)Te photodiodes leading toward realization of such low power focal plane.[1]

In order to demonstrate the viability of on focal plane parallel to serial conversion using CCDs, a breadboard demonstration was made up and tested. This breadboard included current state of the art 9-element photoconductive (Hg,Cd)Te 10.5 to 12.5-micrometer detector array, a cryogenically cooled single stage bipolar preamplifier for each detector, and a 9-channel buried n-channel CCD multiplexer. These were all mounted on the cold pedestal of a variable temperature (80 to 110°K) dewar. Additionally clock drive, bias, and readout circuitry were built up to operate the breadboard. It was found that D* values in the detector were degraded only slightly at the CCD output.

As a demonstration of direct coupling (no preamplifier) the signal from a 5-micrometer (Hg,Cd)Te photovoltaic detectors was directly injected into a CCD multiplexer. Within the experimental error, no degradation in the S/N ratio was experienced in going through the multiplexer. This is an encouraging result towards the realization of a hybrid focal plane with low power consumption. An analysis is presented, taking into account the 1/f noise from the CCD.

II. BURIED CHANNEL CCD MULTIPLEXER

The parallel-to-serial multiplexer used in the IR/CCD experiment is a two-phase, n-channel CCD with 30 parallel inputs. The input MOSFET structure is surface channel. Each input stage consists of an independently accessible pair of source diffusion and control gate, followed by a storage gate and a transfer gate. The shift register is buried, and two adjacent inputs are separated by an empty bit for minimizing crosstalk. A transfer efficiency of 0 99995 has been measured at 1MHz clock frequency. The input/output characteristics of the CCD have been studied in depth for two types of signal injection, i.e , charge equilibration and current integration.[2] Figure 1 describes an I/O characteristic of the equilibration mode for 9 of the 30 available inputs, when signal is entered via the control gate. The relationship is described by

$$V_{out} = C_W(V_W - V_{in}) \times \frac{1}{C_{FD}} \times \alpha \qquad (1)$$

where C_W and V_W are respectively the capacitance and potential of the storage well, C_{FD} is the effective depletion capacitance of the floating diffusion and $\alpha = 0.7$ is the gain of the source follower.

From equation 1, the experimentally measured slope of 0 2 corresponds to $C_{FD} = 3.5\ C_W$, which is in agreement with the CCD geometry. The slope remains the same at 77°K The channel nonuniformity is seen to be small.

Figure 2 depicts the I/O relationship for the current integration mode. For the range of the integration times shown, the channel under the control gate is strongly inverted and the I/O characteristic is given by

$$V_{out} = \frac{\mu C_{ox} Z\tau}{2L} [V_{in} - (V_G - V_T)]^2 \frac{1}{C_{FD}} \alpha \qquad (2)$$

where $\mu_n = 650\ cm^2/V\text{-}s$ at 300°K is the surface channel electron mobility, C_{ox} the gate oxide capacitance per unit area, Z/L the gate aspect ratio, τ the integration time, and V_{in}, V_G and V_T respectively refer to the source, gate and the threshold voltage. In the current integration mode, one has the option of signal entry either at the source diffusion or at the control gate, leading to an identical I/O relationship as given in equation 2. The input impedance is different for the two entries, however. In the source input case, the transconductance is given by

$$g_m = \sqrt{\frac{\mu C_{ox} Z}{2L} I_s} \qquad (3)$$

where I_s is the source diffusion current. The gate is nearly open except for a small capacitance The nonuniformity among the 9 inputs originate mainly from variations in the threshold voltage of ΔV_T=20mV as evidenced by translation and not slope change in Figure 2. The effect of the integration time τ is a change in the slope. Figure 3 illustrates the I/O characteristics of the current integration mode at 300°K and at 77°K, where the major changes occur in V_T (translation) and in μ_n (slope change) The low frequency input referred noise of the two signal input techniques at 300°K and 77°K are shown in Figure 4.

III PHOTOCONDUCTIVE (Hg,Cd)Te IR/CCD

A. 10-MICROMETER PHOTOCONDUCTIVE (Hg,Cd)Te ARRAY

The photoconductive (Hg,Cd)Te array used in the breadboard demonstration consists of 20 linear 5 mil by 5 mil detector elements separated by 1.5 mils Their peak response is at 10.6 micrometers and the cutoff at 13 micrometers. They have an average resistance of 60Ω and are operated with best signal-to-noise ratios at approximately 0.3 volt bias. The $D^*_{\lambda peak}$ values of the array measured at 105°K are plotted in Figure 5 as a function of frequency The average noise voltage of an element at 105°K at 17Hz is of the order of $40nV/\sqrt{Hz}$

B. CRYOGENIC BIPOLAR PREAMPLIFIER

The input referred noise of the CCD MUX in current integration is of the order of $1.8\ \mu V/\sqrt{Hz}$ at 77°K and at 17Hz, and is 45 times larger than the detector noise. In order to make the detector a dominant noise source, a buffer amplifier must be inserted between the detectors and the CCD input. This buffer amplifier array must have 9 channels, have a voltage gain of about 100 times, and operate at focal plane temperatures in the vicinity of 105°K. Figure 6 gives a bipolar preamplifier version consisting of 2N3964 in a common gate and an ac coupled configuration. The gain bandwidth product of the present amplifier is 100MHz and the input referred noise is less than $10nV/\sqrt{Hz}$ at 77°K and at 17Hz. The selection of the transistor was a non trivial task. Most bipolars including the super betas, JFET and MOSFETs may operate perfectly at room temperature and at high frequencies but would fail at 77°K and at 17Hz.

C. PC (Hg,Cd)Te IR/CCD D*

The 10-micrometer PC (Hg,Cd)Te array, the bipolar preamplifier and the CCD MUX are mounted on a common pedestal block assembly. The pedestal block assembly is in (limited)thermal contact with the cold finger of a liquid nitrogen dewar, and an internal heater regulates the focal plane temperature in the range between 80°K and 120°K. Figure 7 illustrates the multiplexed output waveform as well as the sample/hold waveform of a selected channel, showing the chopped blackbody signal. The signal-to-noise ratios of the PC(Hg,Cd)Te IR/CCD at various stages, namely, that of the PC detectors, after the preamplifiers and after the multiplexer, are expressed as $D^*_{\lambda peak}$ and plotted in Figure 8. On the average, a 7% degradation in the S/N is experienced after the preamplifiers and 22% after the CCD multiplexer. The detector noise is 40nV/$\sqrt{Hz}$ and the input noise of the amplifier 10nV/$\sqrt{Hz}$, therefore, the expected average loss in the S/N is given by

$$\left[\left((10nV/\sqrt{Hz})^2 + (40nV/\sqrt{Hz})^2\right)/(40nV/\sqrt{Hz})^2\right]^{-\frac{1}{2}} = 0.97$$

which is to say a loss of 3% is accounted for. The S/N loss in going through the multiplexer is computed to be

$$\left[(40nV/\sqrt{Hz})^2 + (10nV/\sqrt{Hz})^2 + (1.8\mu V/\sqrt{Hz}/100)^2)/(40nV/\sqrt{Hz})^2\right]^{-\frac{1}{2}} = 0.89$$

There is an 11% discrepancy between the observed 0.78 and the calculated 0.89. The discrepancy is a direct result of the noise aliasing suffered when the CCD multiplexer samples the detector signal. In a sampled system, the noise spectrum beyond the integral multiple of the sampling frequency is reflected back into the base signal bandwidth. One method of minimizing aliasing is to reduce the noise bandwidth of the detector/amplifier to less than the sampling frequency. This can be achieved by adding a capacitor next to the collector resistance and forming a low pass filter. This was tried on one channel after which a near theoretical degradation has been observed.

D. POWER DISSIPATION OF PC(Hg,Cd)Te IR/CCD SYSTEM

The average power dissipation in the 10-micrometer PC(Hg,Cd)Te detector is of the order of 1.5mW per one element. Approximately 1mW is consumed in the bipolar preamplifier. In comparison, the power dissipation of the CCD is insignificant. Hence, the PC(Hg,Cd)Te IR/CCD consumes an average of 2.5mW per channel, or 23mW total for the 9 channels.

IV PHOTOVOLTAIC (Hg,Cd)Te IR/CCD

A. DIRECT COUPLING EXPERIMENT

The success of a hybrid focal plane ultimately depends on low power consumption and simplicity of the electronic and mechanical interface between the detector array and the silicon CCD. Photovoltaic (PV) detectors have high impedance and operate with minimal power consumption. It is of interest, then, to explore direct coupling between a PV detector and a CCD without a buffer amplifier.[3]

An experiment was carried out in which a 4.4-micrometer peak photovoltaic (Hg,Cd)Te detector was directly coupled to a source diffusion of a surface p-channel CCD. Within the experimental error, there was no observable degradation in the signal-to-noise ratio when the detector signal was retrieved after the CCD multiplexer. The coupling scheme is of such a simplicity that the preliminary result is an encouraging one towards the realization of a large array hybrid IR/CCD structure with low power dissipation.

Figure 9 describes the experimental setup. The n-type PV detector element and its p-type substrate were directly connected, respectively, to the substrate and a source diffusion of a surface p-channel CCD. Table 1 summarizes the detector specifications. A clock rate of 500 Hz with the aluminum diode gate connected to Ø1, and the polysilicon gate bias in the vicinity of -1 volt, are designed to allow an input current of 0.2 μA to match the background generated photocurrent of the PV detector, therefore assuring the zero bias operation. A 500°K blackbody was chopped at 723 Hz, and the modulation was extracted by a sample and hold amplifier and analyzed by a 304 Quantek Wave Analyzer at 10 Hz bandwidth. The CCD output noise was typically 6μV/$\sqrt{Hz}$ at 723 Hz.

In these experiments, the PV HCT detector was operated with a S/N value of typically 600. When the detector was directly coupled to the CCD, the CCD output exhibited S/N values of 600 ± 100. These values correspond to the detector D* values of 1.6×10^{11} cm^2Hz/W. Signal and noise traces of the PV HCT detector only, and the PV HCT CCD output, are shown in Figure 10.

B. PV IR/CCD D* ANALYSIS

In the directly coupled PV IR/CCD system in Figure 9, the detector noise is in series with that of the CCD. The total detector noise voltage is given by

$$e_D^2 = \left(\frac{4kT}{R_o} + 2qI_\phi\right)R_o^2 \qquad (4)$$

where the first term in the bracket represents the detector Johnson noise current and the second the photon induced shot noise current. $I_\phi = \mu q \phi_B A$ is the diode photocurrent, where μ, ϕ_B, and A are, respectively, the quantum efficiency, photon flux and the photosensitive area of the diode. The CCD noise voltage is expressed by

$$e_{CCD}^2 = \frac{8kT}{3g_m} + e_{1/f}^2 \qquad (5)$$

where the first term is the Johnson noise of the strongly inverted channel region, and the second the 1/f noise. The transconductance gm is given in equation 3, in which I_s is to be replaced by I_ϕ.

The D* value of the IR/CCD is given by

$$D^*_{IR/CCD} = \frac{D^* \text{ DETECTOR}}{\sqrt{N.F.}} \qquad (6)$$

where the noise figure is defined as

$$\text{NOISE FIGURE} = \frac{\text{TOTAL NOISE POWER}}{\text{DETECTOR NOISE POWER}} = 1 + \frac{\text{CCD NOISE POWER}}{\text{DETECTOR NOISE POWER}} \qquad (7)$$

By substitution, one finds that

$$N.F. = 1 + \frac{\frac{8}{3}kT\sqrt{\frac{2L}{\mu C_{ox} Z I_\phi}} + e_{1/f}^2}{R_o^2\left(\frac{4kT}{R_o} + 2qI_\phi\right)} \qquad (8)$$

Using the values q R_o=20MΩ, I_ϕ = 0.2μA, T=77°K, $e_{1/f} = 18/f$ $\mu V/\sqrt{Hz}$ and the CCD parameters given as before, one finds N.F. = 1.00, namely, $D^*_{IR/CCD} = D^*_{DETECTOR}$. This is in agreement with the experiment. In fact, the experimental conditions can be relaxed quite a lot before the CCD starts to contribute a noticeable amount of noise. If for instance one can tolerate a 10% degradation in the system D* value, namely, $D^*_{IR/CCD} \geq 0.9\ D^*_{DETECTOR}$ this corresponds to a maximum noise figure of 1.23. Using equation 9, one can afford any one of the following relaxations when all else are assumed to remain the same.

1. R_o can be as low as 390 KΩ instead of 20MΩ.
2. Background photon flux can be as low as 5×10^{13} photons/cm^{2}sec instead of 9×10^{15} photons/cm^{2}sec.
3. Signal frequency can be as low as 5.4 Hz instead of 723 Hz

The first condition suggests that the actual focal plane temperatures need not be as low as 77°K. It can be as high as when the diode impedance reduces to 390KΩ.

C. POWER CONSUMPTION

The PV(Hg,Cd)Te photodiode element is consuming $I_\phi^2 R_o$ = 0 8 microwatt, which is an insignificant amount compared with that of the PC(Hg,Cd)Te element.

V. SUMMARY

A 9-channel breadboard of 10.6 micrometer peak photoconductive (Hg,Cd)Te detector array, bipolar preamplifiers and a silicon CCD multiplexer, integrated on a focal plane, has demonstrated an electronic scanning. Operated at 105°K and at 17 Hz, the breadboard has yielded an average $D^*_{\lambda peak}$ = 7 5 x 10^9 cmHz$^{\frac{1}{2}}$/W, a 22% degradation from that of the detectors. The power dissipation is 2.5mW per channel.

A 4 4-micrometer peak photovoltaic (Hg,Cd)Te detector has been directly (no preamplifier) coupled to the source diffusion of a CCD. Operating at 77°K and at 723 Hz, the multiplexer has yielded $D^*_{\lambda peak} = 1.6 \times 10^{11}$ cmHz$^{\frac{1}{2}}$/W, with no appreciable degradation from the detector value. The power dissipation was 0.8 μW. The latter configuration promises the realization of a large array hybrid focal plane.

VI. ACKNOWLEDGEMENT

The development of the breadboard demonstration of electronically scanned array was supported by NASA/Goddard Space Flight Center under Contract NAS 5-22339, monitored by K.L. Hallam.

The authors are indebted to D.E. Marshall and N.R. Butler for many helpful discussions. The 10.6-micrometer peak photoconductive (Hg,Cd)Te array was supplied by W.G. Rae, the 4.4-micrometer peak photovoltaic (Hg,Cd)Te array by T.J. Tredwell, and the CCDs by J.S.T. Huang. The hardware was assembled by A.R Carson

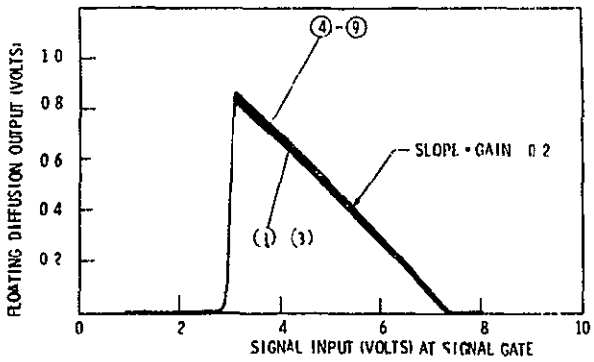

Figure 1. Channel uniformity for fill & spill

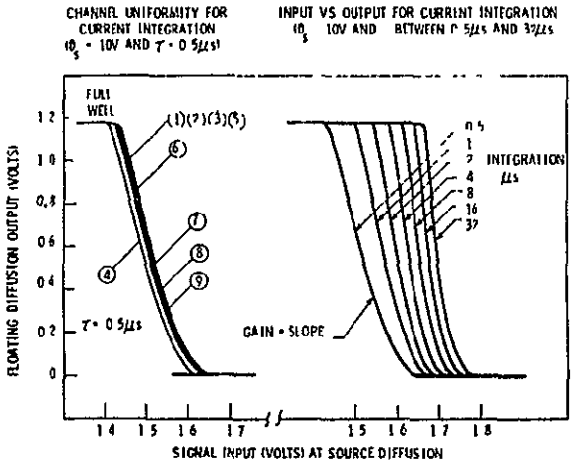

Figure 2. Channel uniformity and input vs output characteristics for current integration

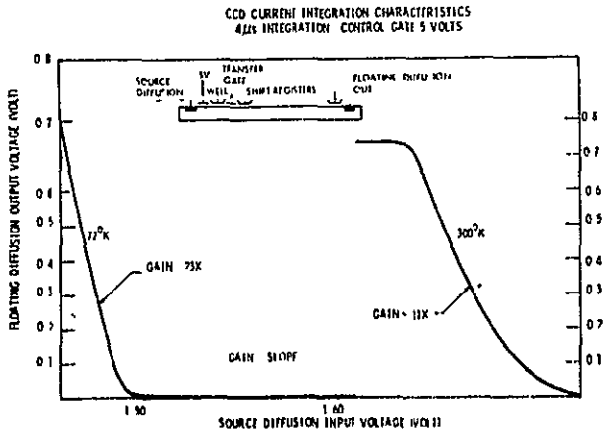

Figure 3. Current integration characteristics for T=300°K & T=77°K

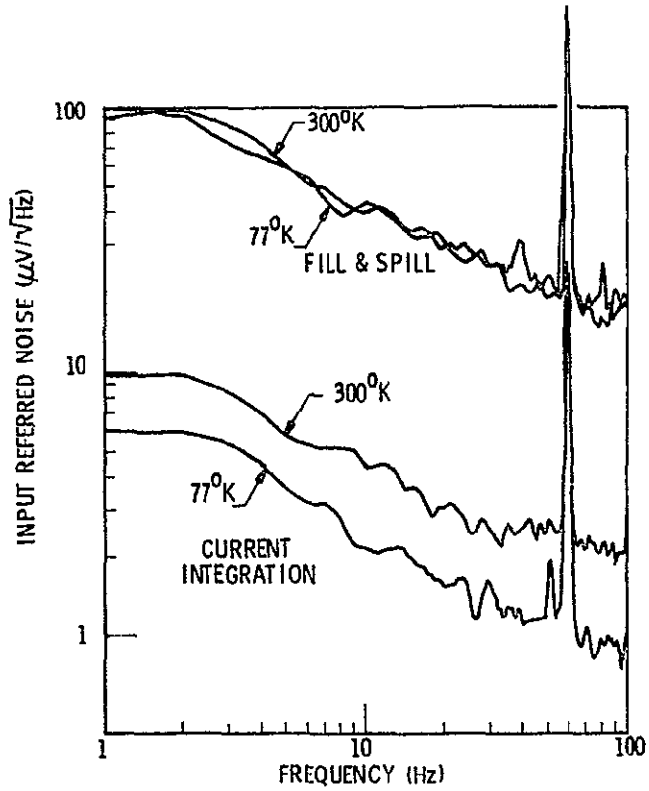

Figure 4. CCD. input referred noise

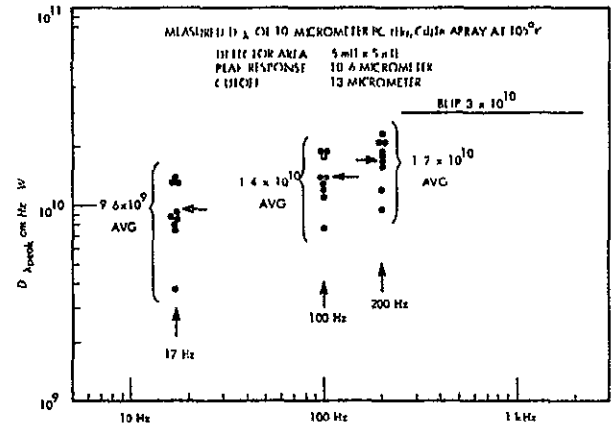

Figure 5. PC HCT array D* vs frequency

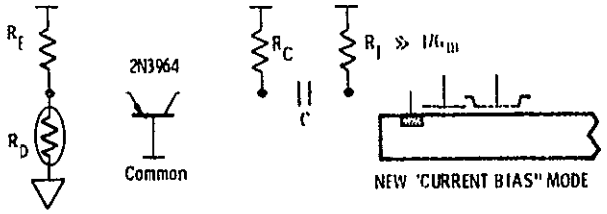

Figure 6. Cryogenic preamplifier configuration

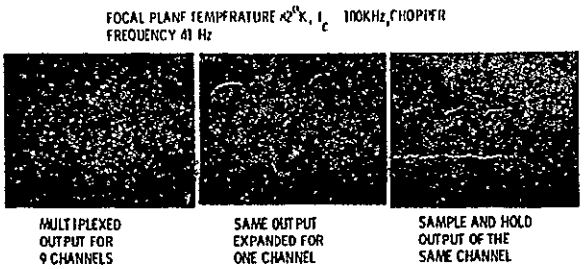

Figure 7. PC HCT IR/CCD MUX output waveforms

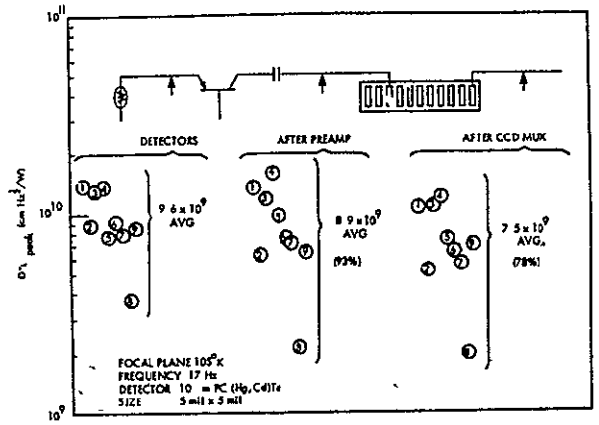

Figure 8. PC IR/CCD D*

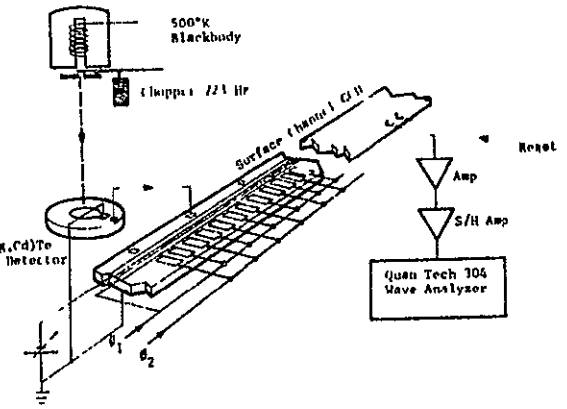

Figure 9. PV HCT direct coupling experiment

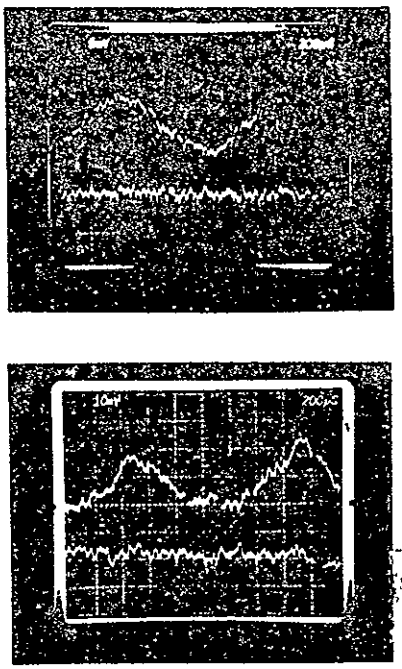

Figure 10. PV HCT detector coupled CCD

Table 1. Photovoltaic (Hg,Cd)Te detector parameters

D* AT 180° FOV, 300°K BACKGROUND 1.6×10^{11} cm^2 Hz/W
D* AT 180° FOV, 77°K BACKGROUND 2.5×10^{12} cm^2 Hz/W

AREA	1.82×10^{-4} cm^2
OPEN RESISTANCE R_0	20MΩ at 77°K
RESPONSE MAXIMUM	4.4 MICROMETERS
RESPONSE CUTOFF	4.76 MICROMETERS
ZERO BIAS DETECTOR CURRENT	0.2 μA
QUANTUM EFFICIENCY η :	0 74
R_0A	3640 AT 77°K

1. Tredwell, T.J., "(Hg,Cd)Te Photodiode Technology," to be published in proceedings of IEDM, December 1976.
2. Tompsett, M.F., "The Potential Equilibration Method of Setting Charge in CCDs," Electron Devices, Vol. ED-22, No. 6, p. 305; June 1975.
3. Steckl, A.J., Nelson, R.D., French, B.T., Gudmundsen, R.A., and Schechter, D; "Application of Charge-Coupled Devices to Infrared Detection and Imaging," Proc. IEEE, Vol. 63, No. 1, p. 67; January 1975.

APPENDIX B

Direct Coupling of Five-Micrometer (Hg,Cd)Te Photovoltaic Detector and a CCD Multiplexer

Sato Iwasa
Honeywell Radiation Center
2 Forbes Road, Lexington, Massachusetts 02173

Abstract

A direct coupling experiment between a 5-micrometer photovoltaic mercury-cadmium telluride detector and a CCD multiplexer is reported No detectable degradation in signal-to-noise ratio was experienced and $D^*_{\lambda\ peak} = 1.6 \times 10^{11}$ cm $Hz^{1/2}/W$ (BLIP) was obtained after the CCD multiplexer, when the photodiode at 77°K was irradiated by the 300 K background with 180-degree field of view, chopped at 723 Hz.

Introduction

The application of infrared detection and imaging is growing steadily, motivated by such diverse areas as military, security, medicine, industrial process control and energy conservation, to name a few The growth is accompanied by an expanding list of solid state sensor materials, and by a natural evolution of going from a single element sensor to linear and mosaic arrays With the advent of charge coupled devices,[1] the concept of a very large and electronically scanned sensor array has become feasible, with the inherent benefit of increased sensitivity and resolution

Large CCD imaging arrays in the visible, having elements numbering in the low 10^5 range, have already been demonstrated, and those in the mid 10^5 range seem just around the corner [2] The infrared counterpart is still a step behind in the development, but it is only a matter of time when large IR sensitive CCD arrays will become practical

The IR/CCD arrays can be divided into two major categories monolithic type in which the IR sensing and the subsequent signal processing are performed on a single material monolithic device, and hybrid type in which a proven IR sensor array is integrated with a Si CCD.[3]

Mercury-cadmium telluride is one of the most promising candidates towards the implementation of a hybrid type IR/CCD. Besides being an efficient quantum detector, its spectral response can be continuously adjusted in the range between 0 8 to 25 micrometers by varying the atomic ratios between Hg and Cd It operates at high temperatures and its thermal expansion coefficient matches closely that of Si. The (Hg,Cd)Te sensors can operate in photoconductive (PC) mode and photovoltaic (PV) mode

A PC sensor is resistive (10 ~ 1000 Ω), while a PV sensor is a diode and hence consists of a high resistance (> 10^6 Ω) in parallel with a capacitance (a few pF) In constructing a hybrid IR/CCD structure, analysis shows that a separate preamplifier is required for the PC (Hg,Cd)Te, while direct coupling is feasible for the PV (Hg,Cd)Te [5]

In addition to direct coupling to a Si CCD, the latter dissipates very little power (less than a μW per sensor), exhibits good linearity and uniformity of response and low 1/f noise, all of which render the PV (Hg,Cd)Te very promising towards a large hybrid IR/CCD [4]

As a demonstration of direct coupling (no preamplifier), the signal from a 5-micrometer (Hg,Cd)Te photovoltaic detector was directly injected into a CCD multiplexer Within the experimental error, no degradation in the S/N ratio was experienced in going through the multiplexer This is an encouraging result towards the realization of a hybrid focal plane with low power consumption. An analysis is presented, taking into account the 1/f noise of the CCD

Photovoltaic (Hg,Cd)Te IR/CCD

Direct Coupling Experiment

The success of a hybrid focal plane ultimately depends on low power consumption and simplicity of the electronic and mechanical interface between the detector array and the silicon CCD Photovoltaic (PV) detectors have high impedance and operate with minimal power consumption It is of interest, then, to explore direct coupling between a PV detector and a CCD without a separate buffer amplifier.

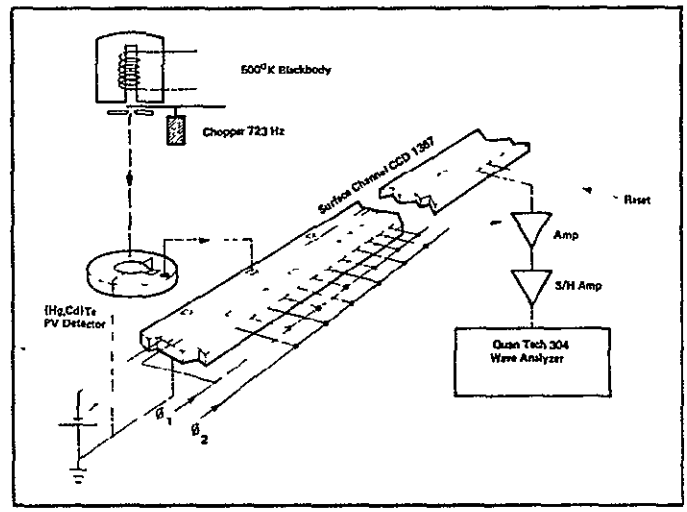

Figure 1. PV HCT Direct Coupling Experiment

Figure 1 describes the experimental setup. The n-type PV detector element and its p-type substrate were directly connected, respectively, to the substrate and a source diffusion of a surface p-channel CCD. Table 1 summarizes the detector specifications. A clock rate of 500 kHz with the aluminum diode gate connected to ϕ1, and the polysilicon gate biased in the vicinity of -1 V, is designed to allow an input current of 0 2

Table 1. Photovoltaic (Hg,Cd)Te Detector Parameters

D* at 180° FOV, 300°K background	1.6×10^{11} cm² Hz/W
D* at 180° FOV, 77°K background	2.5×10^{12} cm² Hz/W
Area	1.82×10^{-4} cm²
Open resistance R_o	20MΩ at 77°K
Response maximum	4 4 micrometers
Response cutoff	4 76 micrometers
Zero bias detector current	0.2 μA
Quantum efficiency η	0 74
R_oA	3640 at 77°K

B2

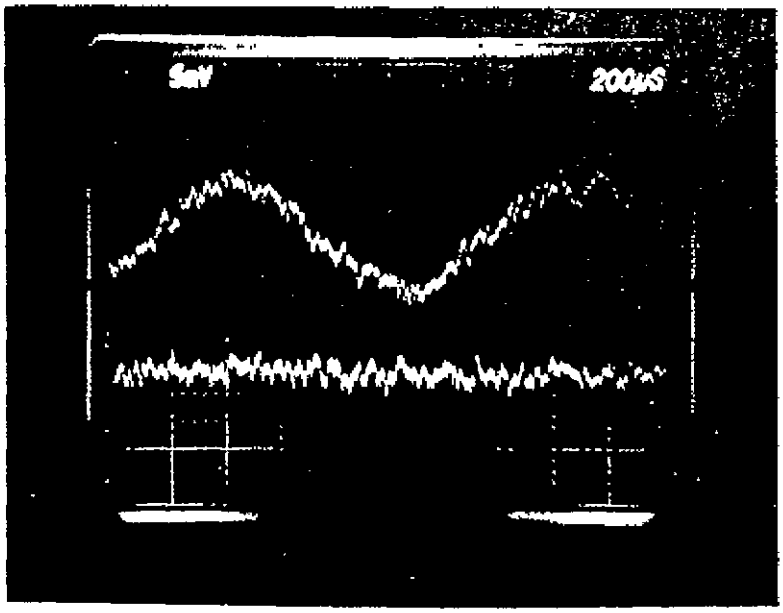

DETECTOR 12

$\lambda_c = 4.8 \mu m$
$R_oA = 3640$
A = 6 mil dia
T = 77°K
$D^* = 1.6 \times 10^{11}$
$Q_B = 300°K$
ZERO BIAS

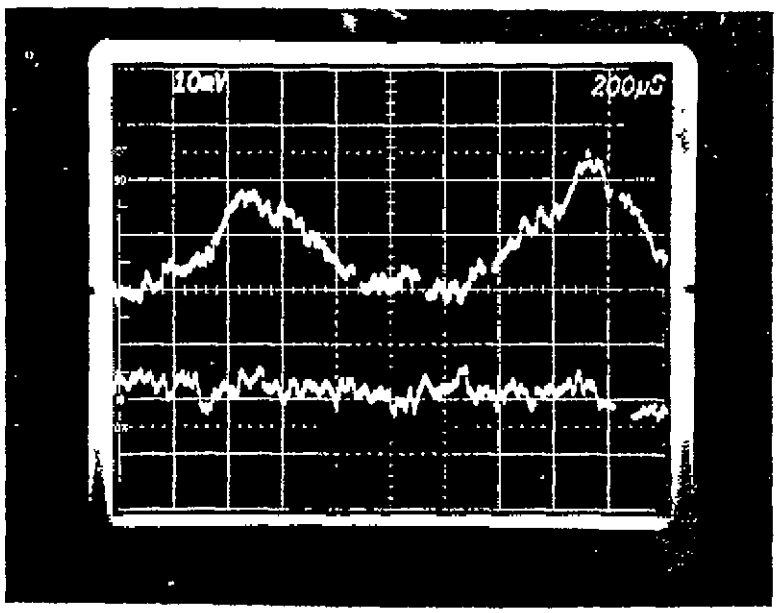

CCD

$f_c = 500K$
T = 300°K
$D^* = 1.6 \times 10^{11}$
COMMON GATE MODE

Figure 2 PV HCT Detector Coupled CCD

μA to match the background generated photo-current of the PV detector, therefore, assuring the zero bias diode operation

A 500 K blackbody was chopped at 723 Hz and the modulation was extracted by a sample and hold amplifier and analyzed by a 304 Quantek Wave Analyzer at 10 Hz bandwidth The CCD output noise was nominally 6 $\mu V/\sqrt{Hz}$ at 723 Hz

In these experiments the PV (Hg,Cd)Te detector was operated with a S/N value of typically 600 When the detector was directly coupled to the CCD the CCD output exhibited S/N values of 600 ± 100 These values correspond to the detector D^* values of 1.6×10^{11} cm Hz/W Signal and noise traces of the PV (Hg,Cd)Te detector only, and the PV (Hg,Cd)Te CCD output, are shown in Figure 2

PV IR/CCD D* Analysis

Direct coupling of photodiodes made of InSb, (Hg,Cd)Te and PbSnTe with Si CCD multiplexers has been reported, and expressions detailing signal-to-noise ratio, injection efficiency and bandwidth have been derived [5-11] The analysis given here is simplified so that the physical mechanism involved is made transparent Only low signal frequency is of interest, and the effects of sampling are neglected An equivalent circuit of the direct coupling is given in Figure 3 As shown in Figure 4, the idealized response of a photovoltaic detector is given by

$$I_D = I_{SAT} \left(e^{\frac{qV}{kT}} - 1\right) + I_\phi \qquad (1)$$

where I_{SAT} is the diode reverse saturation current and I_ϕ is the photo-generated current, the latter is given by

B3

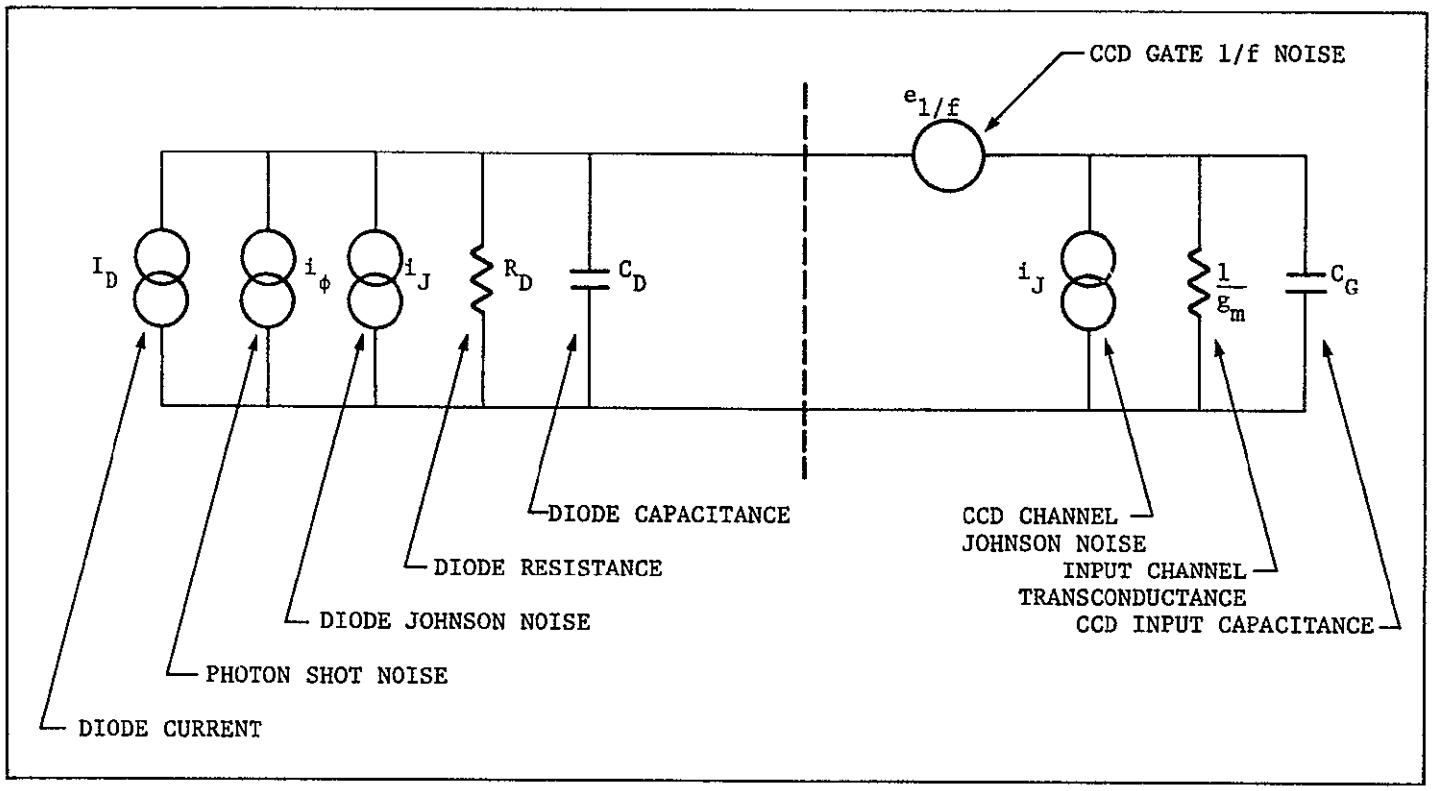

Figure 3 Equivalent Circuit of Direct Injection

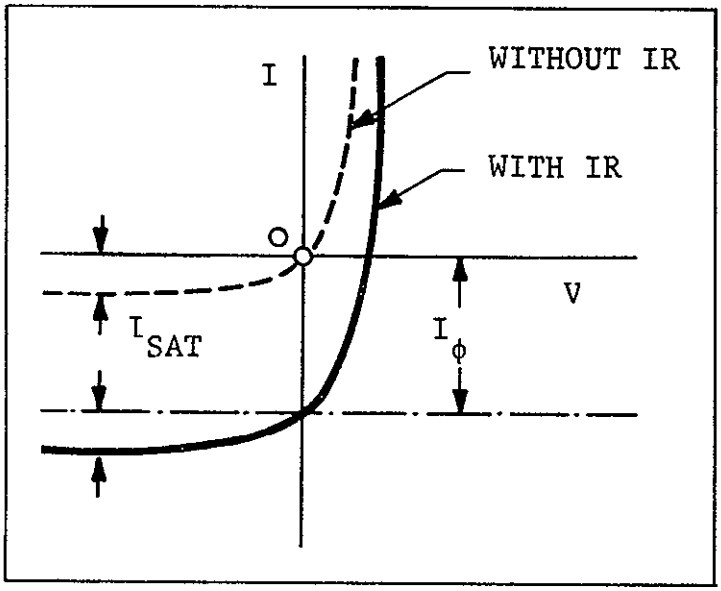

Figure 4 Idealized Photovoltaic Diode Response

$$I_\phi = \eta\, q\, \phi_B\, A_D \tag{2}$$

in which η, ϕ_B and A_D are, respectively, the quantum efficiency, IR photon flux and photosensitive area I_{SAT} is related to the zero bias diode resistance R_O by

$$I_{SAT} = \frac{kT}{qR_O} \tag{3}$$

The signal current distribution at zero diode bias V=O is readily seen to be

$$I_{CCD} = \frac{1}{1 + \frac{1}{g_m R_O}}\, I_\phi \tag{4}$$

The CCD transconductance g_m is given by (5)

$$g_m = \frac{Z}{L}\,\mu C_{ox}\,\left(\frac{kT}{q}\right)\left[\left(1 + \frac{2\, I_{CCD}}{\frac{Z}{L}\,\mu C_{ox}}\left(\frac{q}{kT}\right)^2\right)^{1/2} - 1\right]$$

where Z/L is the CCD input gate aspect ratio, μ the minority carrier mobility and C_{ox} is the oxide capacitance per unit area [12] The signal injection efficiency is the ratio I_{CCD}/I_ϕ, and it is desirable that this value is as close to unity as possible since it means all the photogenerated current in the diode is retrieved in the CCD multiplexer From Eq (4) it is apparent that the product $g_m R_O$ must be large for high injection efficiency, although the dependence of g_m on I_{CCD} as shown in Eq (5) somewhat complicates the picture Instead of mobilizing a computer at this point, we shall examine the so-called subthreshold current regime defined by

$$I_{CCD} \ll \frac{Z\,\mu C_{ox}}{2L}\left(\frac{kT}{q}\right)^2 \tag{6}$$

For a typical CCD input stage, the limiting current, is of the order of 30 nA where values of Z/L = 4, μ = 700 $cm^2 V^{-1} s^{-1}$, C_{ox} = 3 x 10^{-8} farads/cm^2 and T = 300 K have been used. In this current regime the transconductance in Eq. (5) reduces to

$$g_m = \frac{q\, I_{CCD}}{kT} \tag{7}$$

and Eq (4) becomes

$$I_{CCD} = I_\Phi + \frac{kT}{qR_O} = I_\Phi + I_{SAT} \tag{8}$$

It follows then that the condition $I_\phi \gg I_{SAT}$ assures high

B4

percentage signal injection In the language of photovoltaic diodes, this condition is also known as the BLIP (background limited) condition *The BLIP condition is all important* since it means 100% signal injection, linearity of photo-response (between I_{CCD} and Φ_B), and channel uniformity which is independent of the variations in R_O In the present experiment, I_Φ = 0 2 μA and $I_{SAT} = 3\ 3 \times 10^{-10}$ A, easily ensuring the needed BLIP condition

The total detector noise voltage is given by

$$e_D^2 = \left(\frac{4kT}{R_o} + 2qI_\phi\right) R_O^2 \tag{9}$$

where the first term in the bracket represents the detector Johnson noise current and the second the photon induced shot noise current

The CCD noise voltage on the other hand is expressed by

$$e_{CCD}^2 = \frac{8kT}{3g_m} + e_{1/f}^2 \tag{10}$$

where the first term is the Johnson noise of the strongly inverted channel region, and the second the 1/f noise The transconductance g_m is given in Eq (5)

The D* value of the IR/CCD is given by

$$D^*_{IR/CCD} = \frac{D^*\ DETECTOR}{\sqrt{N\,F}} \tag{11}$$

where the noise figure is defined as

$$\text{NOISE FIGURE} = \frac{\text{TOTAL NOISE POWER}}{\text{DETECTOR NOISE POWER}} \tag{12}$$

By substitution, one finds that:

$$N\,F = 1 + \frac{\frac{8}{3}kT\left(\frac{2L}{\mu C_{ox} Z I_\phi}\right)^{1/2} + e_{1/f}^2}{R_o^2\left(\frac{4kT}{R_o} + 2qI_\phi\right)} \tag{13}$$

Using the experimental values of R_o = 20 MΩ, I_ϕ = 0.2 μA, T = 77 K, $e_{1/f}^2$ = 18/f μV^2 / $\sqrt{Hz}$ and the CCD parameters given as before, one finds N.F = 1 00, namely, $D^*_{IR/CCD} = D^*_{DETECTOR}$ This is in agreement with the experiment

Power Consumption

The PV (Hg,Cd)Te photodiode element is consuming $I^2 R_O$ = 0 8 microwatt, which is an insignificant amount compared with that of a photoconductive type detector element

Summary

Following in the footsteps of visible CCD imagers, the development of a large IR/CCD array is a matter of time The hybrid approach attempts to integrate a well developed IR sensor array and a Si CCD signal processor, where (Hg,Cd)Te is one of the most promising candidates A photovoltaic 5-micrometer (Hg,Cd)Te detector has been directly coupled to a Si CCD multiplexer without a detectable degradation in the performance This type of detector consumes little power, making it suitable for the realization of a large integrated focal plane

Acknowledgments

The development of the breadboard demonstration of electronically scanned array was partially supported by NASA/Goddard Space Flight Center under Contract NAS 5-22339

The author is indebted to N R Butler, D E Marshall, and W J. White for many helpful discussions The 4 76-micrometer cutoff photovoltaic (Hg,Cd)Te array was supplied by T J Tredwell, and the CCDs by J. S Huang of the Honeywell Solid State Electronics Center in Minneapolis, Minnesota

References

1 W S. Boyle and G E Smith, "Charge Coupled Semiconductor Devices," Bell Syst Tech J , Vol 49, pp 587-593, Am 1970
2 G W Taylor, G A Antcliffe and G L Streckmann, "Development of Large Area CCD Imagers," Conference on CCD Technology and Applications, Washington, D C , November 1976
3 A J Steckl, R D Nelson, B T French, R A. Gudmundsen and D Schechter, "Application of CCD to Infrared Detection and Imaging," Proc IEEE 63, 67-74 (1975)
4 T J Tredwell, "Advances in 2 to 5-Micrometer (Hg,Cd)Te Photodiodes," International Electron Devices Meeting, Washington, D C , December 1976 Also, the present issue of Optical Engineering
5 A J. Steckl and T Koehler, "Theoretical Analysis of Directly Coupled 8 to 12-Micrometer Hybrid IR/CCD Serial Scanning," Proc CCD Applications Conf , San Diego, CA 247-258 (1973).
6 D M Erb and K Nummedal, "Buried Channel Charge Coupled Devices for Infrared Applications," Proc CCD Applications Conf , San Diego, CA 157-167 (1973)
7 D E French, M Y Pines, I J Renda, P. S Chia, J S Balon and A H Lockwood, "Result of PbSnTe Hetero-Structure Detectors Using Charge Coupled Devices," Proc Nat IRIS Conf , Dayton, Ohio (1974)
8 K Nummedal, M Y Pines, R N Sato and J M Hartmann, "Charge Coupled Device Readout of (Hg,Cd)Te Detectors," Proc Nat , IRIS Conf , Dayton, Ohio (1974)
9 A J Steckl, "Injection Efficiency in Hybrid IR/CCDs," Proc CCD Applications Conf., Edinburgh, 85-91 (1975).
10 A I Milton and M Hess, "Series-Parallel Scan IR/CCD Focal Plane Array Concept," Proc CCD Applications Conf , Edinburgh, 71-83 (1975)
11 S Iwasa and W J White, "A CCD Scanned (Hg,Cd)Te Array for Earth Viewing Applications," Proc Conf. on CCD Device Tech and Applications, Washington, D C (1976)
12 J M Sze, "Physics of Semiconductor Devices," J Wiley & Sons, (New York) 1969

B5

APPENDIX C

OPERATION MANUAL AND PERFORMANCE DATA
FOR
NINE-CHANNEL (Hg,Cd)Te PUSHBROOM IR/CCD SYSTEM

TABLE OF CONTENTS

C/a)

1. INTRODUCTION AND SUMMARY

The objective of this Contract No. NAS5-22339 is to design, build, characterize and deliver a breadboard electronically multiplexed infrared detector array whose D* (10.5 to 12.5 μm, 17 Hz, 60° FOV, 1 Hz) equals or exceeds 1.5×10^9 cm $Hz^{1/2}/W$ at 105 K. The information obtained will be used to create a low power electronically scanned focal plane design for future earth resources systems.

Such an IR/CCD breadboard has been constructed employing a photoconductive (Hg,Cd)Te sensor array, and has demonstrated a 9-channel average $D^*_{\lambda peak}$ value of 7.5×10^9 cm $Hz^{1/2}/W$ (17 Hz, 60° FOV, 1 Hz, 105 K) at the output of the CCD multiplexer. The value exceeds the work statement objective by a factor of 5. The detector array alone exhibits an average $D^*_{\lambda peak}$ value of 9.6×10^9 cm $Hz^{1/2}/W$, and hence the total S/N degradation suffered in the multiplexing electronics amounts to 22%. This document is the operation manual of the demonstration hardware.

2. RECOMMENDATION

Dewar Should Be Kept Evacuated

Although the 9-element (Hg,Cd)Te photoconductor array is nominally passivated, it is nevertheless recommended that the pushbroom dewar be kept evacuated at all times. Disassembly of the dewar for inspection or repair is achieved by letting dry air into the dewar when the pedestal is at equilibrium at room temperature. This operation should be brief and a prolonged exposure to air over several hours should be avoided.

3. THEORY OF OPERATION

The breadboard hardware for the 9-channel 10-μm PC (Hg,Cd)Te IR/CCD MUX system photographed in Figure 1 consists of the following list of subsystem assemblies as sketched in Figure 2:

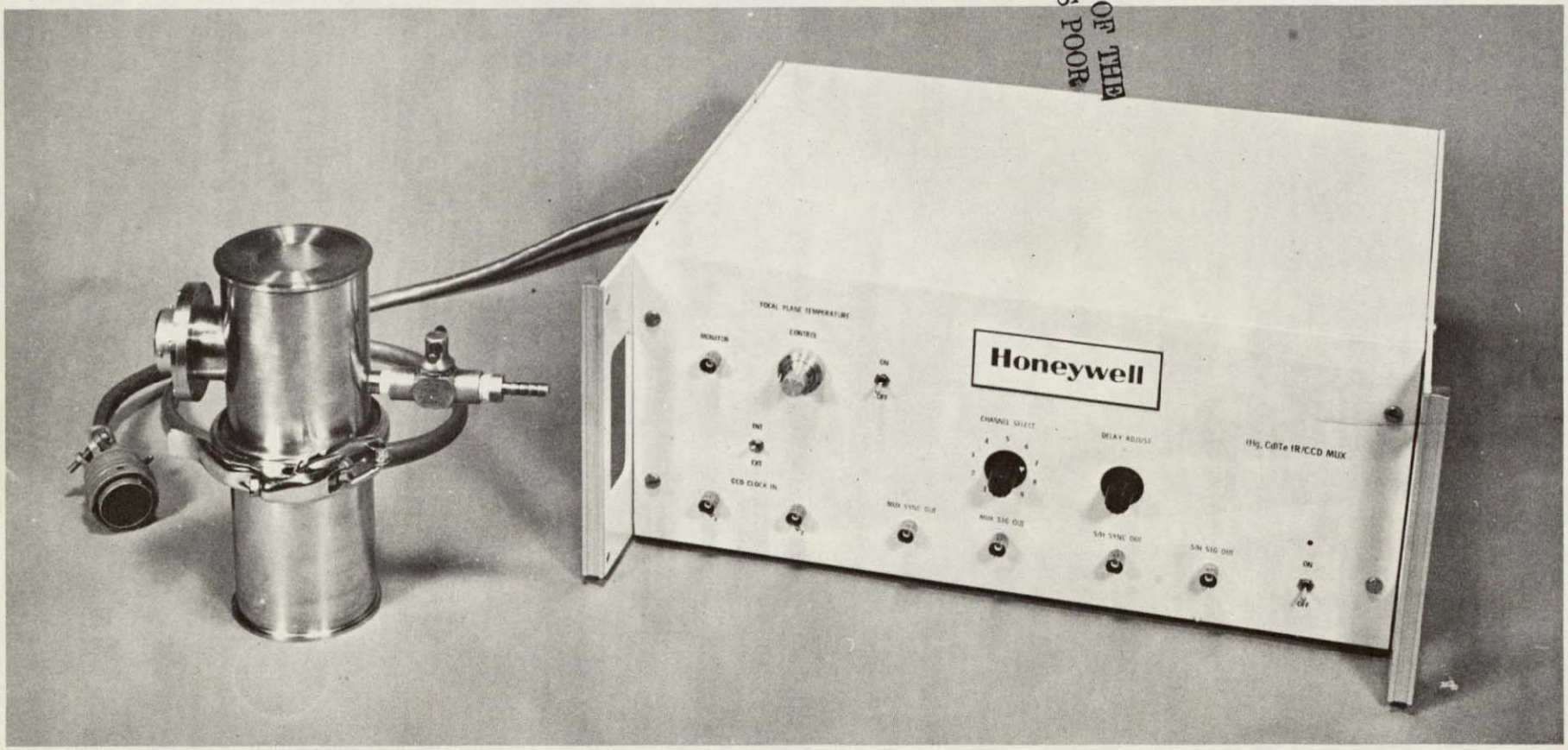

01516

Figure 1 THE 9-CHANNEL 10-μm PC (Hg,Cd)Te IR/CCD MUX BREADBOARD

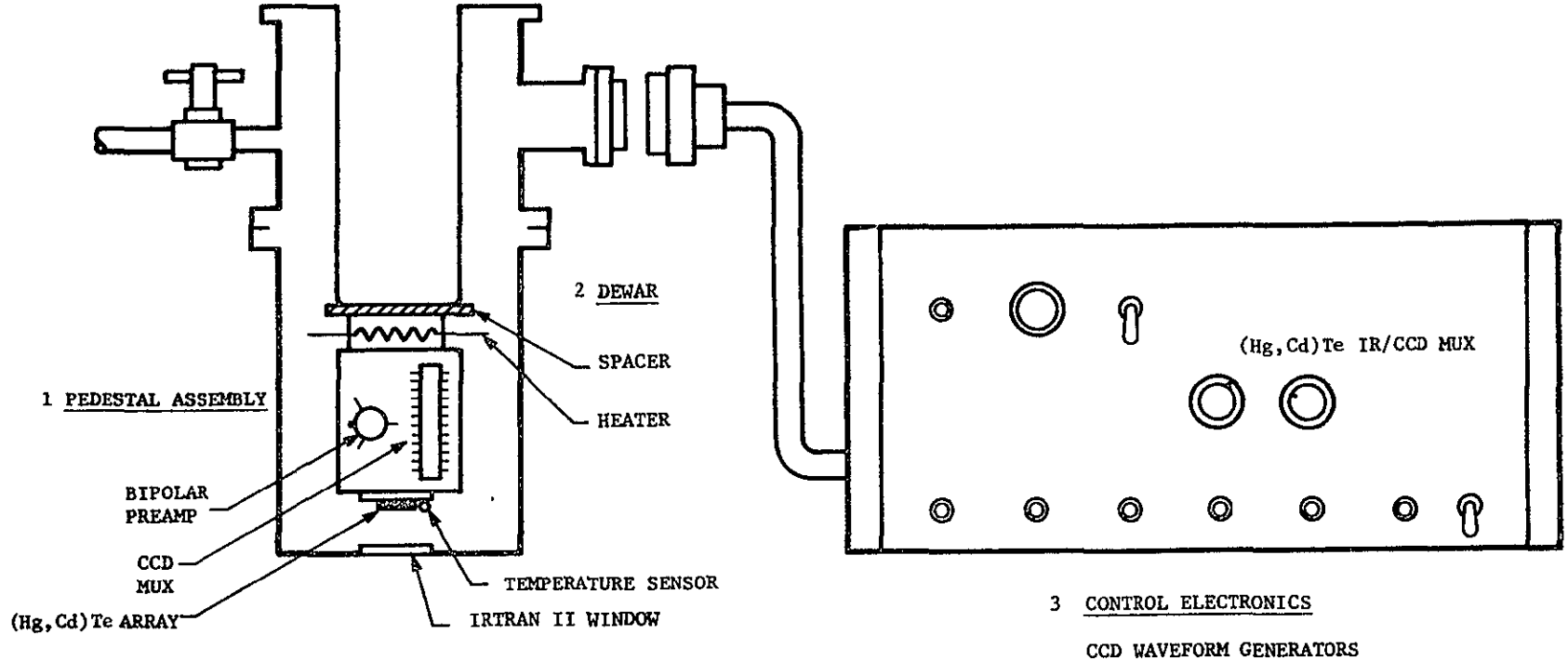

Figure 2 SUBSYSTEM ASSEMBLIES OF THE IR/CCD BREADBOARD

- Pedestal Assembly

  -- 9-channel 10-μm PC (Hg,Cd)Te array
  -- 9-channel bipolar preamplifiers
  -- 30-channel (9 used) buried channel CCD MUX

- Dewar

  -- Variable temperature pedestal
  -- Pedestal temperature sensor
  -- Temperature control heater
  -- IRTRAN II window

- Control Electronics

  -- CCD waveform generators
  -- Low noise bias supplies
  -- Sample and hold amplifier and logic
  -- Pedestal temperature readout electronics
  -- Pedestal temperature controller

In the following, the functions of each of the subassemblies are briefly described, together with the underlying design considerations.

10-μm PC (Hg,Cd)Te Array

Figure 3 shows the interconnection of the breadboard pedestal assembly. One of the nine parallel channels is reproduced in Figure 4 for further clarification. Three dc bias supplies that appear in circles, i.e., V_{EE}, V_B and V_F are independently adjustable from the rear panel of the control electronics assembly. Others are internally set.

A photoconductive detector element is essentially a resistor whose resistance changes with an incident photon flux. A figure-of-merit of that change is called responsivity R_λ and is defined by:

$$R_\lambda = \frac{\Delta V_d}{H_\lambda A_d} \quad \text{(volts/watts)} \tag{1}$$

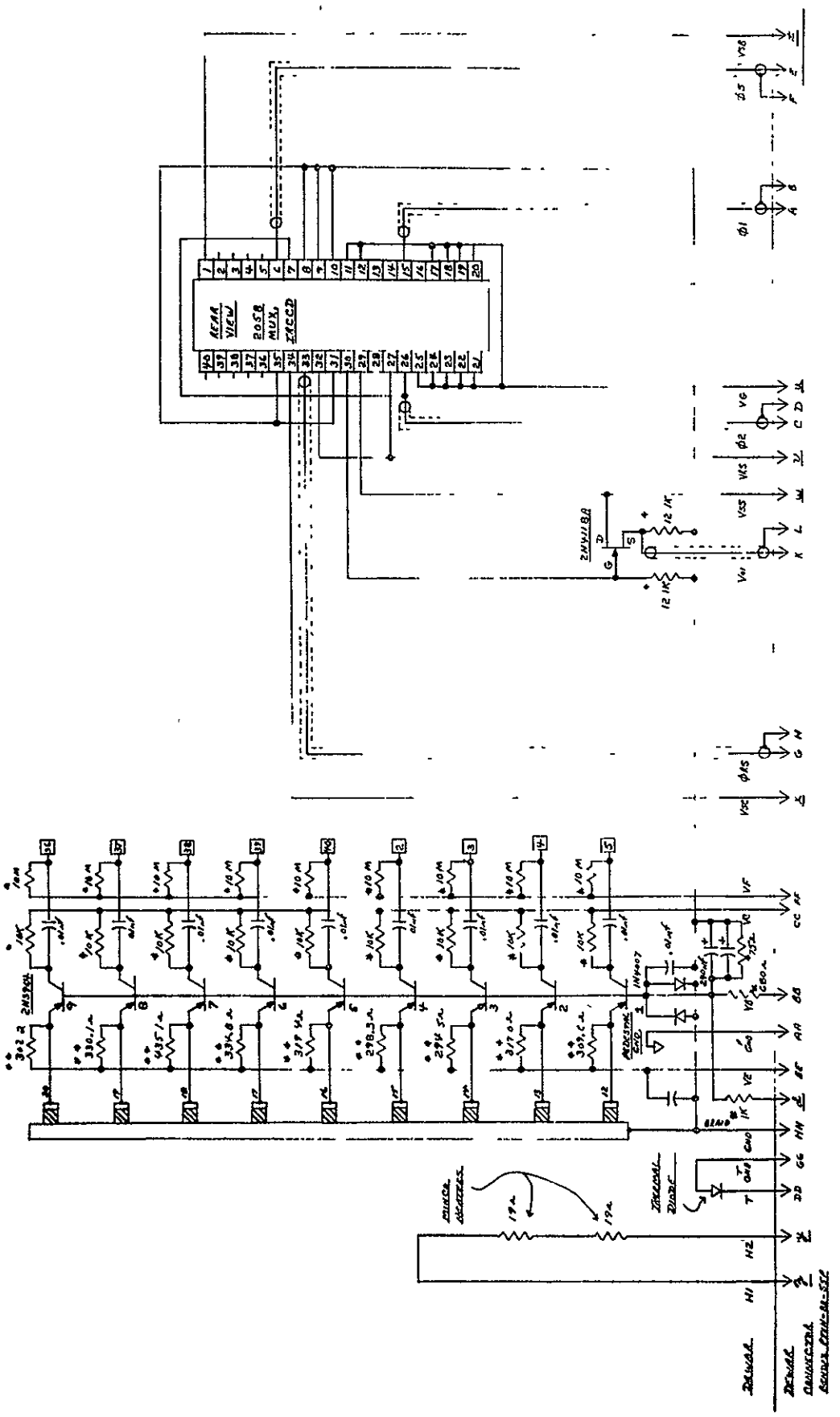

Figure 3 INTERCONNECTION OF THE BREADBOARD PEDESTAL ASSEMBLY

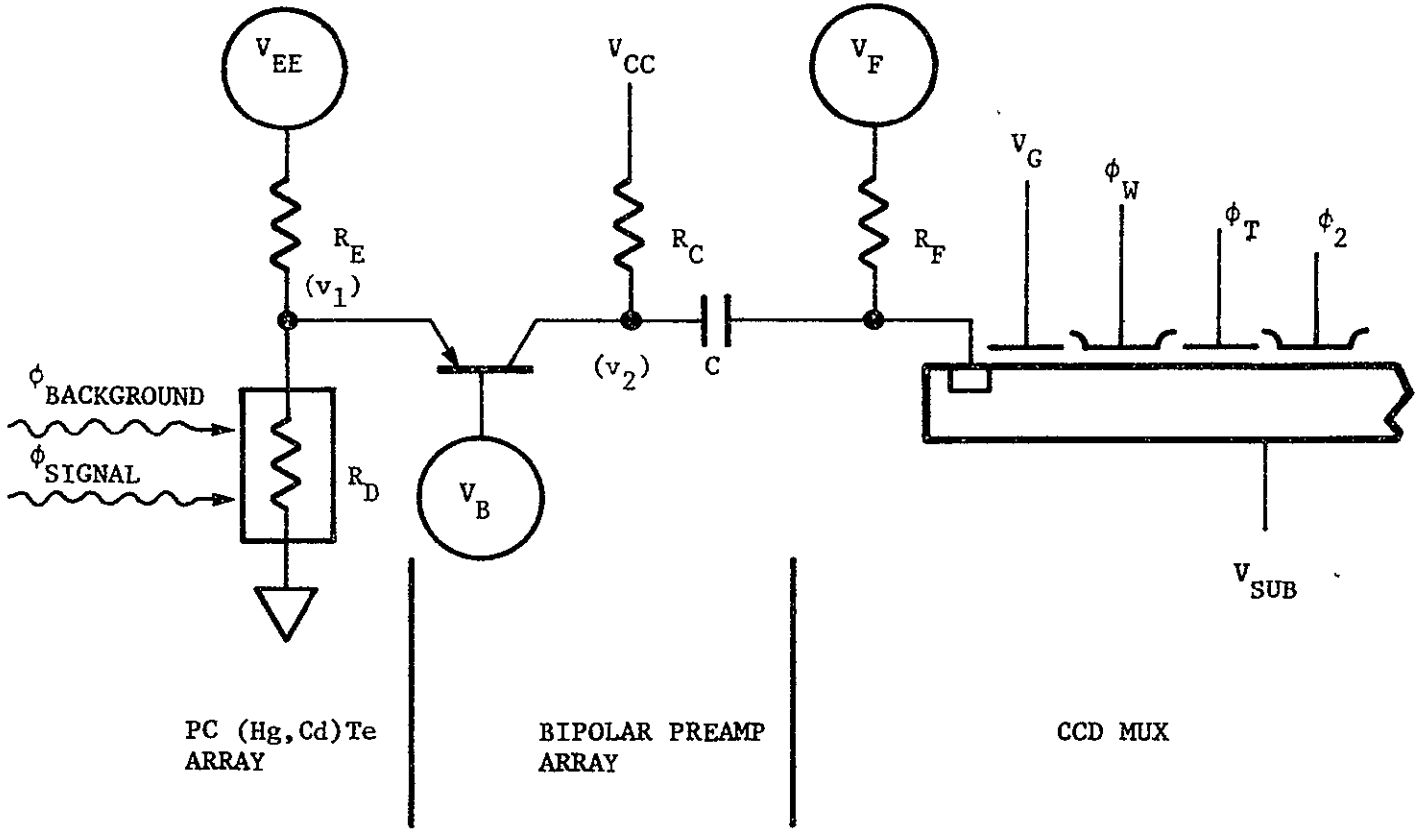

Figure 4 PEDESTAL INTERCONNECTION FOR ONE CHANNEL

where ΔV_d is the photo-induced signal voltage, H_λ is the photon flux density and A_d is the detector cross section. The responsivity for a (Hg,Cd)Te element can be expressed as:

$$R_\lambda = \eta\lambda\tau V_o/hc\ \ell\ wt\ n_o \qquad (2)$$

which clearly shows the basic requirements for high photoconductivity at a given wavelength: one must have high quantum efficiency η, long excess carrier lifetime τ, the highest possible bias voltage V_o, the smallest possible piece of crystal (ℓ is length, w width and t thickness), and a low thermal equilibrium carrier concentration n_o.

In the case of the 10-μm (Hg,Cd)Te array employed in the present breadboard demonstration, there is a broad and optimum bias voltage range for the responsivity maximum, centered around 0.3 volt (see the main text, detector section). The 9-channel average value for $R_{\lambda peak}$ is 30,000 volts/watt at 0.3-volt bias. This bias is achieved through the voltage division of V_{EE} between R_E and R_D. V_{EE} is set at exactly 2.500 volts, and the appropriate value for R_E is determined from a condition $R_E \approx 5\ R_D$.

Bipolar Preamplifier

The photo-induced voltage in R_D is amplified by a common base bipolar transistor which raises the detector noise above the CCD input noise. The advantage of a bipolar transistor rather than an MOS is that the bipolar noise is lower for the same device area. The common base offers the lowest input impedance. The V_{BE} drop of a bipolar at cryogenic temperatures (80 ~ 120 K) is roughly 1 volt. Since the emitter sits at +0.3 volt, the base voltage must be slightly below -0.7 volt for the bipolar to turn on.

The fine control of the base voltage V_B around -0.7 volt is achieved by a 10 turnpot at the rear panel of the control electronics assembly. The transistor turn-on is monitored by the collector current, designed at 200 μA per channel. The rear port marked I.C. measures the total current for nine channels across a 6.8-ohm resistor, hence, it registers $9 \times 2 \times 10^{-4} \times 6.8 =$ 12 mV. The voltage gain of the amplifier is given by:

$$\frac{v_2}{v_1} = \frac{R_c}{\frac{R_d R_E}{R_d+R_E} + \frac{kT}{qI_c} = \frac{R_{bb}}{1+\beta}} = 100 \qquad (3)$$

where R_c = 10 kohm, R_d = 1/5 R_E = 50 ohms, $I_c = 10^{-4}$ amp, T = 105 K, R_{bb} = 40 ohms, and $\beta \geq 10$. At 17 Hz at 105 K the PC (Hg,Cd)Te noise is 50 nV/$\sqrt{\text{Hz}}$ and the CCD input noise is 1.8 μV/$\sqrt{\text{Hz}}$. A gain of 40 dB is optimum for the interface, without causing a significant loss in dynamic range. The collector current is set from:

$$I_c = \frac{h_{FE}\frac{kT}{q}}{(r_{bb'}+R_D)(1+h_{FE})^{1/2}} \approx 200\ \mu A \qquad (4)$$

at which the flat band voltage noise is given by:

$$e_n^2 = 4\ kT\ (r_{bb'} + \frac{r_{bb'}+R_d}{2h_{FE}^{1/2}}) \approx 0.5\ \text{nV}/\sqrt{\text{Hz}} \qquad (5)$$

The details are given in the main text, bipolar amplifier section.

CCD MUX

The CCD MUX circuit samples each of the nine bipolar output voltages during a 5-μs time window $f_c/18$ times a second. Figure 5a shows the CCD clock waveforms, whereas Figure 5b gives the detail.

The sampled bipolar output voltage v_2 is converted into a charge packet of a size Q with the following conversion factor:

$$Q = g_m \tau v_2$$

$$g_m = \frac{Z}{L}\mu C_{ox}\left(\frac{kT}{q}\right)\left[\left(1 + \frac{2I}{\frac{Z}{L}\mu C_{ox}}\left(\frac{q}{kT}\right)^2\right)^{1/2} - 1\right] \qquad (6)$$

and

$$I = \frac{V_w C_w}{2\tau} = \frac{V_w C_{ox} A_w}{2\tau}$$

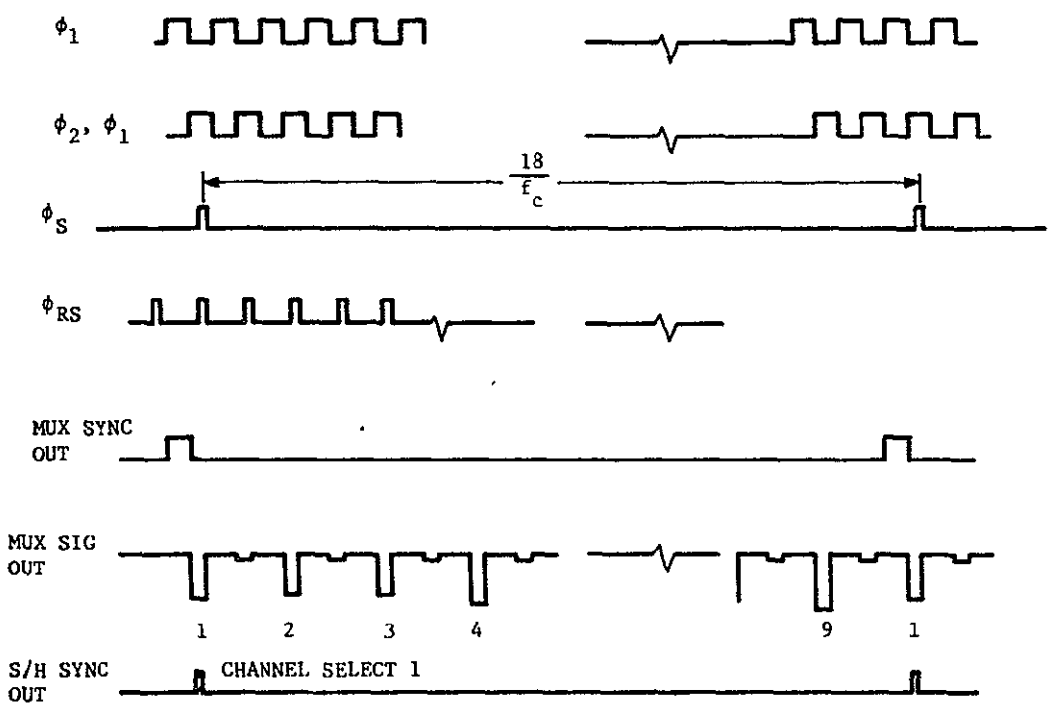

Figure 5a IR/CCD MUX CLOCKING WAVEFORMS

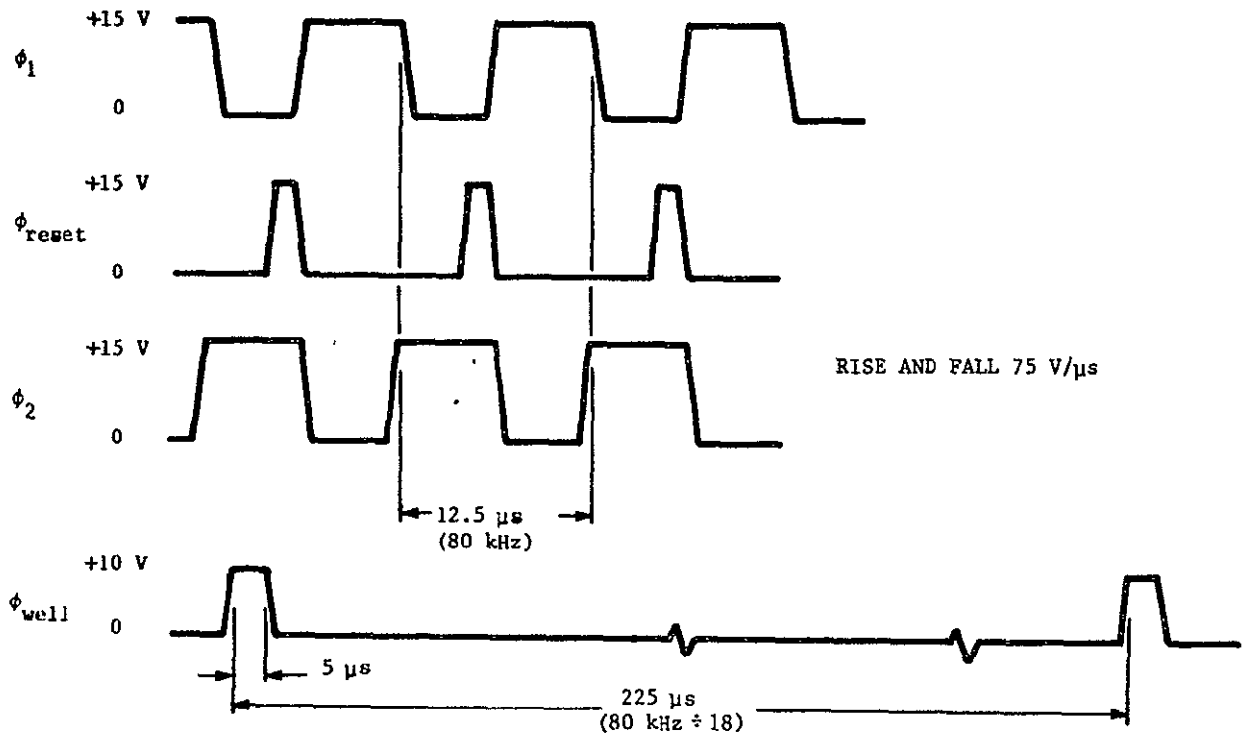

Figure 5b IR/CCD MUX CLOCKING WAVEFORMS

where τ = 5 μs is the integration period, g_m the CCD transconductance, Z/L = 4 the input gate aspect ratio, μ = 700 $cm^2\ V^{-1}\ s^{-1}$ the electron mobility, C_{ox} = 3 x 10^{-8} farads cm^{-2} the gate oxide capacitance, V_w = 10 volts the charge storage well depth, and A_w = 10^{-5} cm^2 is the storage well area. Calculations yield I = 3.2 x 10^{-7} amp, g_m = 6.6 x 10^{-6} mho and Q = 3.3 x 10^{-11} v_2 coulomb.

The current I is set to fill the storage well to one-half the storage capacity in 4 μs every $18/f_o$ = 225 μs. The effective transconductance of the CCD source diffusion is $\tau f_o/18\ g_m$ = 1.17 x 10^{-7} mho and the steady current is $f_o/18$ I = 5.7 nA. The series resistor R_F = 10 MΩ and the bias V_F supply this current.

The charge packet Q is transferred down the CCD shift register with a maximum of N = 120 transfers in the 2-bit, 2-phase, 30-channel 2058 CCD.

$$Q' = (1 - N\epsilon)Q = 0.996\ Q \tag{7}$$

where ϵ = 0.00005 is the transfer inefficiency. No appreciable loss in charge is incurred.

Figures 6a and 6b illustrate the resettable floating diffusion charge sense node where the charge packet Q' is converted to voltage v_3.

The CCD voltage gain is given by:

$$\frac{v_3}{v_2} = \frac{(1 - N\epsilon)\ g\ C_{ox}}{C_{FD} + C_G} \sqrt{\frac{\mu\ Z\ V_w\ A_w\ \tau}{L}} \tag{8}$$

where $(C_{FD} + C_G)$ = 1.2 pF is the effective floating diffusion capacitance and g = 0.8 is the MOSFET follower gain. The calculation yields a gain of 22.5 while the measurement yields 23.

Dewar

The stainless steel dewar should be continuously evacuated to pressures better than 10^{-5} mm Hg for liquid nitrogen operation. A care must be taken not to overfill the cryogen reservoir so as not to freeze the O-ring in the connector flange.

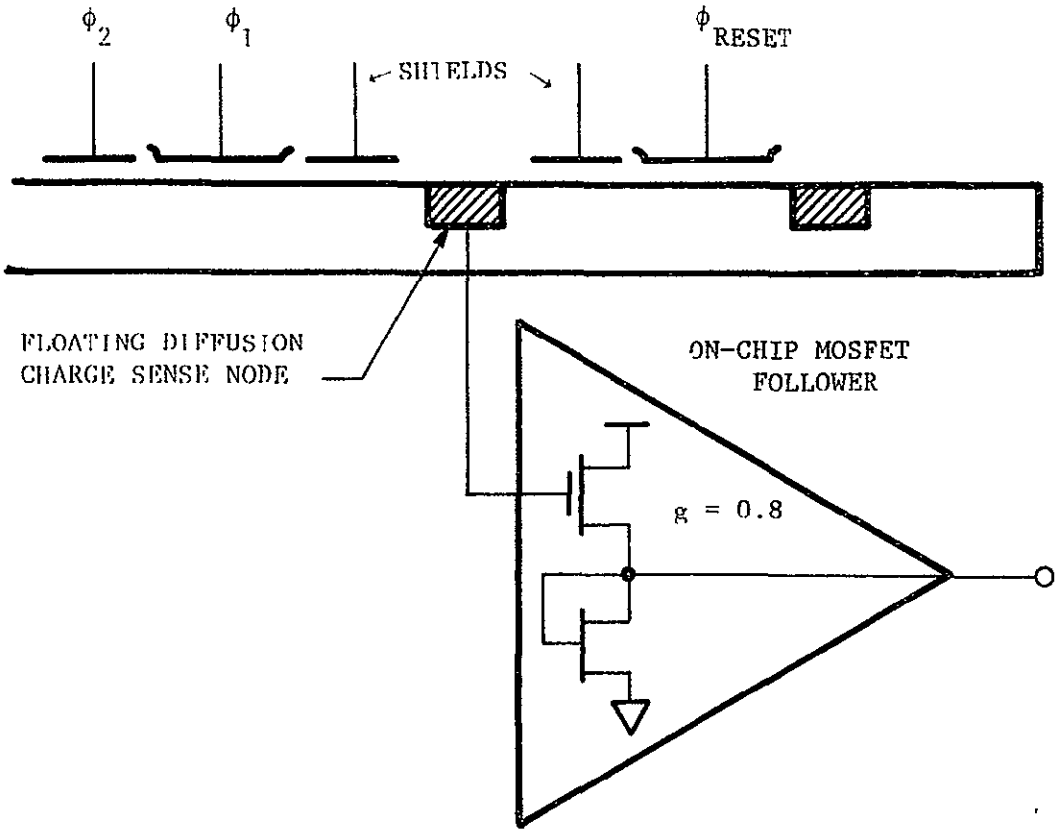

Figure 6a RESETTABLE FLOATING DIFFUSION CHARGE SENSE NODE

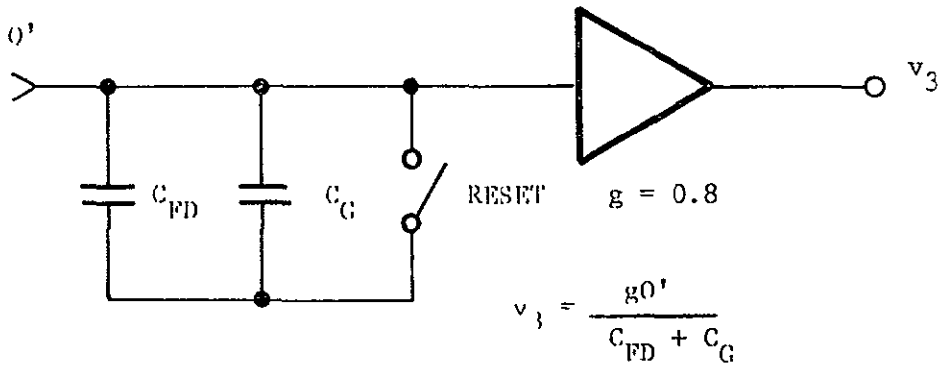

Figure 6b RESETTABLE FLOATING DIFFUSION CHARGE SENSE NODE

The aluminum pedestal housing the pushbroom IR/CCD assembly is separated from the reservoir by an 8-mil thick mylar spacer. Two filament heaters are located in the pedestal with a total maximum dissipation of 18 watts for variable temperature control. A silicon diode temperature sensor is co-located together with the PC (Hg,Cd)Te array and monitors the focal plane temperature to an accuracy of 1 K.

CCD Clock Waveform Generators

Figure 7 is the CCD clock waveform generator circuit. A photograph of the circuit board is shown in Figure 8. All the logic and timing sequence is generated by CMOS chips which are low power consumption and noise-immune devices. In the INT mode, an internal clock of 80 kHz is generated by a triggerable multivibrator chip CD4047. In the EXT mode, a pair of complementary square waveforms are to be supplied to the two BNC terminals marked ϕ_1 and ϕ_2. The externally supplied waveforms should run from 0 volt low to more than +5 volt high ($\phi_2 = \overline{\phi}_1$), and its rep rate should lie between 1 kHz to 80 kHz. When the mode selector switch is in the EXT mode, a Schmidt trigger circuit senses the zero-crossing of the externally supplied clock waveforms and regenerate the rectangular waves with appropriate duty cycle (1 kHz -80 kHz). In either case the rectangular waves go into pulse shaping networks composed of CD4049 opamp and a bipolar buffer. Waveforms ϕ_1, ϕ_2 and ϕ_{RS} are thus created, having the excursion of 0 to +15 volts with a slew rate of 75 volts/μs. A CD4017 decade counter together with CD4027 JKFF divides the clock frequency by a factor 18 (9-channel with 2 bits/channel) and generates ϕ_w which rises from 0 to +10 volts every 18th clock for a 5-μs duration. Altogether, the waveforms depicted in Figures 5a and 5b are provided by the circuit.

Low Noise Bias Supplies

The top center section of Figure 9 is the low noise bias supply network.

The dc bias voltages of V_{EE}, V_B, V_C, V_F and V_{SUB} in Figure 4 are derived from the regulated $\pm$ 24 volts and $\pm$ 15 volt power modules. These power modules exhibit a 1/f noise of the order of 300 nV/$\sqrt{\text{Hz}}$ at 17 Hz. The V_B bias

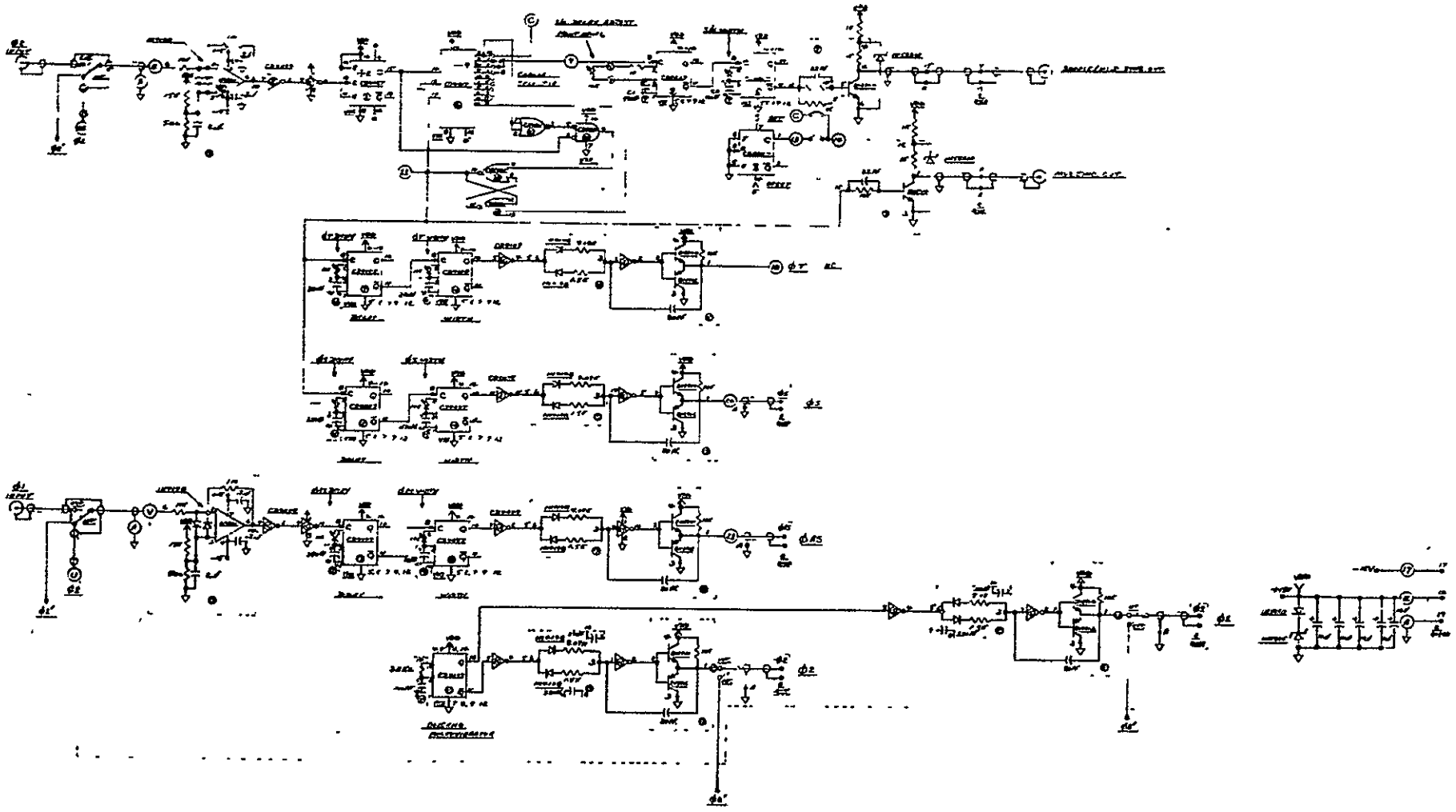

Figure 7 CCD CLOCK WAVEFORM GENERATOR CIRCUIT

Figure 8 CCD WAVEFORM GENERATOR CIRCUIT BOARD

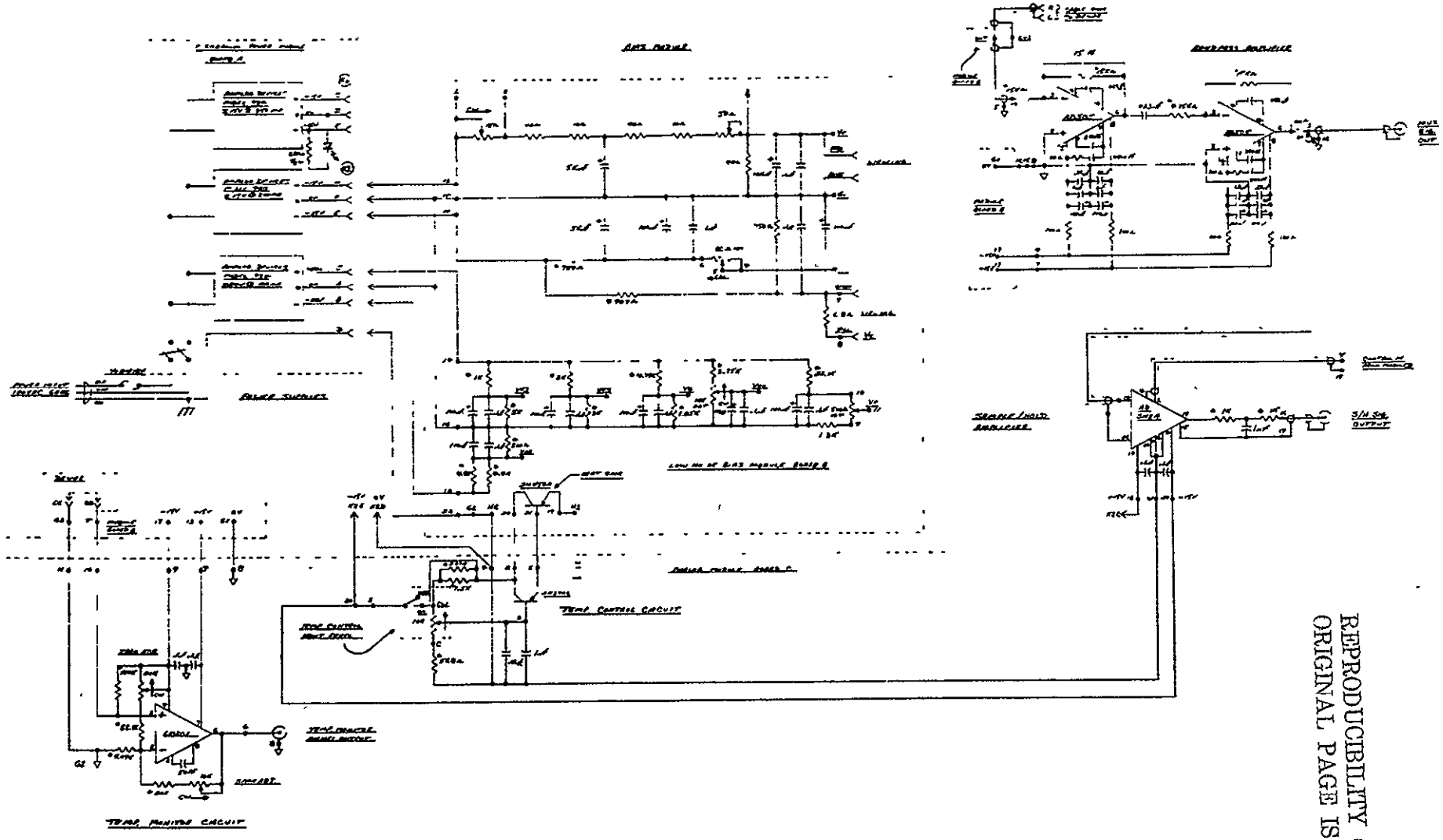

Figure 9 CIRCUIT DIAGRAM CONTAINING BIAS NETWORK, S/H AMPLIFIER, TEMPERATURE CONTROL AND TEMPERATURE READOUT

in particular must see only a few $nV/\sqrt{Hz}$. This is achieved by a voltage division of 0.7 volt/15 volt and an RC filter composed of 700 ohms and 5000 μF. A resultant noise of 2 $nV/\sqrt{Hz}$ at 17 Hz is obtained for V_B.

Sample Hold Amplifier and Logic

The right-hand corner of Figure 9 is the sample and hold amplifier circuit. An Analog Device S/H Amp Model SH/A samples and holds the multiplexed CCD output of a preselected channel (Figure 5a). The channel select switch is provided on the front panel for the channel designation. The delay adjust enables a fine synchronization between the S/H SYNC pulse and the MUX SIG OUT.

Focal Plane Temperature Readout Electronics

Figure 10 gives the calibration curve for the silicon diode used to monitor the focal plane temperature. The linearity and reproducibility is better than 1% in the range 77 to 300 K. By taking advantage of the linearity, a circuit has been devised as given in Figure 9 in which the focal plane temperature is directly converted to $\frac{T \text{ in } K}{100}$ volts. This is a very convenient feature. The filament heaters are powered from 15 volts through a Darlington transistor current regulator. The power dissipation is linearly related to the 10 turnpot on the front panel.

4. LIST OF NECESSARY EQUIPMENT

The following is a list of equipment necessary to test the Pushbroom IR/CCD breadboard:

- Diffusion pump with liquid nitrogen cold trap
- Standard 500 K blackbody source and 17 Hz chopper
- Oscilloscope
- Digital voltmeter
- Spectrum analyzer at 17 Hz

Figure 11 shows the organization.

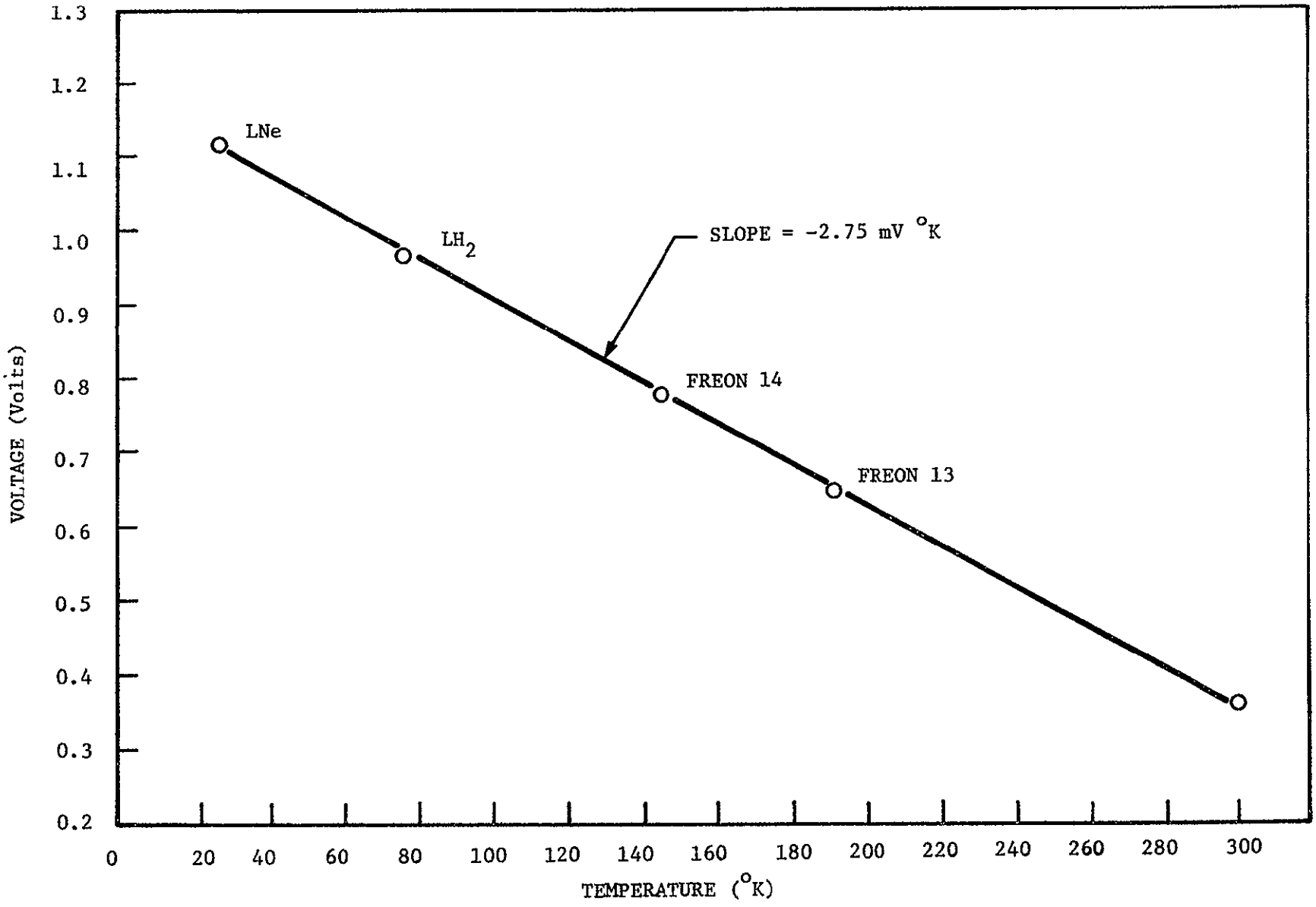

Figure 10 SILICON DIODE TEMPERATURE SENSOR CALIBRATION

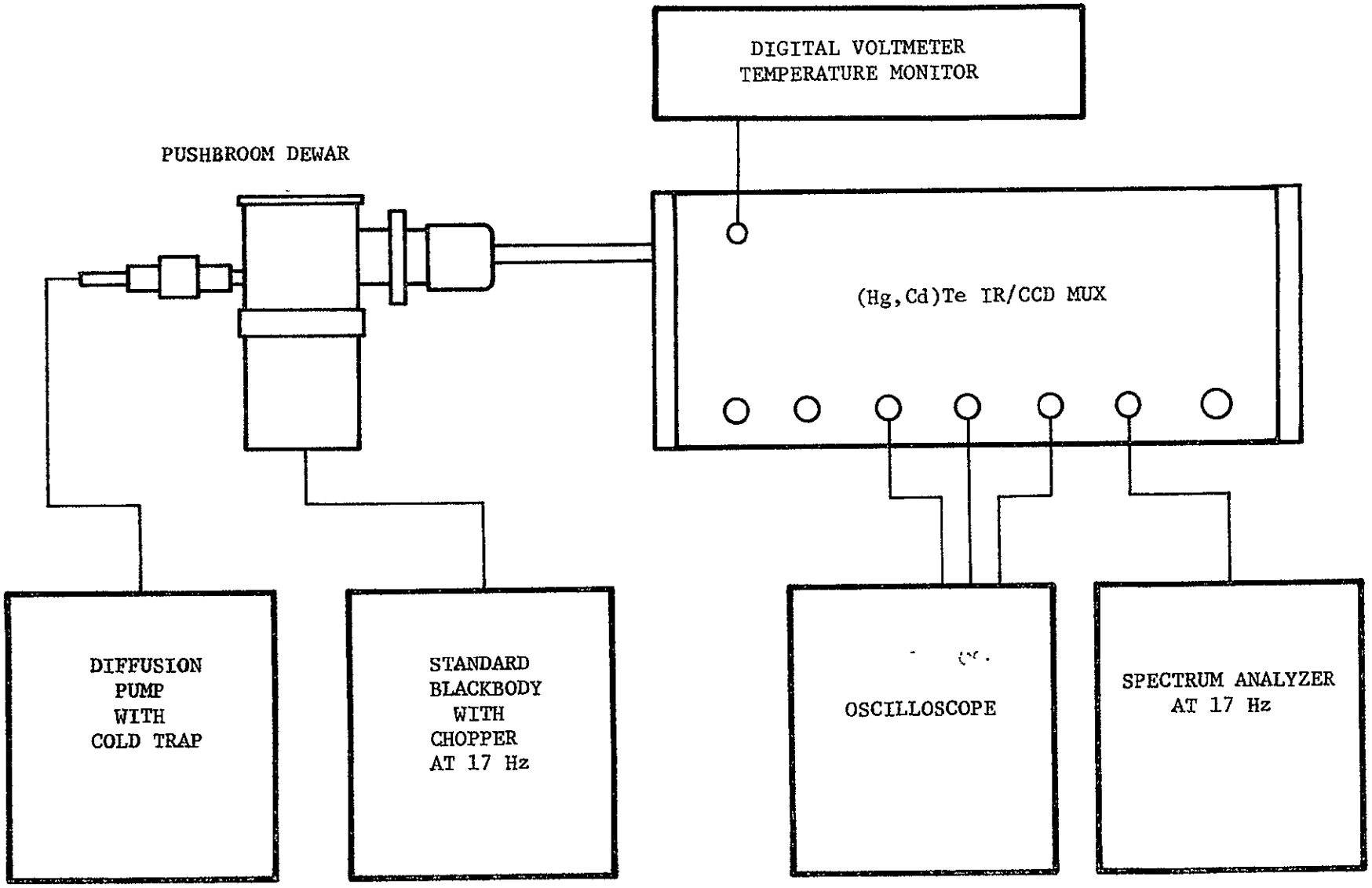

Figure 11 ORGANIZATION OF ANCILLARY EQUIPMENT FOR IR/CCD TEST

5. TEST PROCEDURE

Figure 12 is the front panel arrangement of the Pushbroom IR/CCD MUX breadboard. The operating sequence of the Pushbroom IR/CCD MUX breadboard is as follows:

- Power off in the control electronics.
- Remove the anti-static plug made of black foam rubber from the Pushbroom dewar connector.
- Connect the dewar to the control electronics.
- Evacuate the dewar to pressure less than 10^{-5} mm Hg with a pump equipped with a liquid nitrogen trap.
- Cool the dewar with liquid nitrogen.
- Power on.
- Monitor the focal plane temperature with a digital voltmeter. Direct reading T(K)/100 volt.
- The INT/EXT switch of the CCD clock to INT.
- Trigger the oscilloscope using MUX SYNC OUT. Horizontal sweep should be approximately 23 μs/div for 9-channel display.
- Display MUX SIG OUT and S/H SYNC OUT simultaneously. The waveform displayed is the multiplexed output of the 9-channel Pushbroom IR/CCD array (see Figure 14).
- CHANNEL SELECT switch slides the sample/hold pulse among 9 discrete time slots, corresponding to the 9-channel PC (Hg,Cd)Te elements. DELAY ADJUST allows fine tuning of the S/H SYNC OUT pulse with respect to the multiplexed output peak. S/H SIG OUT yields the sampled detector signal of a particular channel designated by CHANNEL SELECT switch.

6. BIAS READJUSTMENT PROCEDURE

After the system has been down for a period, it may become necessary to reestablish the proper dc bias conditions in the IR/CCD circuit (see Figure 4). The procedure listed below should be followed in sequence. Figure 13 shows the rear panel of the Pushbroom Control Electronics Assembly. The pedestal temperature must stabilize prior to the bias readjustments.

Figure 12 FRONT PANEL ARRANGEMENT OF PUSHBROOM IR/CCD MUX BREADBOARD

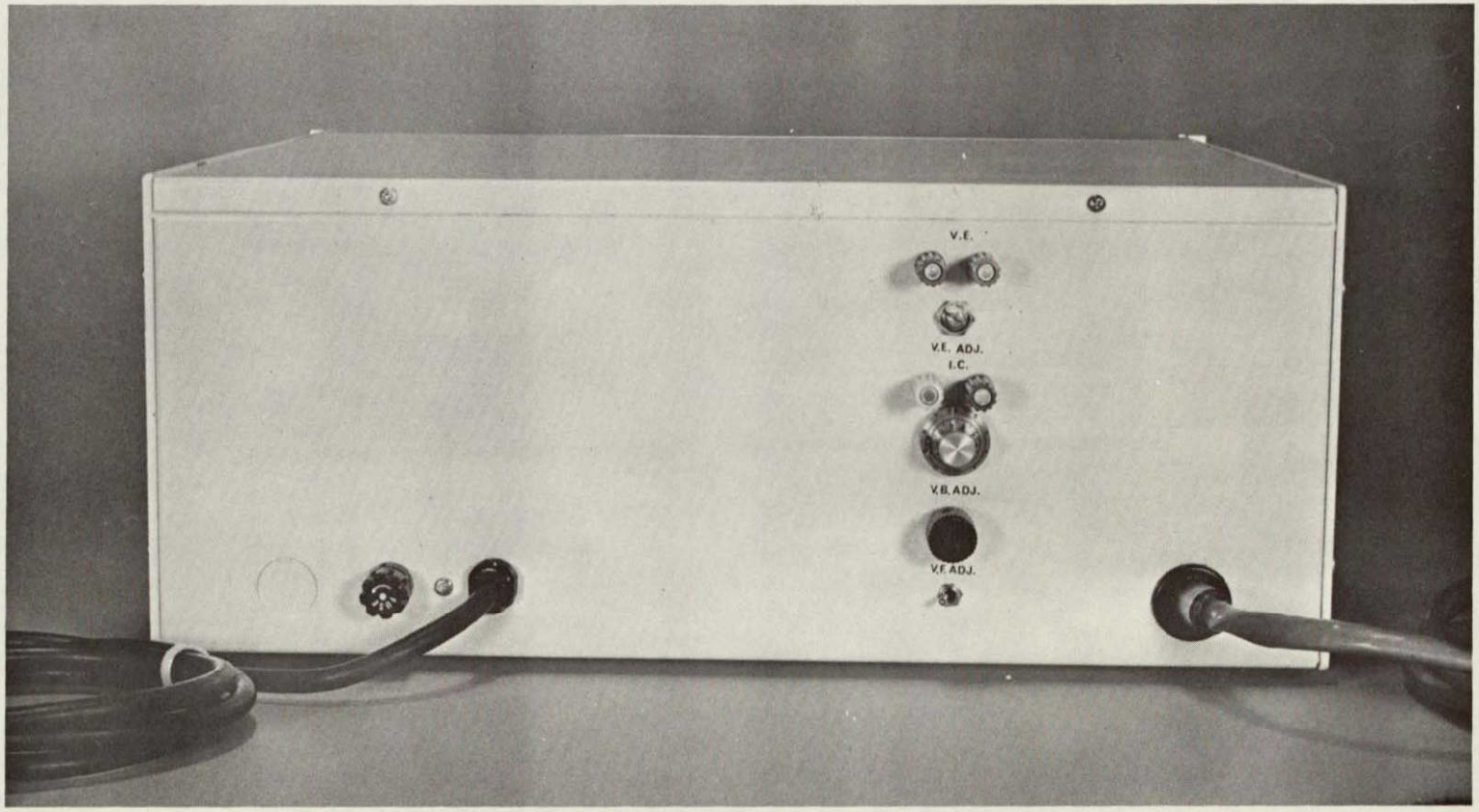

Figure 13 REAR PANEL ARRANGEMENT OF PUSHBROOM IR/CCD MUX BREADBOARD

- Turn V.E. ADJ. so that the voltage reading on V.E. is 2.500 volt.
- Turn the 10 turnpot V.B. ADJ. so that the voltage reading on I.C. is 12 mV.
- Monitor MUX SIG OUT of the front panel as V.F. ADJ. is turned on the read panel. As it is turned clockwise, the output waveform transitions from 0 charge to full well injection (Figures 14). It is set for the half-full well condition.

7. PERFORMANCE SPECIFICATIONS

Detector

1. Material: Photoconductive (Hg,Cd)Te
2. Array configuration: Linear 9 contiguous elements
3. Element size: 125 x 125 μm ± 20% average
4. Spacing between elements: 25 μm
5. Operating temperature: 80 to 120 K
6. Background temperature: 300 K
   Spectral response: 10.6 μm peak, 13 μm cutoff
7. $D^*_{\lambda peak}$ (17 Hz, 60° FOV, 1 Hz): 9.6×10^{10} cm $Hz^{1/2}/W$
8. Responsivity: 30,000 volts/watts 9-channel average
9. Resistance: 55 ohm 9-channel average
10. Power consumption: 1.5 mW/element

Bipolar Preamp

1. Transistor: 2N3964 PNP
2. Configuration: Common base
3. Gain: 40 dB
4. Input voltage noise: 10 $nV/\sqrt{Hz}$ at 17 Hz at 105 K
5. Current gain: $\beta > 10$ at 77 K
6. Collector current: 200 nA

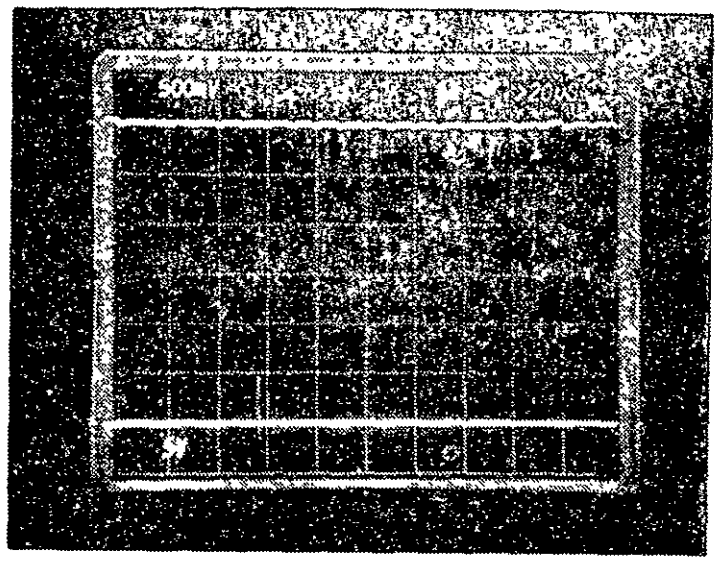

Upper trace: CCD MUX SIG OUT

Lower trace: S/H SYNC OUT

a 0 CHARGE INJECTION

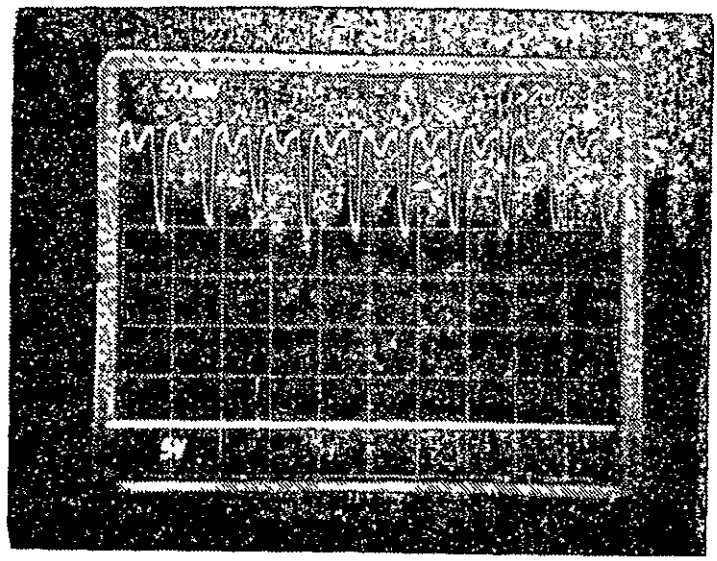

b 1/2 WELL CHARGE INJECTION (OPERATING POINT)

Figure 14 PUSHBROOM IR/CCD OUTPUT SIGNAL

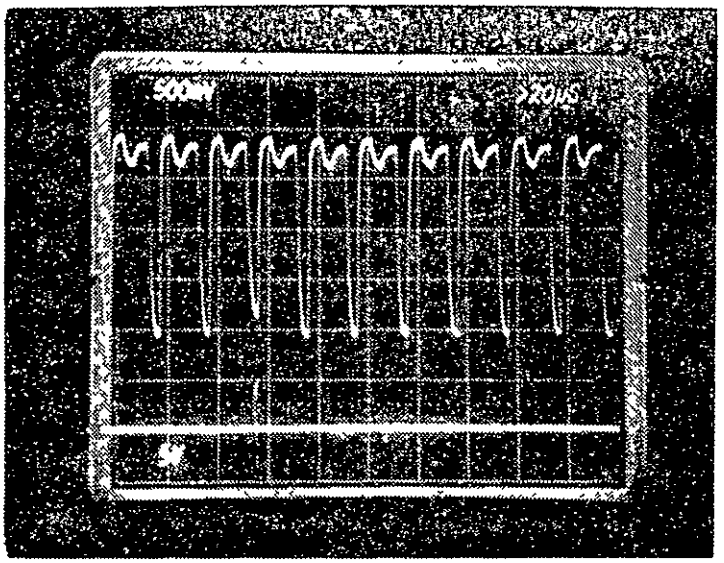

c FULL-WELL CHARGE INJECTION

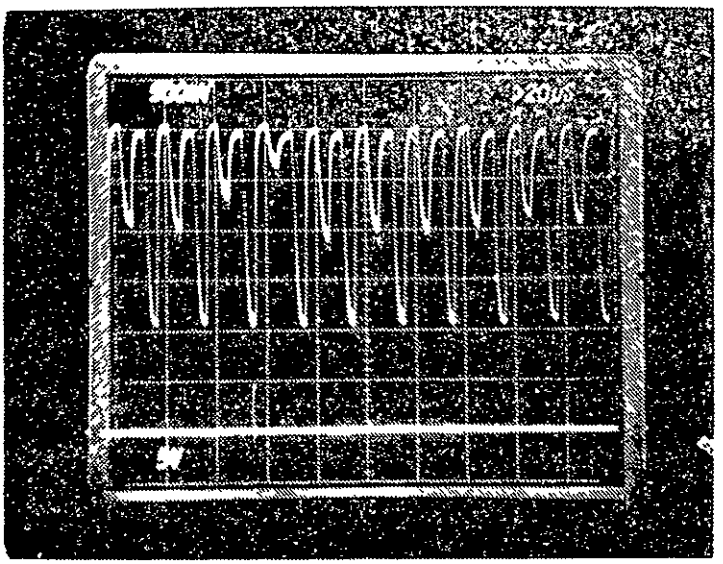

d OVERFILLING

Figure 14 PUSHBROOM IR/CCD OUTPUT SIGNAL

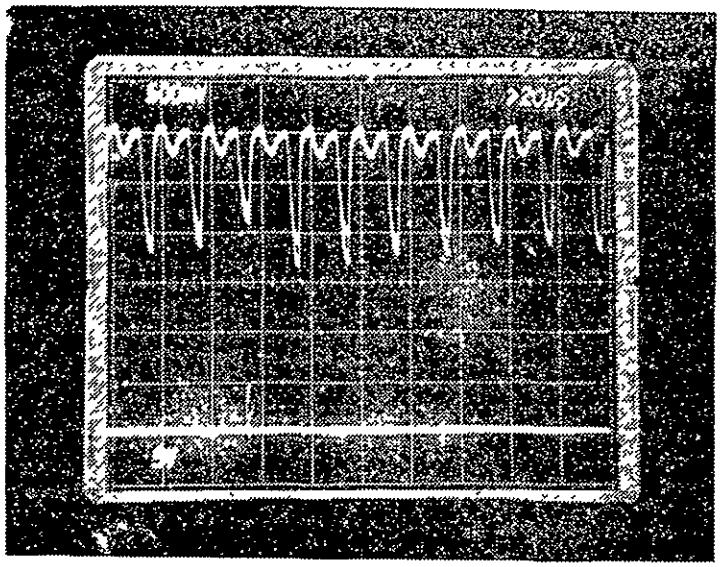

e 17 Hz BLACKBODY SIGNAL MODULATION OF 9 CHANNELS

Figure 14 PUSHBROOM IR/CCD OUTPUT SIGNAL

7. Gain bandwidth: 100 MHz

8. Power dissipation: 2 mW

CCD

1. Type: Buried n-channel CCD

2. Function: 30 parallel input MUX

3. Input configuration: Current integration for 5 μs

4. Uniformity: 10% (9 inputs, current integration)

5. Transfer efficiency: 0.99995 at 1 MHz

6. Dark current: 5% of full well at 1 kHz

7. Input referred noise: 1.8 $\mu V/\sqrt{Hz}$ at 17 Hz at 105 K

8. Voltage gain at half well: 23 at 17 Hz at 105 K

9. Dynamic range: $25{,}000/\sqrt{Hz}$ at 17 Hz

IR/CCD

1. $D^*_{\lambda peak}$: 7.5×10^9 cm $Hz^{1/2}/W$ 9-channel average: focal plane temperature 105 K, 10.6 μm peak, 300 K background, 60^o FOV, 17 Hz, 1 Hz bandwidth.

2. Responsivity uniformity: $\pm$ 40%

3. Temperature dependence: $\frac{D^*}{T} = -1.4 \times 10^8/K$ (90 ~ 120)K range